Stiffness reduction of cantilever I-beams through lateral torsional buckling for compliant beams

L. T. Staats

Master Thesis Report, June 2021

TU Delft

Stiffness reduction of cantilever I-beams through lateral torsional buckling for compliant beams

by

L. T. Staats

to obtain the degree of Master of Science
at the Delft University of Technology,
to be defended publicly on Wednesday July 7, 2021 at 14:00.

Student number:	4328582	
Project duration:	December 14, 2019 – July 7, 2021	
Thesis committee:	Prof. dr. ir. J. L. Herder,	TU Delft, supervisor, chair
	Dr. ir. G. Radaelli,	TU Delft, daily supervisor
	Dr. ir. A. Sakes,	TU Delft
	Ir. A. Amoozandeh Nobaveh,	TU Delft, daily supervisor

This thesis is confidential and cannot be made public until July 7, 2022.

TU Delft

Preface

Writing this preface marks the very end of my thesis project and thereby my time as a student at the TU Delft. Reflecting on the various student projects over the years I find myself grateful for the fun experiences I got to be part of. A few examples are a walking beer crate, a feedback video system for a surf board and a compliant mechanism ice cream scoop. This thesis project formed a worthy final successor to these student projects.

Although it was not easy to perform an already highly individual project in times of a global pandemic I am happy with the end result and I look forward to future challenges with more confidence, knowing that even during a global pandemic I managed to pull off a master thesis project.

Of course this project would not be what it is now without some much appreciated support. I would like to thank my supervisors, Ali and Giuseppe, for their help, feedback and interesting discussions. As students we are lucky to receive the level of interest and support that you provide as supervisors. Also I want to thank my fellow students, especially those from the shell skeletons group, for the interesting meetings, helpful feedback and relaxing lunch walks. Last but not least I would like to thank my parents and sister for their love and support at all times through my student career.

L. T. Staats
Leiden, June 2021

Contents

1 Introduction

Patients suffering from Duchenne muscular dystrophy (DMD) experience deterioration of muscle over time. Among other consequences a major consequence for the ability of patients to continue practicing activities performed in daily life is the loss of strength in the upper limb and more specifically the wrist [15]. Depending on the phase of DMD patients struggle to lift weight or hold the weight of their hand such that the hand is in a neutral position. The inability of the muscles to support the hand in a neutral position leads to hyperextension of the wrist which causes tissue damage to the muscles and ligaments of the wrist [15].

A solution to prevent tissue damage and increase the range of motion of the wrist would be to have wrist support that keeps the hand in a neutral position and supports the weight of the hand throughout the motion of the wrist such that only a slight additional force needs to be provided by the muscle to use the wrist. In order to have a functional wrist support it should be capable of supporting the hand for its two major degrees of freedom: flexion/extension and pronation/supination. Figure 1.1 obtained from the work of Kayhan et al. [9] illustrates these degrees of freedom as well as the neutral position. In order to support the weight of the hand a conceptual wrist support could be made based on the principle of static balancing [8]. The principle of static balancing uses a pendulum with a spring attached to a vertical reference. The spring is selected such that the potential energy of the system remains constant and thus no additional energy is required to lift the pendulum.

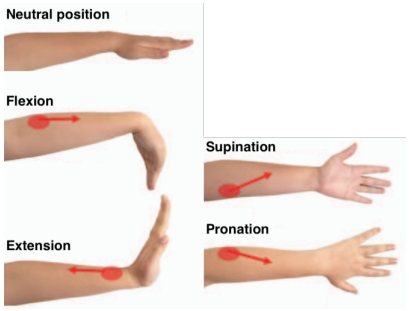

Figure 1.1: The image obtained from the work by Kayhan et al. [9] illustrates the motion of flexion/extension and pronation/-supination

If the hand would be modelled as a pendulum with the wrist modelled as a rotational joint as illustrated in figure 1.2 the motion of flexion and extension could be supported. The gravitational force of the hand would be supported by the spring, resulting in a supported hand throughout a range of flexion/extension.

However, when considering the additional degree of freedom of pronation and supination, the concept becomes more complex. When modelling pronation/supination as a rotation about the x-axis, the concept of a hand supported by a spring by means of static balancing no longer works. When rotating the pendulum, which represents the hand, about the x-axis, the line of action of gravity and the spring force are no longer in the same plane which causes the pendulum to be pulled such that the spring

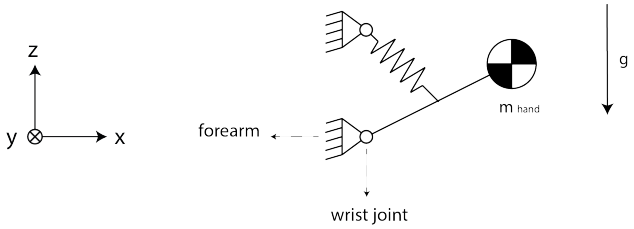

Figure 1.2: When modelling the wrist and hand as a weight on a pendulum, tha addition of a spring would keep the potential energy of the system constant which means that the weight of the hand would be supported

returns to its rest length. Thus simply designing a wrist support based on gravity balancing does not satisfy the support for both flexion/extension and pronation/supination.

What is needed to support both degrees of freedom is a method to have rotational compliance while supporting the load induced by the weight of the hand. This is where inspiration came up from the world of civil and structural engineering. In these fields there is a well known phenomenon called lateral torsional buckling (LTB) of open section beams [4], [10]. This type of buckling concerns open section beams becoming unstable when subjected to bending beyond a critical load. For the case of cantilever I-beams specifically, when subjected to a bending load beyond a critical value, an elastic instability occurs because the bottom flange in compression tends to move laterally while the top flange in tension tends to keep the beam straight [5]. This causes a beam, when subjected to a bending load beyond a critical value, to become unstable and thereby deflect laterally as well as twist about its longitudinal axis. Figure 1.3, obtained from the work by Herman Venter [14], displays the unloaded and buckled orientation of a cantilever I-beam subject to LTB by an applied tip load, P, with a lateral deflection indicated by δ_{Lc} and co-occurring longitudinal rotation indicated by ϕ_{C}.

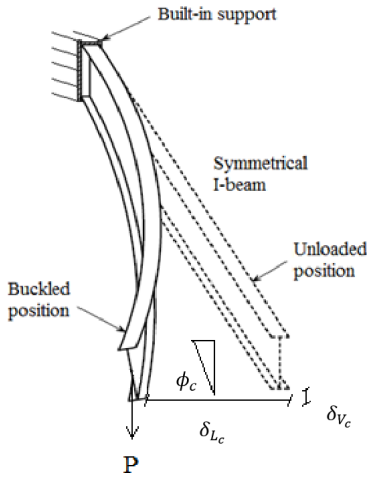

Figure 1.3: The figure obtained from the work by Herman Venter [14] displays the unloaded and buckled orientation of a cantilever I-beam subject to LTB by an applied tip load, P, with a lateral deflection indicated by δ_{Lc} and co-occurring longitudinal rotation indicated by ϕ_{C}.

When an elastic instability is present, the structure generally exhibits a form of zero or negative stiffness. A cantilever I-beam subject to LTB due to an applied tip load at the free end, appears to go from a stable equilibrium state when subjected to a load lower than the critical load to a new equilibrium state when loaded beyond the critical load. In this new equilibrium state the beam is deflected laterally and rotated about its longitudinal axis. Due to the observed tendency of a cantilever beam subject to LTB to suddenly twist about its longitudinal axis and deflect laterally, it is suspected that, in the buckled state, the cantilever beam displays significantly reduced, potentially negative or zero, rotational stiffness behaviour about its longitudinal axis at the free end.

This is where beams subject to LTB become a potentially interesting solution for a wrist support, since in the buckled state the beams still support a bending load while being compliant about the longitudinal axis. As a concept for a wrist support the weight of the hand could form the critical load

which is still supported by the beam and the rotational stiffness about the longitudinal axis is reduced, which allows for pronation and supination. However a beam subject to LTB displays both a rotation and lateral deflection at the free end of the beam. This lateral deflection is undesirable as, when implemented as a wrist support, it would cause the hand to move laterally for pronation/supination.

1.1. Thesis objective

Current literature does not consider lateral torsional buckling as a potential working principle for negative and/ or zero stiffness mechanisms, let alone a wrist support. Therefore, the aim of this work is to investigate the potential of exploiting lateral torsional buckling to reduce the rotational stiffness about the longitudinal axis of cantilever I-beams with minimal co-occurring lateral deflection. By minimising the lateral deflection the twisting behaviour approaches the behaviour of a rotational joint, making the outcome of this work suitable to an even wider range of applications. In this work the potential of reducing longitudinal rotational stiffness through LTB is investigated for cantilever I-beams, since I-beams are known for their susceptibility to LTB [5], [13].

This investigation is structured by 3 objectives: (i) a verification of negative rotational stiffness behaviour for a beam subject to LTB, (ii) a parameter study of both cross-sectional geometrical properties as well as cross-sectional dimensions of tip loaded cantilever I-beams at their critical load and (iii) an optimisation case to find the dimensions of a tip loaded straight cantilever I-beam that has minimal lateral deflection while being torsionally compliant when applying the buckling load at its free end. The optimisation results are verified by means of an experiment on a 3D printed beam.

1.2. Thesis outline

This thesis is outlined as following: the main work is presented in the form of a paper on the objectives mentioned above in chapter 2. The following chapters present supplementary information on the topics of the estimation of the critical buckling loads (chapter 3), the numerical modelling of LTB through a 3-step loading scheme (chapter 4), supplementary results of the parameter study (chapter 5), a detailed explanation of the optimisation process (chapter 6) and details on the experimental setup (chapter 7). Finally a discussion and conclusion of this work are presented in chapter 8 and chapter 9 respectively.

2

Paper: Stiffness reduction of cantilever I-beams through lateral torsional buckling for compliant beams

Stiffness reduction of cantilever I-beams through lateral torsional buckling for compliant beams

Laurens Staats

Precision and Microsystems Engineering Department, Delft University of Technology, 2628CD, Delft, The Netherlands

Abstract

Lateral torsional buckling (LTB) of I-beams is an established buckling phenomenon in civil and structural engineering known for causing structural failures. However when a buckling instability is present the structure contains a form of negative stiffness. Due to the observed tendency of I-beams subject to LTB to twist about their longitudinal axis it is suspected that such I-beams contain a form of negative rotational stiffness about their longitudinal axis. Rather than considering LTB as a failure mode for structures, this work aims to investigate the potential of cantilever I-beams subject to LTB having a reduced rotational stiffness about their longitudinal axis with minimal lateral deflection on demand by subjecting the beam to LTB. By minimising the lateral deflection the longitudinal twisting behaviour approaches the behaviour of a compliant rotational joint. The occurrence of negative rotational stiffness in the buckled state is verified and a parameter study is executed to evaluate the stiffness reduction and co-occurring lateral deflection by means of 1-dimensional finite element modelling. Finally an optimisation is performed to obtain a beam with minimal lateral deflection and a significant reduction in longitudinal rotational stiffness. The simulated behaviour is experimentally validated. The simulation and experiment showed that rotational stiffness can be significantly reduced through LTB. Additionally the experiment verified the significant reduction of lateral deflection for the optimised beam. Overall this work forms an initial step towards the use of reduced rotational stiffness of beams by exploiting lateral torsional buckling.

Keywords: Lateral torsional buckling, variable stiffness, compliant beams, beam optimisation

1. Introduction

Lateral torsional buckling (LTB) of open section beams is a well studied phenomenon in civil and structural engineering [1], [2]. This type of buckling concerns open section beams becoming unstable when subjected to bending beyond a critical load. For the case of I-beams specifically, when subjected to a bending load beyond a critical value, an elastic instability occurs because the bottom flange in compression tends to move laterally while the top flange in tension tends to keep the beam straight [3]. This causes a beam, when subjected to a bending load beyond a critical value, to become unstable and thereby deflect laterally as well as twist about its longitudinal axis. Figure 1, obtained from the work by Herman Venter [4], displays the unloaded and buckled orientation of a cantilever I-beam subject to LTB by an applied tip load, P, with a lateral deflection indicated by δ_{Lc} and co-occurring longitudinal rotation indicated by ϕ_{C}.

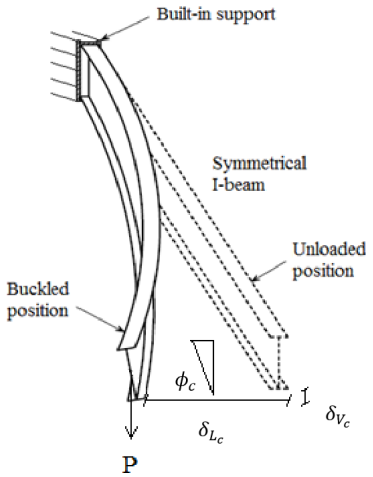

Figure 1: The figure obtained from the work by Herman Venter [4] displays the unloaded and buckled orientation of a cantilever I-beam subject to LTB by an applied tip load, P, with a lateral deflection indicated by δ_{Lc} and co-occurring longitudinal rotation indicated by ϕ_{C}.

Existing literature on LTB covers the buckling behaviour as a failure mode of beams as structural supports. Research topics include end support conditions [5], loading types [6], simulations [7] beam types and dimensions [8], [9], [10], [11] and experimental validations of simulations [12], [13]. Approximations of critical loads for beams subject to LTB are defined by Eurocode design regulations for structures [14]. Overall, the focus of literature regard-

*Corresponding author: Laurens Staats

Email address: L.T.Staats@student.tudelft.nl (Laurens Staats)

ing beams subject to LTB lies on preventing beams from becoming unstable and causing structures to fail.

However when an elastic instability is present, the structure generally exhibits a form of zero or negative stiffness. A general example of an elastic instability is buckling of a slender beam in compression while the beam is fixed at both ends. This example is illustrated by figure 2 as shown in the work of Fulcher et al. [15] which displays the behaviour of a beam that is axially compressed by a load larger than the critical buckling load. Initially the beam is in an ideal unstable equilibrium due to the absence of geometric or loading perturbations, displayed by position (2) in figure 2a. However when a loading perturbation is present in the form of an applied transverse force, F_t, the beam displays negative stiffness behaviour in the transverse direction of the applied F_t and transverse displacement u_y. After displacing through a range of displacement with negative stiffness two stable equilibrium states (1) or (3) in figure 2a can be obtained from the middle configuration (2) with corresponding values for F_t of 0 N. The stable equilibrium states of the buckled beam are displayed in terms of force - displacement in figure 2b (1) and (3).

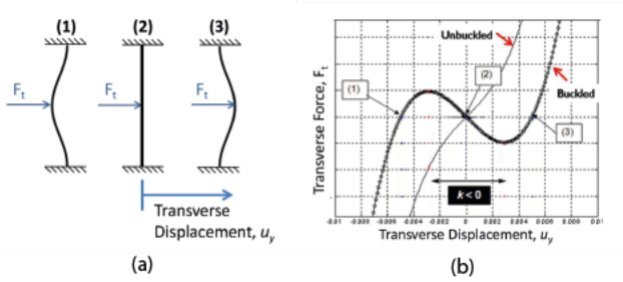

Figure 2: The figure obtained from the work by Fulcher et al. [15] displays: (a) The beam in compression in unstable equilibrium state (2) and 2 stable equilibrium states (1) and (3). (b) The corresponding transverse force - displacement behaviour shows a region of negative stiffness and bistable behaviour between the stable equilibrium states (1) and (3) for the buckled beam. The unbuckled beam shows a positive stiffness behaviour throughout the entire applied transverse displacement.

A cantilever I-beam subject to LTB due to an applied tip load at the free end, appears to go from a stable equilibrium state when subjected to a load lower than the critical load to a new equilibrium state when loaded beyond the critical load. In this new equilibrium state the beam is deflected laterally and rotated about its longitudinal axis. Due to the observed tendency of a cantilever beam subject to LTB to suddenly twist about its longitudinal axis and deflect laterally, it is suspected that, in the buckled state, the cantilever beam displays significantly reduced rotational stiffness behaviour about its longitudinal axis at the free end.

Thereby, rather than being a failure mode for structures, the phenomenon of a cantilever I-beam subjected to LTB offers potential as a mechanism with reduced rotational stiffness on demand. This is particularly interesting for the field of compliant mechanisms, since these often consist of elastically deformable elements with an inherent positive stiffness, thus requiring energy to deform these elements and actuate the mechanism [16]. Being able to reduce the rotational stiffness of a beam significantly on demand may be beneficial to reduce or eliminate the positive stiffness of compliant mechanisms. When the rotational stiffness of beams is reduced significantly through LTB, the beams may approach zero rotational stiffness mechanisms which require no increase in actuation load and thus no additional energy to rotate [17].

Additionally, being able to reduce the rotational stiffness on demand by purely applying a tip load can be beneficial for a variety of applications. Variable stiffness applications are of interest in a variety of fields. Examples are the field of aerospace [18], medical devices [19] and soft robotics [20].

Current literature does not consider lateral torsional buckling as a potential working principle for negative and/or zero stiffness mechanisms.

Therefore, the aim of this work is to investigate the potential of exploiting lateral torsional buckling to reduce the rotational stiffness about the longitudinal axis of cantilever I-beams with minimal co-occurring lateral deflection. By minimising the lateral deflection the twisting behaviour approaches the behaviour of a rotational joint, making the outcome of this work suitable to a wider range of applications. In this work the potential of reducing longitudinal rotational stiffness through LTB is investigated for cantilever I-beams, since I-beams are known for their susceptibility to LTB [3], [14].

This investigation is structured by 3 objectives: (i) a verification of negative rotational stiffness behaviour for a beam subject to LTB, (ii) a parameter study of both cross-sectional geometrical properties as well as cross-sectional dimensions of tip loaded cantilever I-beams at their critical load and (iii) an optimisation case to find the dimensions of a tip loaded straight cantilever I-beam that has minimal lateral deflection while being torsionally compliant when applying the buckling load at its free end. The optimisation results are verified by means of an experiment on a 3D printed beam.

The outline of this paper is as follows. The method is described in section 2 with subsections 2.1, 2.2 and 2.3 covering modelling steps used throughout the 3 objectives and section 2.4, 2.5 and 2.6 cover the method per objective. Subsection 2.7 covers the experimental setup. The respective results are described per objective in section 3 with subsections 3.1 on the verification of negative rotational stiffness due to LTB, 3.2 on the parameter study, 3.3 on the optimisation case and 3.4 on the experimental validation. Section 4 provides the discussion and the work is concluded in section 5.

2. Method

The aim of this work is to investigate the potential of exploiting LTB to reduce the rotational stiffness of cantilever I-beams with minimal lateral deflection through 3 objectives.

Before proposing the detailed methods for these objectives this section will first cover the used FEM model in section 2.1, the need for and the details on an estimation of the critical buckling load in section 2.2 and a 3 step loading scheme in section 2.3. These modelling steps form the foundation of what is investigated for each of the 3 objectives. Finally, for each of the 3 objectives the specific methods are elaborated on in sections 2.4, 2.5 and 2.6. The experimental validation is described in 2.7

2.1. FEM model

The beam simulations for both the parameter study and the optimisation case are performed using a three dimensional beam model with a custom finite element method (FEM) solver based on geometrically non-linear co-rotational beam elements using the Euler-Bernoulli beam formulation as proposed by Battini [21].

The one dimensional beam model creates a beam structure based on a set of one dimensional nodes with user defined locations, nodal mechanical material properties (E,G) and nodal geometrical properties (Iyy, Izz, J). The beam orientation and shape is set by specifying the nodal coordinates and nodal connections. Computation of the deformation behaviour is based on the nodal properties. Application of forces, moments, displacements and rotations is simulated through the custom FEM solver. This solver was selected over commercially available FEM tools, since it allows for highly custom loading options and for faster computation as well as optimisation.

2.2. Buckling load approximation

Before any post-buckling behaviour can be investigated, the simulated beam needs to become unstable through lateral torsional buckling. Therefore the first step is the estimation of the buckling load or critical load. Various literature covers the topic of critical load estimation for open-section beams subject to LTB. However, the geometrically non-linear nature of LTB results in literature that is mostly case specific in terms of applied loads, beam support conditions and beam shapes [5], [6], [7], [8], [13], [9], [10], [11], [14]. Therefore, in this work a self-developed, more universal, numerical approach is taken to estimate the critical buckling load.

The numerical approach for approximation of the buckling load is based on the observation of a cantilever I-beam subject to LTB. An I-beam subject to a gradually increasing tip load applied at the free end initially shows bending behaviour. Once the force has increased up to the critical buckling load the beam will no longer purely bend. Rather, due to the occurrence of LTB the beam will deflect laterally and twist about its longitudinal axis. Thus an increasing tip load initially results in no lateral deflection. However, once the critical buckling load is reached an increase of the tip load results in significant lateral deflection.

This sudden change in lateral deflection is the foundation to the approximation of the buckling load used throughout this study.

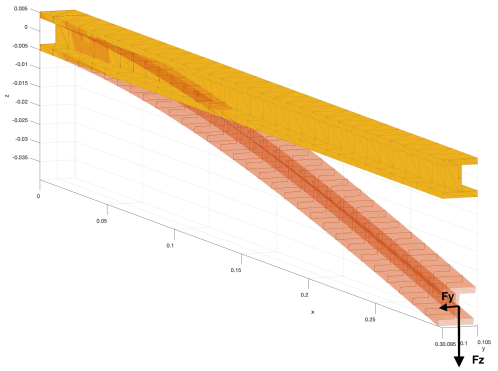

Figure 3: A vertical tip load, Fz, is applied at the free end while a lateral perturbation load, Fy, with a magnitude of 1/1000 of Fz provides a slight imperfection to the model to enable simulation of buckling. Fy is not drawn to scale for illustration clarity

In the FEM model LTB is simulated by application of a vertical tip load Fz applied at the free end of a cantilever I-beam. Additionally a perturbation force, Fy, with a magnitude that is 1/1000 of the tip load is applied in the lateral direction. Figure 3 displays the vertical tip load Fz and lateral perturbation load Fy.

An example graph of the resulting behaviour of the applied load and resulting lateral deflection, Fz - Δy, is displayed in figure 4.

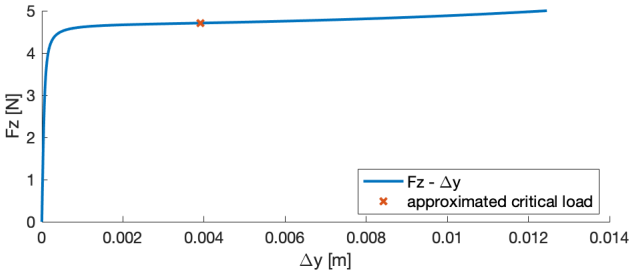

Figure 4: The graphs shows an example of the applied load - lateral deflection, Fz - Δy, behaviour for an I-beam loaded as shown in figure 3. Up to a load of about 4.7 N the slope dF/dΔy decreases and to then start increasing again

Figure 4 shows the corresponding relation between Fz and Δy for this example case. Around a load of 4.6 N and above, an increment in applied load, Fz, suddenly results in a large increment in lateral deflection compared to the applied force, Fz, up to 4.6 N.

Also the example shows that the slope of the Fz-Δy behaviour decreases greatly from an initially large value at the origin, displayed as a seemingly vertical graph, to

almost a horizontal line around 4.7 N.

For further increased loads, the slope then starts increasing again. This inflexion point at around 4.7 N is appointed as the approximation of the critical load, since it is close to the transition from having barely any to a lot of increase in lateral deflection per increment in applied tip load Fz. The inflexion point is easily identified mathematically by looking for the minimal slope dFz/dΔy and co-occurring ddFz/ddΔy = 0. This mathematical property is beneficial for universal automated approximation of many different I-beams for both the parameter study and optimisation.

A final feature is used throughout the numerical buckling load approximation to avoid occasionally falsely allocated buckling loads: the minimal slope dFz/dΔy at the inflexion point with ddFz/ddΔy = 0 should have at most a magnitude of 10% of the magnitude of the slope dFz/dΔy at the initial increments in load from 0.

For the example graph of figure 4 the estimation procedure described above approximated a buckling load of 4.7 N, indicated by the orange cross in the graph.

2.3. 3-step loading scheme

Once the buckling load has been estimated, a 3 step loading scheme is applied to investigate the moment - rotation and longitudinal rotational stiffness behaviour at the end point of the beam in a buckled state. First the approximated critical load is applied as a vertical tip load at the free end of the cantilever beam (fig. 5-a). Consequently the beam bends down in the xz plane (fig. 5-b).

Secondly, the beam and applied tip load are realigned by rotating the orientation of the beam and the applied load about the y axis by angle α such that the longitudinal axis normal to the cross-section at the free end of the beam, is oriented parallel to the global x-axis (fig. 5-c). This is required for the application of a pure rotation about the longitudinal axis of the free end of the beam. Before this rotation is applied, the beam is kept at an unstable equilibrium by setting the critical load as preload on the free end of the beam. This preload remains present and stays constant throughout the application of the rotation.

Thirdly, a rotation β is incrementally applied about the longitudinal axis, normal to the final cross-section, which is now parallel to the global x axis (fig. 5-d). Throughout the rotation the reaction moment as well as the co-occurring displacements and rotations are traced to determine the longitudinal rotational stiffness as well as the co-occurring lateral deflection.

2.4. Verification of negative rotational stiffness behaviour due to LTB

The first sub objective of this work is the verification of negative rotational stiffness behaviour due to LTB. To validate that the longitudinal rotational stiffness becomes negative when the beam is loaded beyond the critical buckling load, the 3-step loading scheme(fig. 5) is applied for preload values, indicated by Fb in 5, that are smaller, equal and larger than the approximated buckling load. The preload is varied as a factor of 0 to 1.4 times the buckling load with 0.2 increments.

Preload levels smaller than the buckling load with magnitude of 0.2 to 0.8 of the buckling load simulate a preloaded, yet stable, unbuckled beam, while the preload levels of 1.2 and 1.4 of the buckling load simulate an unstable beam subject to LTB. The preload level equal to the buckling load forms the boundary between the stable, unbuckled beam and unstable, buckled beam.

For each level of preload the rotational stiffness profile is derived about the longitudinal axis of the final beam element by applying a rotation of $-60°$ to $60°$ about the longitudinal axis of the final beam element and tracing the corresponding reaction moment. The applied rotation is displayed as β about the x-axis in step (d) of figure 5 and the reaction moment is taken about the same x-axis to obtain the moment - rotation and thereby rotational stiffness behaviour about this axis.

2.5. Parameter study

The second sub objective of this work is a parameter study of both cross-sectional geometrical properties and cross-sectional dimensions of a tip loaded cantilever I-beam at the buckling point. The cantilever I-beam is selected since it is not only a structure known for its susceptibility to lateral torsional buckling, but also variation of its dimensions can span a wide range of values for the geometrical properties of the second moments of inertia, Iyy, Izz and torsional constant, J. For the parameter study the I-beam is modelled with mechanical material properties E = 1750 MPa and G = 361 MPa, corresponding to Polyamide12 (PA12), a nylon [22]. PA12 is selected as a material, since it allows for precise 3D printing of I-beams.

The geometry of the I-beam for the parameter study is based on a cross-section defined by dimensions H, B, h and b as displayed in figure 6. The variation of parameters is based on a base beam with beam length L = 0.3 m and the base dimensions of the cross-section are H = 0.007 05 m, B = 0.010 m, h = 0.0017 m, b = 0.0010 m. The cross-sectional geometrical properties are given by the moments of inertia, Iyy and Izz and the torsional constant J. For the cross-section in figure 6 with dimensions H, B, h and b the moments of inertia Iyy and Izz and the torsional constant J are expressed by:

$$Iyy = \frac{H * b^3}{12} + 2 * \frac{h * B^3}{12} \tag{1}$$

$$Izz = \frac{b * H^3}{12} + 2 * \frac{B * h^3}{12} + 2 * h * B * \frac{(H + h)^2}{4} \tag{2}$$

$$J = \frac{2 * B * h^3 + H * b^3}{3} \tag{3}$$

The performance of the cantilever I-beam for variation of both the cross-sectional geometrical properties as well

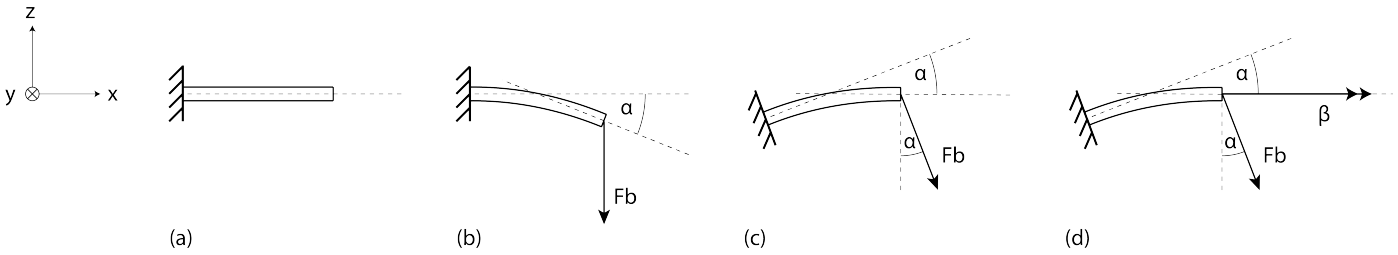

Figure 5: The cantilever beam (a) is loaded by the buckling load, Fb, at its free end (b). The beam is realigned by rotation about the y-axis (c). The rotation is applied about the local longitudinal axis at the free end of the beam which coincides with the global x-axis while the critical buckling load, Fb, is present as preload

as variation of the cross-sectional dimensions is evaluated over an applied rotation of 60° about the longitudinal axis of the final beam element with an applied preload at the free end that is equal to the estimated critical load. Application of a rotation on a beam with preload is done through the 3 step loading scheme explained in 2.3.

The performance of the beam is classified by the lateral deflection, Δy, co-occurring with the applied rotation and the resulting secant rotational stiffness over the range of the applied rotation. The secant rotational stiffness is defined as net the reaction moment about the global horizontal x-axis divided by the final applied angle about the same axis. The final performance metric is the reduction in secant rotational stiffness about the longitudinal axis normal to the cross-section at the free end of a beam that is unstable at its buckling point versus an unbuckled beam to which only a rotation of 60° is applied..

2.5.1. Cross-sectional geometrical properties

The goal of varying geometrical properties Iyy, Izz and J and A is to exploit the numerical beam model by not limiting deformation behaviour to the shape of a physical I-beam. By looking beyond the possible geometrical properties of I-beam sections a broader range of LTB behaviour can be investigated. Even though this means that unrealistic sets of geometrical properties are investigated, since the geometrical properties Iyy, Izz and J are dependent on the cross-sectional dimensions H, B, h and b. However, variation of the dependent cross-sctional geometrical properties allows for insight for what sets of dependent geometrical properties could give the desired behaviour of significantly reduced rotational stiffness and minimal lateral deflection. Future beams section can then be designed towards these potentially ideal sets of geometrical properties. Starting from the geometrical properties of the I-beam mentioned above Iyy, Izz and J are varied as a percentage of their values corresponding to the value of the base I-beam. The range of variation is 25% to 200% with increments 0f 5%.

2.5.2. Cross-sectional dimensions

Since variation of cross-sectional geometrical properties does not yield concrete cross-sectional dimensions for a tip loaded cantilever I-beam with significantly reduced rotational stiffness and minimal lateral deflection, the cross-sectional dimensions are also varied. Dimensions H, B, h and b (figure 6) are varied as a percentage of their values corresponding to the original I-beams mentioned above. The range of variation is 25% to 200% with increments of 5%.

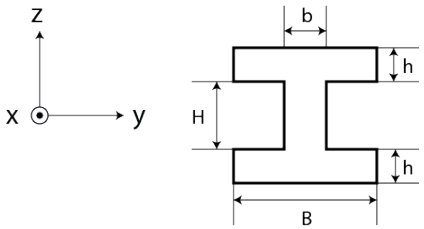

Figure 6: The cross-sectional dimensions of the I-beam are defined by parameters H, B, h and b

2.6. Optimisation case

The final sub objective is to perform an optimisation to obtain a beam with minimal lateral deflection and a significantly reduced longitudinal rotational stiffness due to LTB.

The optimisation case is based on a cantilever I-beam to which a tip load is applied at its free end. The cross-sectional dimensions as well as the beam length are optimised within a bounded region.

The optimisation is created using the same 1 dimensional beam model with the custom FEM solver as described in section 2.1 for its custom options for the applications of forces, moments displacements and rotations.

The optimisation process is performed using the Matlab® functions 'Multistart' and 'fmincon' which are both obtained from the optimisation toolbox. 'Multistart' starts with a set of optimisation variables with user defined values and a user defined number of additional starting sets of input variables for which the values are randomly selected by the function within the bounds. Then, within the bounds, 'Multistart' iteratively looks for the values of the input variables with a minimal value for the objective function through the 'fmincon' function.

2.6.1. Objective function, constraints, free variables

The objective of the optimisation is to find a I-beam that has significantly lower rotational stiffness due to LTB

with minimal lateral deflection. Therefore the objective function is defined as the lateral deflection, Δy. This value should be as low as possible while the beam is in a buckled state. The buckled state should reduces the rotational stiffness of the beam compared to the unbuckled state. To ensure the condition of a buckled state and a significant amount of stiffness reduction between the unloaded beam and the buckled beam, the following constraints are implemented:

(i) The applied load should at least have the magnitude of the critical load and (ii) the resulting longitudinal secant rotational stiffness in the buckled state should be at least 50% lower than the longitudinal secant rotational stiffness of the same beam in the neutral, unloaded and thus non-buckled, state for an applied angle of 60°. If the critical load does not result in at least 50% decrease in rotational stiffness, the applied load is iteratively increased by 10% until the applied force results in at least 50% decrease in longitudinal rotational stiffness about the final beam element. This can result in the optimised I-beam having an absolute applied load that is larger than the absolute critical load and the beam thus being loaded beyond the critical load.

The optimisation loading scheme is similar to the loading scheme explained in section 2.3. The major addition is the constraint that ensures the beam having at least a 50% decrease in longitudinal secant rotational stiffness. The final optimisation loading scheme is as following: first a rotation of 60° is applied about the longitudinal axis of a beam in the unloaded and thus unbuckled state. This gives the value of the longitudinal secant rotational stiffness of a neutral beam. Secondly, the 3 step loading scheme is applied (figure 5): The critical load is estimated, the critical load is applied, the orientation of the beam and applied critical load are realigned to have a horizontal final beam element at the free end of the beam, a rotation of 60° is applied about the longitudinal axis of this final beam element and the reaction moment and resulting secant rotational stiffness are computed. Thirdly, the constraint is implemented and if necessary the load is increased incrementally to ensure a 50 % reduction of secant rotational stiffness in the buckled state with respect to the unloaded, unbuckled state. Finally once the constraint is satisfied the resulting lateral deflection is taken as the value for the objective function that is to be minimised.

The beam optimisation is based around the cross-sectional dimensions and the beam length. The input variables defining the cross-sectional dimensions of the I-beam are H, B, h, and b as displayed in figure 6]. The optimisation uses the input variables as defined by H, B, hH and bB of which hH and bB are the ratios of h/H and b/B respectively. The ratios hH = h/H and bB = b/B serve to maintain a cross-sectional profile of an I-beam. The final input variable is the beam length. The cross-sectional dimensions are set to be constant over the length of the beam.

The input variables are free within a bounded region. The lower and upper bounds are set such that the result with the lowest lateral deflection of each individual parameter variation should at least be obtainable through the optimisation process.

2.7. Experimental validation

An experiment is performed to (i) validate the magnitude of the critical buckling loads, (ii) validate the reduction of rotational stiffness through LTB and (iii) investigate the reduction in lateral deflection through optimisation in the buckled state of the beam. These objectives are investigated for the base beam, the best performing beam of the parameter study and the optimised beam.

For the validation of critical loads each beam is clamped as a cantilever and loaded at the free end by an attached weight that forms a pure tip load (figure 7, left). The applied load is varied by varying the amount of weight. Thereby the beam is loaded to different states of deformation. To determine the magnitude of the critical load, for each applied load a frontal and side image is taken and the images are processed using the 'imageJ' software package. The angle of twist about the longitudinal axis is traced by image processing. It is expected that for loads equal to or larger than the critical load a sudden increase in the angle of twist will occur. The lateral deflection was not selected as a variable to determine the critical load as the optimised beam is optimised to have a minimal lateral deflection. Therefore a much less sudden increase in lateral deflection is expected for loads equal to or larger than the critical load, making this a less suitable metric to determine the critical load based on image processing.

For the validation of reduction of rotational stiffness each beam is loaded by an applied moment in the neutral unbuckled state with no preload and an applied moment in the unstable, buckled state, with a preload equal to the critical buckling load found in the first experiment.

The beam without preload is subjected to a pure moment by placing a moment arm through the centreline of the cross-section of the beam at the free end of the beam. At both ends of the moment arm an equal but opposite load is applied to ensure that a pure moment is applied with a net zero tip load. A weight is hung directly on end of the moment arm. At the other end of the moment arm a string is attached which is connected to a weight and hung around a pulley. The setup for the application of a pure moment is displayed in figure 7 (middle).

For the application of the moment to a beam with preload equal to the critical load, the load case is based on step 2 of the 3-step loading scheme presented in figure 5c: The beam is clamped at an angle, α in figure 5c, and the critical load, Fb in figure 5c, is applied as a preload at an angle such that the free end of the beam has a longitudinal axis parallel to the horizontal global x-axis. The clamping angle and the angle of the preload are set by the bending angle for the vertically applied critical load obtained in the first experiment.

Figure 7: The critical load is validated by attaching weight at the free end of the cantilever (left). A pure moment is applied to the free end of the beam to determine the resulting angle in a state without preload by placing a moment arm to the centre of the cross-section of the beam and applying equal but opposite loads on each end of the moment arm (middle). The preload is applied at the free end of the beam by a horizontal component by a weight hung around a pulley and a by vertical component by a weight attached directly. The moment about the longitudinal axis is applied by placing the weight, representing the vertical component of the preload, on a small moment arm at a slight distance from the centroid of the cross-section

The values of the critical load that are to be applied as preload are also taken from the first part of the experiment to ensure that the moment is applied for a preload that is true to the true critical load rather than a simulation based value. To apply the preload at an angle α, it is decomposed in a horizontal (+x direction) and vertical (-z direction) component. The vertical component is applied as a weight attached directly at the free end of the beam. The horizontal component is applied through a horizontal string attached to the the free end of the beam and routed around a pulley with a weight attached on the other end of the string.

The moment is applied about the horizontal x-axis by placing the weight, representing the vertical component of the preload hung directly at the free end of the beam, at a distance from the exact centre of the beam cross-section on a moment arm. This ensures that the beam is subjected to a vertical preload component, a moment about the horizontal x-axis and a horizontal preload by a second string without additional parasitic force components that are absent in the simulation. The setup for the application of a moment to a clamped beam with preload is displayed in figure 7 (right).

The magnitude of the moment is based on the magnitudes found in the simulation at the end of the applied rotation.

For both the cases of an applied moment with and without preload a rotation as well as a lateral deflection occurs due to the net nonzero applied moment. The values of the rotation and lateral deflection are determined through image processing of a frontal image of the beam without preload and an applied moment and the beam with preload and an applied moment.

The applied moment and corresponding rotation present a value for the secant rotational stiffness for the beam with and without preload. The values for the secant rotational stiffness are compared to to estimate the reduction in secant rotational stiffness that is expected due to the preload causing a state of LTB.

3. Results

The results section is divided by the sub objectives of (i) verification of negative rotational stiffness behaviour (ii) the parameter study and (iii) the optimisation. Section 3.1 provides results on the verification of negative rotational stiffness behaviour due to LTB. Section 3.2 shows the results on the parameter study. Finally section 3.3 displays the results on the optimisation case of a straight cantilever beam with minimal lateral deflection.

3.1. Verification of negative rotational stiffness behaviour due to LTB

Figure 8 displays the reaction moment, RMx, about the longitudinal axis of the final beam element for an applied rotation range of -60 ° to 60°. For preload values lower than the critical load the rotational stiffness of the RMx-β behaviour is always positive. When a rotation is applied while the critical load is present, corresponding to an applied load factor of 1, the initial increments in rotations up to around $-10°$ and 10° show a flat line which corresponds to zero stiffness behaviour. When the beam is loaded beyond the buckling load by a force of 1.2*Fb and 1.4*Fb, the initial angular deviations show negative stiffness behaviour between $-20°$ and 20° and $-15°$ and 15° respectively.

3.2. Parameter study

In addition to these performance measures the buckling load per variable per variation factor is plotted.

Figure 9 a-d displays the lateral deflection, secant rotational stiffness, buckling loads and stiffness reduction per varied parameter for the cross-sectional geometrical properties Iyy, Izz an J. Figure 9 e-h display these performance measures for the cross-sectional dimensions H, B, h and b.

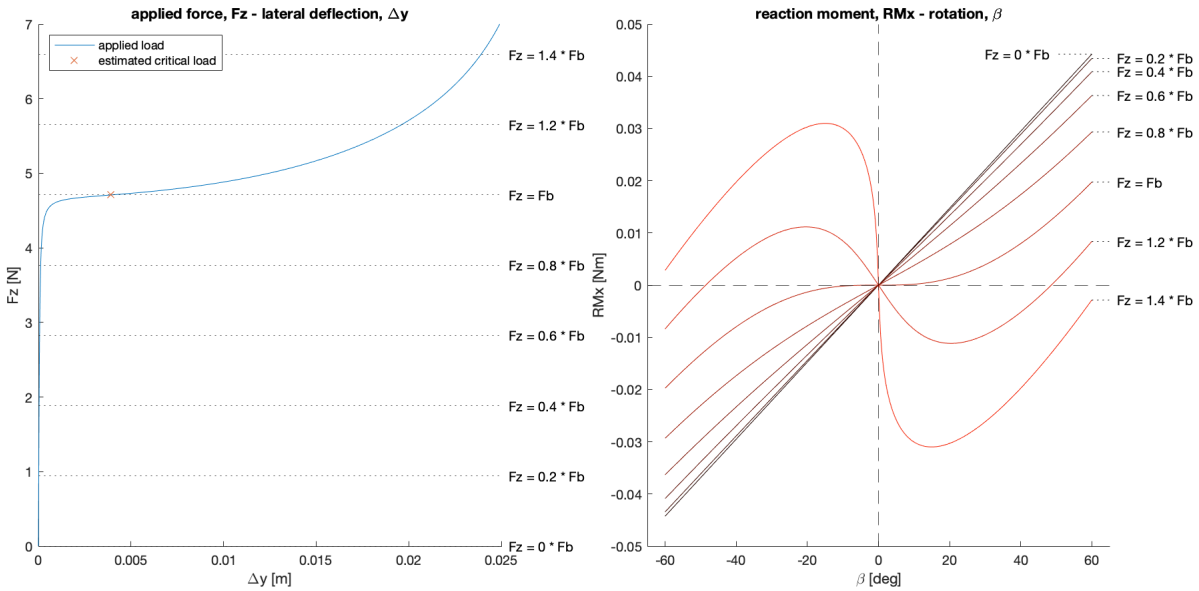

Figure 8: The applied vertical load, Fz and the lateral deflection, Δy show lateral deflection from the buckling point, Fz = Fb and beyond and the preload levels are illustrated with respect to the Fz - Δy behaviour (left). Applying a rotation for different levels of preload results in positive rotational stiffness before the buckling point Fz¡Fb, zero stiffness at the buckling point Fz = Fb and negative rotational stiffness beyond the buckling point Fz¿Fb about the longitudinal axis of the final beam element

3.2.1. Cross-sectional geometrical properties

For increasing Iyy the rotational stiffness as well as the lateral deflection decreases. The lowest lateral deflection for all geometrical properties is obtained for a variation of Iyy of 200%. The highest lateral deflection for all geometrical properties is obtained for a variation of Iyy 25%. The buckling load increases for larger a variation percentage, while the stiffness reduction increases as well. The smallest and largest value of the buckling load for all geometrical properties occur for a variation of 25% and 200% respectively. The lowest stiffness reduction for all geometrical properties occurs at a variation of 25%.

For an increasing value of Izz the secant rotational stiffness remains almost constant with respect to J. For an increase of Izz the lateral deflection increases while the buckling load and the stiffness reduction decrease. For a variation of 25% the FEM model showed no convergence, which results in a shorter line than for the other variables.

The variation of J displays that for an increase of J the secant rotational stiffness increases along with the lateral deflection and the buckling load. The minimum value for the secant rotational stiffness value is the overall minimum value for the variation of the geometrical properties at a variation of 25%. The corresponding co-occurring value for the lateral deflection is not the overall minimum, but is close to the minimal lateral deflection values of the variation of Iyy and Izz at respectively 200% and 50%. The reduction of secant stiffness shows a fluctuating downward trend between 55% and 56%.

3.2.2. Cross-sectional dimensions

Increasing the variation of H shows no tradeoff in performance of secant rotational stiffness and lateral deflection. Increasing secant rotational stiffness co-occurs with increasing lateral deflection for an increased variation. For increasing H the buckling load and stiffness reduction decrease. Compared to the performances for the variation of B and h the magnitudes of the stiffness and deflection are moderate. With respect to B and h the buckling load shows only a slight decrease. The stiffness reduction decreases for increasing H, but remains within the range of 55% and 56%.

Variation of B shows a tradeoff between secant rotational stiffness and lateral deflection in the sense that an increase of B results in increasing rotational stiffness and in decreasing lateral deflection. The minimum lateral deflection of the variation of B at 150% is also the overall minimum across the variation of the cross-sectional dimensions H, B, h and b. The buckling loads increase for increasing variation factors. Beyond 125% the buckling load increases more rapidly than for the variation between 50% and 125%. The stiffness reduction increases for an increasing variation factor. The overall lowest stiffness reduction occurs at a variation of 25% For a variation of 25%, 175% and 200% no convergence was found, which results in a shorter line than for the other variables.

Variation of h shows no tradeoff between secant rotational stiffness and lateral deflection. An increase of h results in an increase of rotational stiffness, an increase of lateral deflection, along with an increase of the buckling load. The stiffness reduction decreases for an increase of h,

but compared to the H, B and b the decrease is moderate. The range of rotational stiffness values contains both the overall minimum at a variation of 25% and overall maximum at 200% for all cross-sectional dimensions.

Variation of b leads to the least change in behaviour with respect to H, B and h and no presence of a tradeoff between secant rotational stiffness and lateral deflection. An increase of h does show an increase of secant rotational stiffness along with an increase of lateral deflection. The buckling load remains practically constant with respect to H, B and h. The stiffness reduction remains almost constant with a fluctuation at a variation of 150%.

3.3. Optimisation case

The optimisation process converged to a solution with cross-sectional dimensions H = 0.006 659 m, B = 0.014 62 m, h = 0.001 731 m, b = 0.001 465 m and beam length L = 0.2971 m. The resulting cross-sectional profile is displayed in figure 10a, the lateral deflection for an applied angle of 60° was 0.001 825 m and the applied load required to satisfy the constraint was equal to the buckling load with an absolute value of 93.92 N.

As displayed in figure 10c, the optimisation objective lateral deflection, Δy = 0.001 825 m, is lower than the lateral deflection of the best result of the parameter study, Δy = 0.002 831 m, and lower than the lateral deflection of the original base beam, Δy = 0.015 74 m. The optimised result has a 36 % and 88% reduction in lateral deflection with respect to the best beam of the parameter study and the base beam respectively.

Figure 10b shows buckling behaviour for the optimised beam by having a sudden large increment in lateral deflection, Δy, per increment in applied tip load, Fz, at the approximated critical load at Fz = 93.92 N.

The reaction moment rotation plot of figure 10d shows a flat line up to an angle around 7° which corresponds to zero stiffness behaviour. The constraint to ensure a reduction of 50% for the secant rotational stiffness was satisfied by application of the buckling load, since the reaction moment at the end of the applied rotation of 60 degrees is still lower than 50% of the reaction moment for the same beam without a preload.

As displayed in figure 10a the optimised cross-sectional dimensions are fairly similar to the best result from the parameter study which was the cross-section with a flange width, B, of 150% of the flange width of the base beam. Both the best result of the parameter study and the optimised result have relatively wide flanges, corresponding to similar values for B. The optimised values for H, b and h are similar to those of the original base beam.

3.4. Experimental validation

The experiment served to validate simulation based results for the magnitude of the critical loads, the reduction in rotational stiffness and the reduction in lateral deflection through optimisation.

The critical loads can be derived from the applied force and resulting angle of twist. Figure 11 shows the applied force, Fz, and the resulting angle of twist captured on image. The raw data is displayed in blue and a smooth spline (red) is fitted using the Matlab® function 'fit' as 'smoothingspline' with smoothing parameters p = [0.5 0.5 0.25] for the base, best parameter and optimised beam case respectively. The graphs show a trend that beyond a certain magnitude of the applied load the angle of twist suddenly increases much more per increment in applied load. This indicates that the critical buckling load was reached. The observed critical loads are around 4.5 N for the base beam, 20 N for the best beam of the parameter study and 18 N for the optimised beam. However, the magnitude of the critical buckling loads of all three beams are less than the simulation based values: for the base beam the experimentally obtained 4.5 N is 4.5% less than the simulation based value of 4.71 N, for the best beam of the parameter study the experimentally obtained 20 N is 55% less than the simulation based value of 44.73 N and the experimentally obtained 18 N for the optimised beam is 81% less than the simulation based value of 93.92 N. Furthermore, the best beam of the parameter study failed when loading beyond the critical buckling load and could therefore not be analysed in the second part of the experiment.

Table 1 displays the critical load, Fb, the applied moment, Mx, the corresponding rotation, θx, and the reduction in secant rotational stiffness for the base beam, the best beam of the parameter study and the optimised beam for both the values obtained in the simulation (sim.) and the experiment (exp.) and for beams in the state without preload and beams in the buckled state with the buckling load present as critical preload.

The moment angle provided vastly different results between simulation and experiment. In the experiment The secant rotational stiffness reduced by 49% for the base beam and 35% for the optimised beam. In the simulation the secant rotational stiffness reduced by 86.0% for the base beam and 84.8% for the optimised beam evaluated at the same angles as were obtained by application of the moment in the experiment.

The applied moment caused a rotation of 27 degree and a lateral deflection of 8 mm for the base beam and a rotation of 25 degree and lateral deflection of 0.8 mm for the optimised beam.

4. Discussion

The optimisation case showed that optimal performance in terms of a minimal lateral deflection can be obtained that was undiscovered through the parameter study. However, it is fair to note that even though a reduction in lateral deflection from 0.0028 m to 0.0018 m, which could be presented as reduction of 36%, may, in reality, be invisible on the scale of an unstable beam with a length of 0.297 m due to modelling inaccuracies and limitations of the 1D FEM model. Nonetheless with respect to the base beam

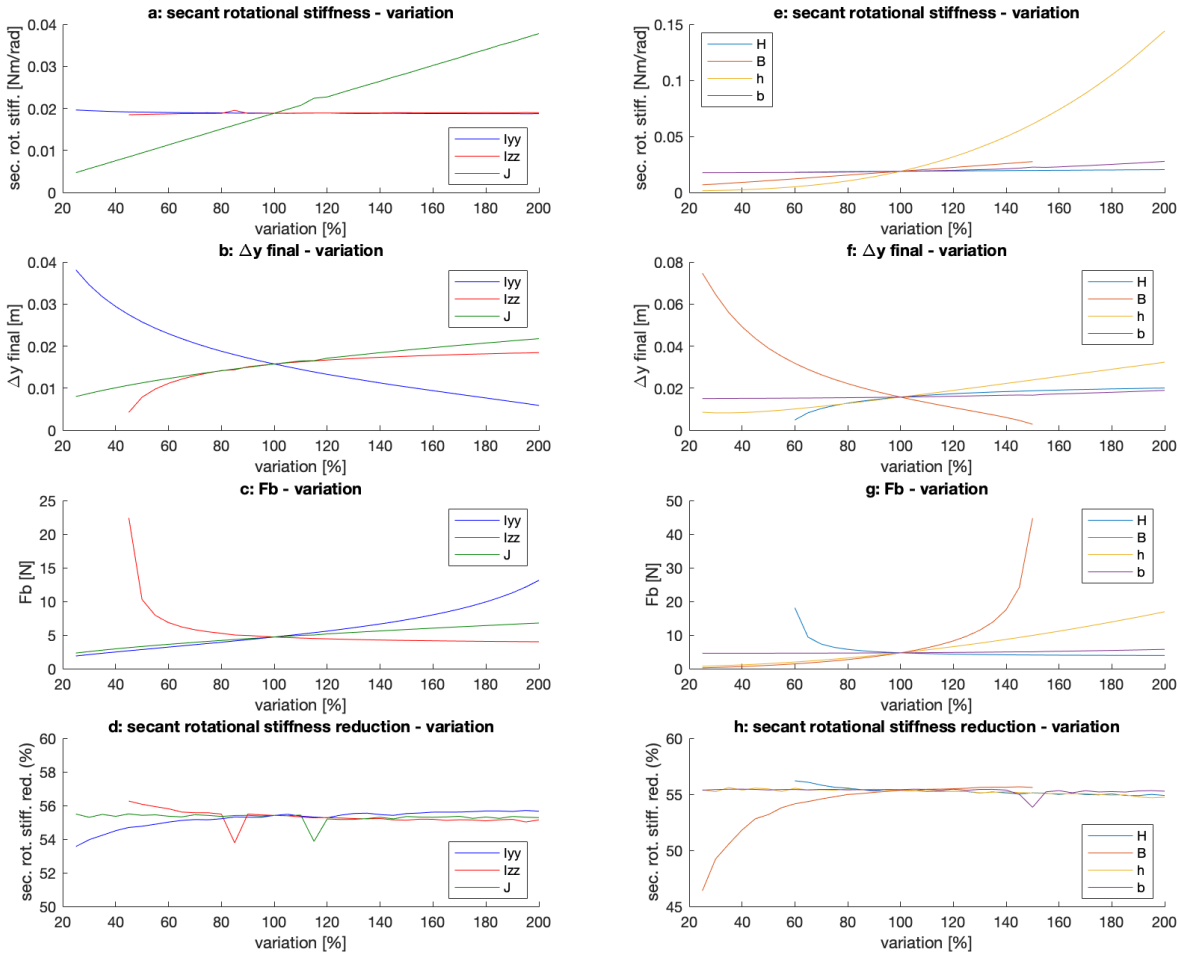

Figure 9: (a) the lateral deflection, Δy, (b) secant rotational stiffness, sec. rot. stiff., (c) critical load, Fb, (d) secant rotational stiffness reduction, sec. rot. stiff. red., for cross-sectional geometrical properties and the variation. (e) the lateral deflection, Δy, f() secant rotational stiffness, sec. rot. stiff., (g) critical load, Fb, (h) secant rotational stiffness reduction, sec. rot. stiff. red. for cross-sectional dimensions and the variation.

with a deflection of $\Delta y = 0.015\,74\,\mathrm{m}$ the optimised beam showed a significant reduction of 88%.

Regarding potential modelling inaccuracies, a remark is to be made with respect to the selected method of applying a rotation about an axis that is always parallel to the global x-axis to obtain the reaction moment, rotation behaviour of the cantilever beam. Before the application of the rotation, the beam, in its preloaded and realigned state (fig. 5c), has a longitudinal axis normal to the cross-section at the free end that is initially parallel to the global x-axis. However, throughout the incremental application of the rotation, the orientation of the longitudinal axis normal to the cross section of the free end changes, since the beam deflects laterally and twists longitudinally due to LTB.

Thereby the resultant moment - rotation behaviour and corresponding stiffness profile is also determined about this fixed orientation axis instead of an axis that is always normal the cross-section at free end of the beam. However, for future work or the design of applications an orientation specific stiffness profile may be more difficult to use than a stiffness profile about a fixed axis.

For the optimisation case it should be noted that the magnitude of the buckling load was not considered as part of the constraints or objective function. The magnitude of the buckling load was free as long as the load was at least equal to the buckling load of the beam at hand such that the beam would become unstable. For applications aimed at exploiting reduced rotational stiffness of beams by LTB this may be different and the magnitude of the buckling load may in fact become a relevant constraint.

On the outlook of the simulation results it should be noted that the applied angle significantly affects the values for the performance metrics of the secant rotational

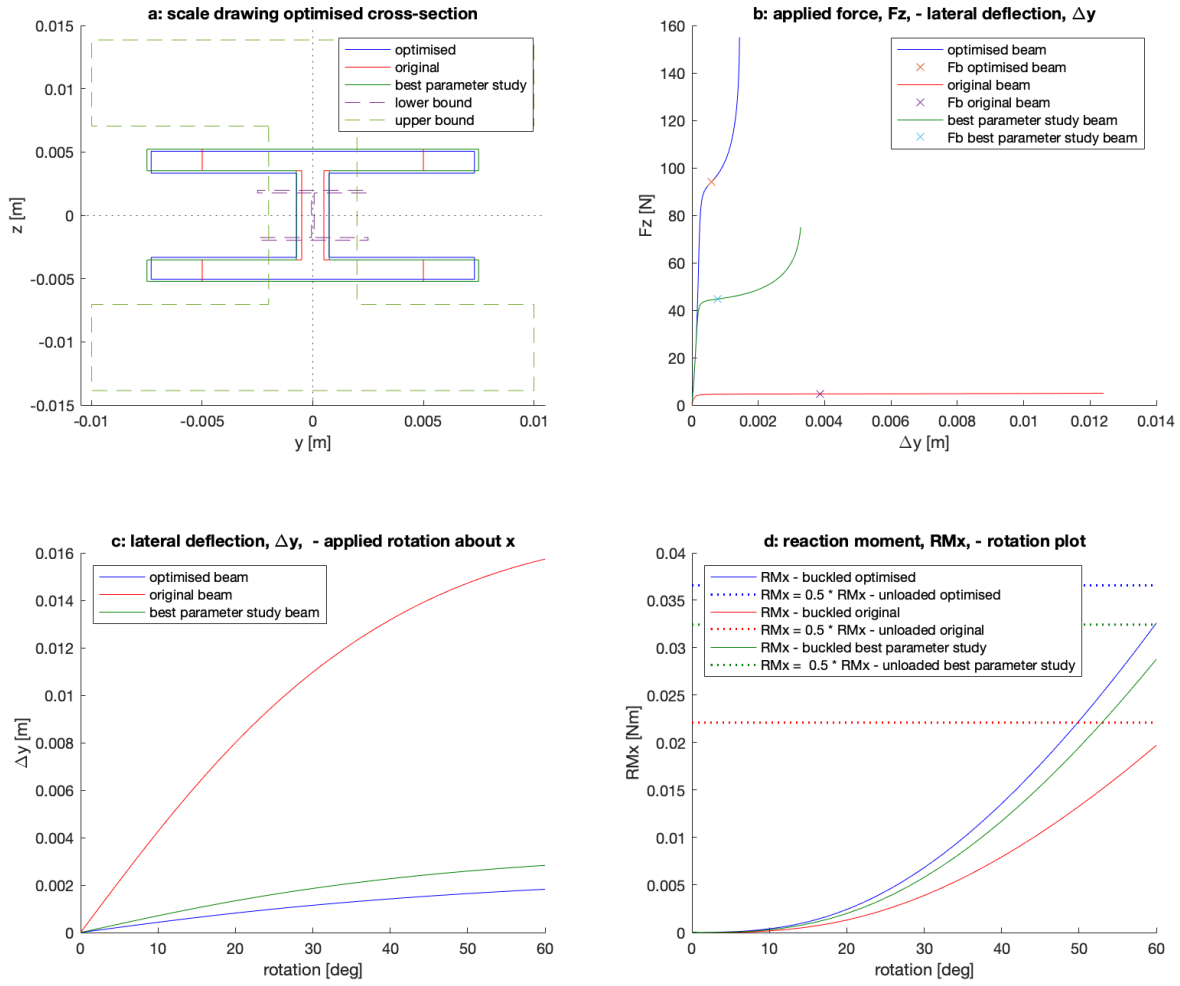

Figure 10: (a) The optimised cross-sectional dimensions are similar to the manually varied dimensions with a flange width B that is 150% of the original flange width. (b) The buckling load of the optimised beam has a larger absolute magnitude than the buckling load of both the original beam as well as the best manually found beam. (c) The lateral deflection at the final value of the applied rotation is smaller than both the result of the original beam as well as the best manual result. (d) The base beam, best manually found beam and the optimised beam fulfill the stiffness reduction constraint for application of the buckling load and show zero stiffness behaviour up to about 8°.

stiffness and the reduction of secant rotational stiffness. Especially for relatively small angles near the region of zero rotational stiffness, the secant rotational stiffness may be much lower and thus the stiffness reduction percentage would become much higher.

The applied angle is also influencing the outlook of the results of the optimisation, since a smaller applied angle would result in a much lower secant rotational stiffness and higher values for the corresponding stiffness reduction. This would allow the constraint of a minimal stiffness reduction of 50% to be satisfied more easily. Alternatively, by using a smaller fixed value for the applied angle, the stiffness reduction constraint can easily be increased to larger values.

Another aspect that influences the outlook of the results for the secant rotational stiffness and the reduction of the secant rotational stiffness is the selected method of applying the approximated critical buckling load as preload before application of the rotation for the parameter variation and the optimisation case. As was shown in this work, whenever LTB is detected application of the buckling load consistently shows an initial moment - rotation behaviour with zero stiffness regardless of the exact beam dimensions.

From section 3.1 it was observed that the if the applied load is increased beyond the magnitude of the absolute critical load the initial increments in rotation show negative stiffness behaviour. This means that the reaction moment for the final value of the same applied angle is lower for a beam loaded by a force larger than the criti-

Table 1: Experimental and simulation results: the critical load, Fb, the applied moment, Mx, the corresponding rotation, θx, and the reduction in secant rotational stiffness are stated for the base beam, the best beam of the parameter study and the optimised beam for both the values obtained in the simulation (sim.) and the experiment (exp.) and for beams in the state without preload and beams in the buckled state with the buckling load present as critical preload. For all cases the critical load, Fb, was present as the net preload

beam type		critical load	no preload	no preload	critical preload	critical preload	critical preload	critical vs no preload
		Fb [N]	Mx [Nm]	θx [deg]	Mx [Nm]	θx [deg]	Δy [m]	stiffness reduction [%]
base	sim.	4.71	0.0229	29	0.0030	27	0.016	86.0
	exp.	4.5	0.038	29	0.018	27	0.008	49
parameter study	sim.	44.73	0.0649	60	0.0288	60	0.0028	55.6
	exp.	20	-	-	-	-	-	-
optimised	sim.	93.92	0.0378	33	0.0043	25	0.0018	84.8
	exp.	18	0.061	33	0.030	25	0.0009	35

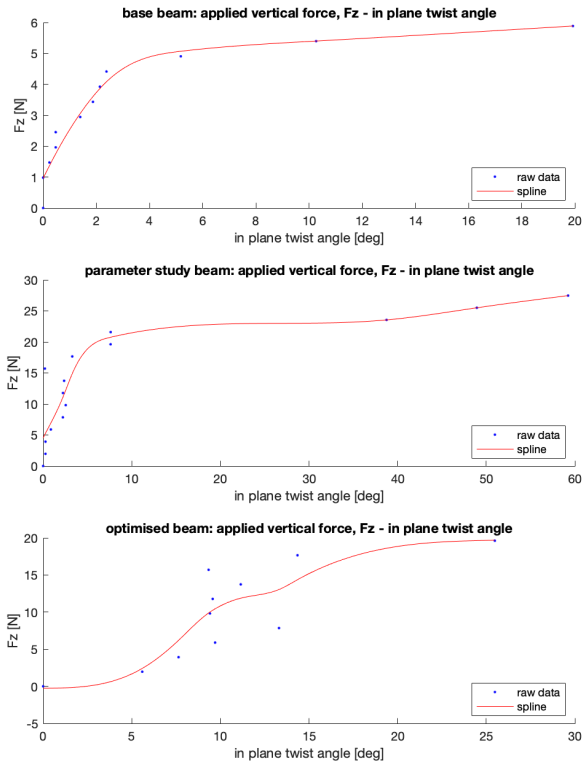

Figure 11: The experimental results for the approximation of the critical load for the base (upper), parameter study (middle) and optimised beam (lower). The blue dots represent raw data points. A smooth spline is fitted and displayed as a red line by the Matlab® function 'fit' as 'smoothingspline' with smoothing parameters p = [0.5, 0.5, 0.25] for the base, parameter study and optimised beam respectively.

cal load than the reaction moment for a beam loaded by the exact critical load. Consequently the secant rotational stiffness would be lower and the stiffness reduction higher. The behaviour of beams becoming unstable due to LTB could even be tuned to have a secant rotational stiffness of zero if the reaction moment for the final value of the applied angle results in a reaction moment of zero.

The experimental validation results showed different values for the critical loads, stiffness reductions and the lateral deflections with respect to the simulation. However the results showed a significant reduction in secant rotational stiffness by 49% for the base beam and 35% for the optimised beam. Thereby the stiffness reduction through a beam subject to LTB is validated.

The differences between the observed critical loads in the experiment and the model are much larger for the best parameter study beam and the optimised beam than the critical load obtained for the base beam. For beams with wide flanges the beam model appears to be less reliable as for wider cross-sections effects of cross-sectional distortion become more prevalent in the overall force deformation behaviour of the beam. Especially for less slender beams with wider flanges simulation with shells or solids may provide more accurate results.

The observed reduction in lateral deflection in the experimental results between the base beam and the optimised beam are to be taken with consideration as they are based on different magnitudes of applied moments applied to different beams. In the simulation all beams are preloaded, subjected to a fixed rotation and then the resulting angle and lateral deflection are obtained. To keep the experiment simple a moment, rather than a rotation, is applied to a beam subjected to preload and the resulting rotation is observed. These moments are not identical for all beams as they are based on the reaction moments obtained in the simulation for a fixed applied angle.

Additionally the application of a moment by hanging weights on strings resulted in a moment that was dependent of the resulting rotation as the rotation caused shortening of the effective moment arm. Since the lateral deflections are now experimentally obtained for different angles of rotation and different moments, the lateral deflection of the base beam and the optimised beam cannot be directly be compared to one another.

However it was observed that the rotation resulting from the applied moment are fairly close, 27° for the base beam and 25° for the optimised beam, whereas the lateral

deflection is 90% less for the optimised beam. Therefore it is considered plausible that the optimised beam results in significantly lower lateral deflection than the base beam if an identical angle were to be applied to both beams.

Furthermore the differences between the simulation and model can also be attributed to manufacturing inaccuracies as well as inaccuracies in the experimental setup. Manufacturing of the prototype beams resulted in a slight beam curvature in the xy-plane. Also the experimental setup presented additional forces to the system because of friction of the string on the pulleys and the orientations of the string not always being exactly parallel to the global x-axis.

5. Conclusion

This work proposes an investigation of the potential of exploiting lateral torsional buckling to reduce the longitudinal rotational stiffness with minimal co-occurring lateral deflection for cantilever I-beams through: (i) a verification of negative rotational stiffness behaviour in the buckled state, (ii) a parameter study of both cross-sectional geometrical properties and cross-sectional dimensions and (iii) an optimisation case for a straight cantilever I-beam with minimal lateral deflection and reduced secant rotational stiffness.

Simulations showed that for an applied load equal to the critical load a region of zero stiffness occurred for the initial range of the applied rotation. For an applied load larger than the critical load a symmetric negative rotational stiffness behaviour occurred.

Overall for the variation of the cross-sectional geometrical properties the variation of J showed the largest change and thus possible range in performance. Variation of Iyy, Izz and J all show no tradeoff between secant rotational stiffness and lateral deflection. Variation of Iyy and Izz showed that while the lateral deflection can be reduced significantly the corresponding secant rotational stiffness reduces only slightly.

For the variation of cross-sectional dimensions variation of the flange width B shows a trade off between low secant rotational stiffness and low lateral deflection. Variation of flange height H, web thickness h and flange thickness b do not show this trade off. Low values of h and H and a large value of B present low values for the lateral deflection. It should be noted that the large value of B also results in a large critical buckling load and relatively large value for the secant rotational stiffness.

The optimisation resulted in a beam with lower lateral deflection than any of the beams in the parameter study. The best beam of the parameter study and the optimised beam have a similar geometry as both have relatively wide flanges. Simulation of the optimised beam showed a reduction of lateral deflection of 36% with respect to the best beam in the parameter study and a reduction of 99% with respect to the base beam.

The experimental validation showed different values for the critical loads and applied moment - rotation behaviour. However the experiment confirmed that the secant rotational stiffness reduces significantly by subjecting the beam to lateral torsional buckling. Also the results show a trend that the optimisation resulted in a beam that has significantly less lateral deflection than the base beam.

Overall this work forms an initial step towards the use of reduced rotational stiffness of beams by exploiting the phenomenon of lateral torsional buckling. It was shown that rotational stiffness can be significantly decreased by applying the buckling load to a cantilever I-beam. Having a strongly reduced rotational stiffness may be beneficial for the application of compliant mechanisms or variable stiffness applications for which a simple method to reduce rotational stiffness on demand is desired.

For future work the results of this study can be expanded by tailoring the performance towards specific applications with variable rotational stiffness. Also to further improve the performance of the beams in terms of achieving lower lateral deflection and larger reductions of rotational stiffness the magnitude of the applied angle should be considered as well as the application of a load larger than the buckling load.

Finally, apart from straight cantilever I-beams, cross-sections other than an I-profile and beam shapes other than purely straight cantilevers may be worth exploring. Cantilever beams with a (local) non straight shape or (local) non bi-symmetric I-beam like cross-section may pose interesting behaviour in terms of lateral deflection. Different beam shapes and cross-sectional profiles may result in even further minimised lateral deflection when implemented in an optimisation procedure similar to the optimisation presented in this work.

References

[1] V. Boonyapinyo, H. Yamada, T. Miyata, Wind-induced nonlinear lateral-torsional buckling of cable-stayed bridges, Journal of Structural Engineering 120 (2) (1994) 486–506.

[2] S. Movaghati, Strengthening beam sections of industrial buildings against lateral torsional buckling, in: Proceedings of the Annual Stability Conference Structural Stability Research Council, Vol. 1, 2019, pp. 1–12.

[3] M. Brettle, Lateral torsional buckling and slenderness (Oct 2006).

[4] S. H. Venter, et al., The effect of the adjacent span on the lateral-torsional buckling capacity of overhang beams, Ph.D. thesis, University of Pretoria (2017).

[5] R. Piotrowski, A. Szychowski, Lateral-torsional buckling of beams elastically restrained against warping at supports, Archives of Civil Engineering 61 (4) (2015) 155–174.

[6] N. Challamel, C. M. Wang, Exact lateral–torsional buckling solutions for cantilevered beams subjected to intermediate and end transverse point loads, Thin-Walled Structures 48 (1) (2010) 71–76.

[7] A. Andrade, D. Camotim, P. B. Dinis, Lateral-torsional buckling of singly symmetric web-tapered thin-walled i-beams: 1d model vs. shell fea, Computers & Structures 85 (17-18) (2007) 1343–1359.

[8] A. Andrade, D. Camotim, P. P. e Costa, On the evaluation of elastic critical moments in doubly and singly symmetric i-section cantilevers, Journal of Constructional Steel Research 63 (7) (2007) 894–908.
[9] W.-b. Yuan, B. Kim, C.-y. Chen, Lateral–torsional buckling of steel web tapered tee-section cantilevers, Journal of Constructional Steel Research 87 (2013) 31–37.
[10] R. A. Bhat, L. M. Gupta, Moment-gradient factor for perforated cellular steel beams under lateral torsional buckling, Arabian Journal for Science and Engineering 45 (10) (2020) 8727–8743.
[11] I. G. Raftoyiannis, T. Adamakos, Critical lateral-torsional buckling moments of steel web-tapered i-beams, The Open Construction and Building Technology Journal 4 (1) (2010).
[12] J. Jankowska-Sandberg, J. Kołodziej, Experimental study of steel truss lateral–torsional buckling, Engineering Structures 46 (2013) 165–172.
[13] A. L. Demirhan, H. E. Eroğlu, E. O. Mutlu, T. Yılmaz, Ö. Anil, Experimental and numerical evaluation of inelastic lateral-torsional buckling of i-section cantilevers, Journal of Constructional Steel Research 168 (2020) 105991.
[14] A. Steel, Ncci: Elastic critical moment for lateral torsional buckling, Access Steel (2005).
[15] B. A. Fulcher, D. W. Shahan, M. R. Haberman, C. Conner Seepersad, P. S. Wilson, Analytical and experimental investigation of buckled beams as negative stiffness elements for passive vibration and shock isolation systems, Journal of Vibration and Acoustics 136 (3) (2014).
[16] L. L. Howell, Introduction to Compliant Mechanisms, John Wiley Sons, Ltd, 2013, Ch. 1, pp. 1–13. arXiv:https://onlinelibrary.wiley.com/doi/pdf/10.1002/9781118516485.ch1, doi:https://doi.org/10.1002/9781118516485.ch1.
URL https://onlinelibrary.wiley.com/doi/abs/10.1002/9781118516485.ch1
[17] M. Schenk, S. D. Guest, On zero stiffness, Proceedings of the Institution of Mechanical Engineers, Part C: Journal of Mechanical Engineering Science 228 (10) (2014) 1701–1714.
[18] S. Barbarino, O. Bilgen, R. M. Ajaj, M. I. Friswell, D. J. Inman, A review of morphing aircraft, Journal of intelligent material systems and structures 22 (9) (2011) 823–877.
[19] L. Blanc, A. Delchambre, P. Lambert, Flexible medical devices: review of controllable stiffness solutions, in: Actuators, Vol. 6, Multidisciplinary Digital Publishing Institute, 2017, p. 23.
[20] M. Manti, V. Cacucciolo, M. Cianchetti, Stiffening in soft robotics: A review of the state of the art, IEEE Robotics & Automation Magazine 23 (3) (2016) 93–106.
[21] J.-M. Battini, Co-rotational beam elements in instability problems, Ph.D. thesis, KTH (2002).
[22] Pa 12 (mjf).
URL https://www.materialise.com/en/manufacturing/materials/pa-12-mjf

3

Supplementary Material: Critical buckling load estimation

This chapter provides additional insight of the numerical buckling load estimation method used throughout this work.

3.1. Development of the universal numerical buckling load estimation

Various literature covers the topic of critical load estimation for open-section beams subject to LTB. However, the geometrically non-linear nature of LTB results in literature that is mostly case specific in terms of applied loads, beam support conditions and beam shapes ([11], [6], [2], [1], [7], [16], [3], [12], [13]). Therefore, in this work a self-developed, more universal, numerical approach is taken to estimate the critical buckling load using the 1D FEM beam model.

Since this thesis project is aimed at exploring LTB behaviour for tip loaded cantilever beams, a first step towards universal approximation of the critical tip load was to simulate LTB. Simulation of LTB was done by applying a vertical tip load at the free end of the beam. Since the model does not have any geometrical or loading imperfections a purely tip loaded beam would show unrealistic infinite bending rather than LTB behaviour when loaded beyond the critical load. Therefore an imperfection is applied by a perturbation force in the lateral direction, Fy, applied at the free end of the beam with a magnitude of 1/1000 of the vertically applied tip load Fz. This is illustrated in figure 3.1. Plotting the Fz and displacements in y direction showed a clear increase of Δy beyond a value of Fz around 4.5 N displayed in figure 3.2.

3.1.1. Minimal slope

Taking a closer at the graph of 3.2 it can be observed that the slope of the Fz - Δy graph decreases from an applied load of Fz = 0 N until an applied load slightly beyond the notch in the graph at roughly 4.5 N. Beyond approximately 4.5 N the increase of lateral deflection per increment of applied load, Fz, becomes much larger than before. From a mathematical point of view this infers that a minimal slope $dF/d\Delta y$ coincides with the critical load. The $dF/d\Delta y$ behaviour was numerically evaluated by taking the gradient of Fz and corresponding Δy using the Matlab® gradient function.

A drawback of solely considering the location of the minimal slope is that Fz - Δy behaviour which does not show buckling in the sense that there is no value for Fz beyond which the lateral deflection per increment Fz becomes significantly bigger, may falsely get a buckling critical load appointed. An example is that the for any part of the Fz-Δy graph there is a minimum slope, then purely taking the load with a minimum value of the slope often results in a value at the boundaries of the range of the applied force.

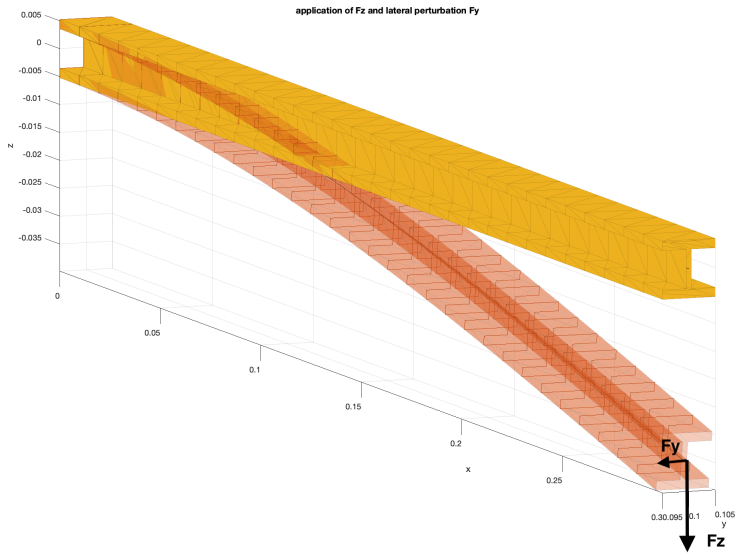

Figure 3.1: A vertical tip load, Fz, is applied at the free end while a lateral perturbation load, Fy, with a magnitude of 1/1000 of Fz provides a slight imperfection to the model to enable simulation of buckling. Fy is not drawn to scale for illustration clarity

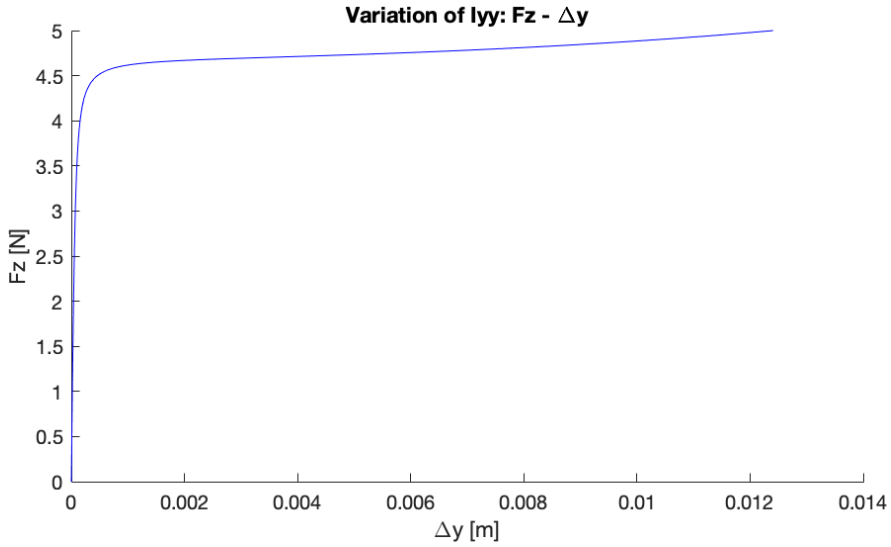

Figure 3.2: Application of the vertical tip load, Fz, and the resulting lateral deflection, Δy, show a significant increase in lateral deflection per increment in applied load, Fz. This is characteristic for buckling behaviour

3.1.2. Requirement: inflexion point

To prevent this false allocation of the critical load an additional estimation feature is implemented to make sure that the minimal slope is actually a local minimum of the Fz - Δy behaviour. The Fz - Δy graph of figure 3.2 shows that when going beyond the sudden decrease in slope with loads larger than 4.5 N, the slope starts to increase again. Thus for buckling behaviour the critical load appears to be very near to the minimum slope which coincides with an inflexion point of the graph. Thus for the approximation of the critical load the requirement is implemented that for the critical load value of Fz, the slope dF/dΔy is minimal and that the second derivative ddFz/ddΔy is passing through 0.

3.1.3. Numerical evaluation of the second derivative

Since the beam model is based on a discrete set of solutions points, the evaluations of first and second derivatives dF/dΔy and ddF/ddΔy are also evaluated numerically based on the gradients of Fz - Δy. The analytical expression for the second derivative of ddFz/ddΔy = 0 for the minimum of dFz/dΔy is

approximated by detection of the point for which the ddFz/ddΔy changes from a negative to a positive value. This is based on the observation that the slope of the graph decreases from 0 to the minimum and then increases again. Trying some example cases for various beam dimensions showed that this added constraint consistently picks a point in the Fz - Δy graph for which the sudden big increase of Δy per increment of Fz had just passed.

3.1.4. Requirement: limiting the magnitude of decrease in slope

However when varying beam parameters as cross-sectional dimensions some exceptions occurred for which the located minimum slope dFz/dΔy would coincide with ddFz/Δy = 0, but without corresponding to a point in the graph of Fz - Δy that showed the characteristic behaviour for LTB of a sudden big increase of Δy per increment of Fz. Therefore a third and final constraint is added in the form of the following constraint: if the slope dFz/dΔy is minimal and ddFz/ddΔy passes through 0 the slope dFz/dΔy should also be at most 10% of the initial slope for the initial increments in applied load from 0 N. This is based on the observation that graphs showing buckling behaviour have a very steep upward line up to approximately the critical buckling load, then greatly flatten and then slowly become steeper again. The inclusion of this third constraint resulted in consistent numerical approximation of the buckling load.

3.1.5. Automatic range extension of the applied load

A final feature is needed to have automatic approximation of the buckling load. Up to now the requirements of having a minimal slope with a coinciding inflexion point have been evaluated for a given load range of 0 N to 5 N in the example graphs displayed earlier in this section. However if no buckling is detected within this range, it does not mean that the beam cannot buckle. Therefore the range is automatically extended if no buckling behaviour is detected. The range extension is set as twice the previous range. The new force setting the end of the applied force range, Fend, is defined by:

$$F_{end,i+1} = F_{end,0} + 2 * F_{end,i}$$

During testing it appeared that some I-beams will not show any buckling behaviour in the used 1D beam model regardless of the applied load and the applied perturbation. AN example is an I-beam with extremely wide flanges. Therefore an upper limit to the number of range extensions can be set.

For an initial guess of F_{end} = 0 N to F_{end} = 5 N this means that the magnitude of the range evaluated evolves as: 5, 15 (= 5+2*5), 35 (= 5+2*15), 75 (= 5 + 35*2), 155 (= 5 + 2*75), 315 (= 5 + 2*155), 635 = (5 + 2 * 315). For the case of beams with the order of magnitude of dimensions in this work made of the material PA12, polyamide 12, the range is set to be increased 6 times as manual iteration to larger limits never showed buckling behaviour for beams in higher orders of magnitude.

3.2. Overview buckling load estimation process

To summarise, the buckling load approximation is performed through the following steps:

1. An initial guess is made for the vertical tip load Fz for which the range from 0 to Fz in which buckling is suspect to occur.
2. The vertically applied tip load, Fz, is incrementally applied while having perturbation load Fy of 1/1000 * Fz
3. The resulting graph is checked if the minimal dFz/dΔy co-occurs with the approximated inflexion point for which ddFz/ddΔy switches from negative to positive as a numerical alternative to locating the exact point for which ddFz/ddΔy = 0 and if the dFz/dΔy of the allocated point has a dFz/dΔy which is only 10% of the initial dFz/dΔy for the initial increment in applied load from 0.
4. If yes, the approximated Fz for which the constraint of point 3 is true is appointed as the approximated buckling load
5. If no, the applied range of force is increased and steps 2, 3 and 4 are repeated until the constraint of point 4 is satisfied.

The resulting algorithm proved to consistently find buckling behaviour from the Fz - Δy graphs for beams with many different dimensions throughout the entire parameter study. Also multiple optimisation

runs resulted in each solution having a buckling point allocated in the Fz -Δy graph that were very similar to the Fz - Δy graph shown in figure 3.2. Iteratively testing this for beams with different lengths and shape showed similar Fz - Δy behaviour with a sudden large increment in Δy per increment in applied load Fz. An example of the different Fz - Δy behaviour is shown for beams with varying web heights in figure 3.3.

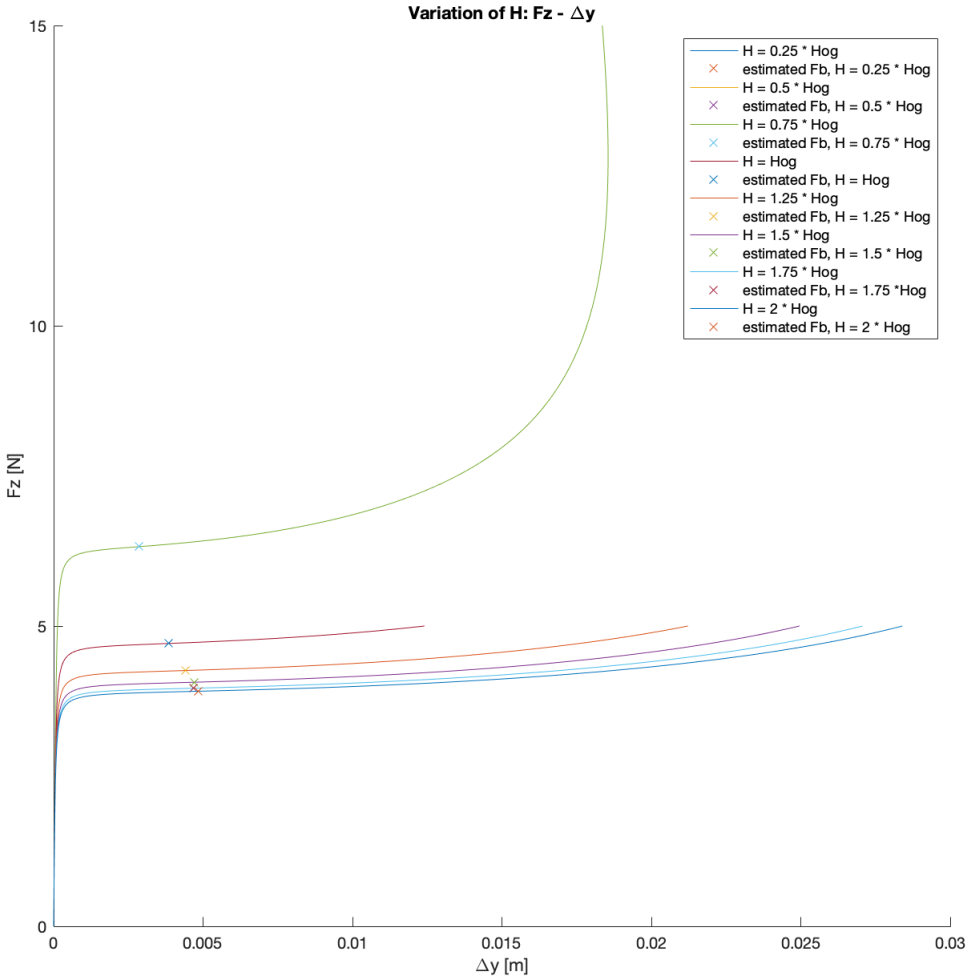

Figure 3.3: Application of the vertical tip load, Fz, and the resulting lateral deflection, Δy, show characteristic buckling behaviour and estimated critical loads near the notch in the graph indicating the buckling point for an I-beam with different web heights, H, varied as a factor of the original web height, H og.

4

Supplementary Material: 3-step loading scheme

This chapter provides additional detail on the 3-step loading scheme that is used for all 3 objectives of this work: the verification of negative rotational stiffness behaviour due to LTB, the parameter study and the optimisation case. The 3-step loading scheme serves to investigate the moment - rotation and longitudinal rotational stiffness behaviour at the end point of the beam in a buckled state. Before the 3-step loading scheme is applied, the buckling load is estimated.

1. Since the critical buckling load has been estimated, the first step is to apply the estimated critical load as a vertical tip load at the free end of the cantilever beam (fig. 4.1-a). Consequently the beam bends down in the xz plane (fig. 4.1-b, fig. 4.2-left).

2. As the second step the beam and applied estimated critical load are realigned by rotating the orientation of the beam and the applied load about the y axis by angle α such that the longitudinal axis normal to the cross-section at the free end of the beam, is oriented parallel to the global x-axis (fig. 4.1-c, fig. 4.2-middle). Even though the tip load is equal to the estimated critical load, no LTB behaviour will be observed yet as the model contains no imperfections yet. Therefore the beam will show pure bending in the xz plane. The realignment of the free end of the beam is required for the application of a pure rotation about the longitudinal axis of the free end of the beam which forms the third step of the loading scheme.

3. As the third step a rotation β is incrementally applied about the longitudinal axis, normal to the final cross-section of the free end of the beam, which is now parallel to the global x axis while the estimated critical load is present as preload for the entire range of the applied rotation (fig. 4.1-d, fig. 4.2-right). Throughout the rotation the reaction moment as well as the co-occurring displacements and rotations are traced to determine the longitudinal rotational stiffness as well as the co-occurring lateral deflection. The rotation forms the imperfection that will change the state of the beam from bending to a state of lateral torsional buckling.

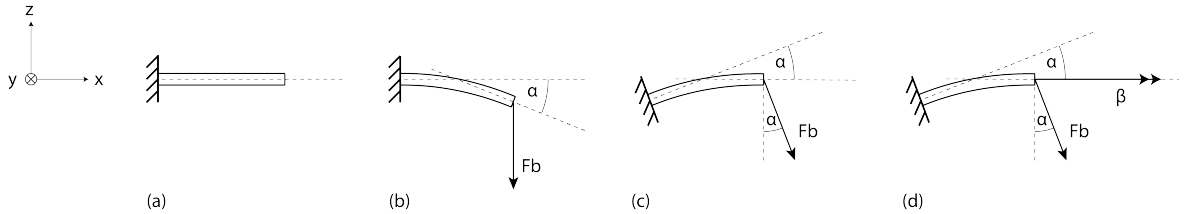

Figure 4.1: The cantilever beam (a) is loaded by the buckling load, Fb, at its free end (b). The beam is realigned by rotation about the y-axis (c). The rotation is applied about the local longitudinal axis at the free end of the beam which coincides with the global x-axis while the critical buckling load, Fb, is present as preload

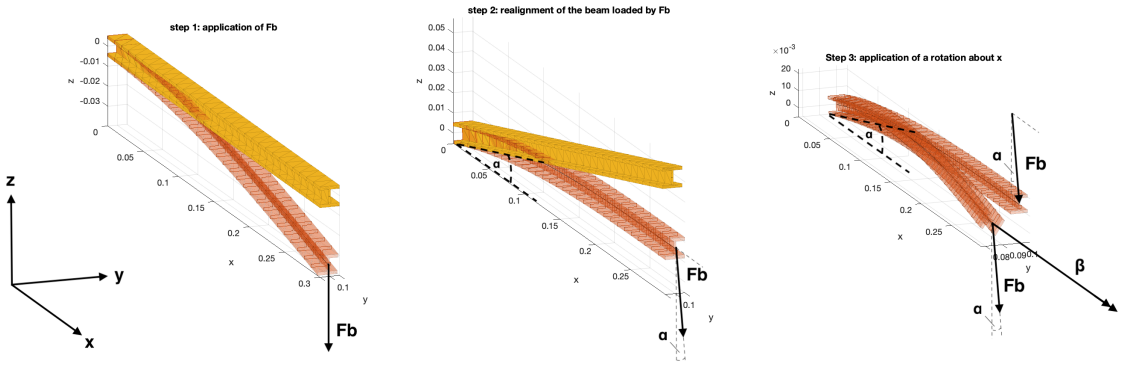

Figure 4.2: The cantilever beam is loaded by the buckling load, Fb, at its free end (left). The beam is realigned by rotation about the y-axis and the critical buckling load is applied (middle). The rotation is applied about the local longitudinal axis at the free end of the beam which coincides with the global x-axis while the critical buckling load, Fb, is present as preload (right)

5

Supplementary Material: Additional results parameter study

This chapter provides additional insight in the results of the parameter study. These results serve to display that the simulations consistently showed buckling behaviour of a sudden large increment in lateral deflection per increment applied force and that the critical buckling load was consistently estimated near this characteristic change in behaviour. Also the corresponding reaction moment rotation plots, investigated at a preload equal to the estimated buckling load, consistently showed an initially flat line indicating a range of zero stiffness.

5.1. Variation of cross-sectional geometrical properties

The I-beams considered in this work are defined by the cross-sectional dimensions: web height, H, flange width, B, flange thickness, h, and web thickness, b as illustrated in figure 5.1.

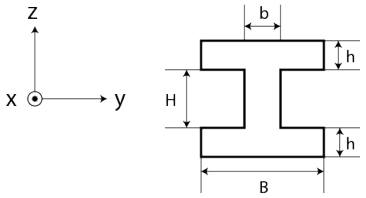

Figure 5.1: The cross-sectional dimensions of the I-beam are defined by parameters H, B, h and b

The corresponding cross-sectional geometrical properties are defined by the moment of inertia about the y-axis, Iyy, the moment of inertia about the z-axis, Izz, and the torsional constant, J. Iyy, Izz and J are defined by:

$$Iyy = \frac{H * b^3}{12} + 2 * \frac{h * B^3}{12} \tag{5.1}$$

$$Izz = \frac{b * H^3}{12} + 2 * \frac{B * h^3}{12} + 2 * h * B * \frac{(H + h)^2}{4} \tag{5.2}$$

$$J = \frac{2 * B * h^3 + H * b^3}{3} \tag{5.3}$$

For variation of Iyy, Izz, and J, the vertically applied tip force - lateral deflection, Fz - Δy, behaviour and reaction moment - applied rotation, RMx - β for an applied preload equal to the estimated critical buckling load, Fb, is displayed in figure 5.2, figure 5.3 and figure 5.4 respectively. For each variation percentage the Fz - Δy behaviour shows characteristic buckling behaviour for lateral torsional buckling: a sudden large increment in lateral deflection, Δy, per increment of the vertically applied tip load, Fz. When the estimated buckling load, Fb, is present as preload, the RMx - β behaviour consistently shows

a flat line for the initial increments in applied angle, β corresponding to a range of zero rotational stiffness.

The lines in the Fz - Δy graphs of figure 5.2, 5.3 and 5.4 show a different range of applied force, Fz, and thus a different evaluated range of Fz - Δy. This indicates that the buckling load estimation process required different values for the range of the applied force, Fz, for different variation percentages to detect buckling behaviour and estimate the critical buckling load, Fb.

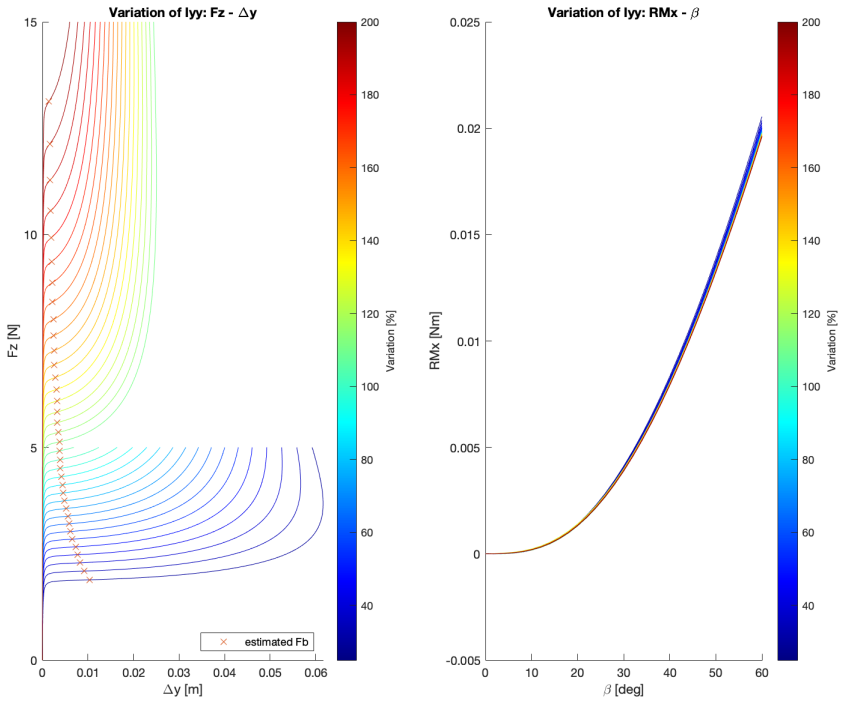

Figure 5.2: The Fz - Δy behaviour obtained in the estimation process of the critical buckling load is shown per variation percentage of the geometrical property Iyy (left). The estimated critical buckling load, Fb, is indicated by an orange cross for each variation. The reaction moment, RMx, is plotted for the applied angle, β, per variation percentage of the geometrical property Iyy (right).

5.2. Variation of cross-sectional dimensions

For variation of the cross-sectional dimensions H, B, h, b as illustrated in figure 5.1, the vertically applied tip force - lateral deflection, Fz - Δy, behaviour and reaction moment - applied rotation, RMx - β, for an applied preload equal to the estimated critical buckling load, Fb, is displayed in figure 5.5, figure 5.6, figure 5.7 and figure 5.6 respectively. For each variation percentage the Fz - Δy behaviour shows characteristic buckling behaviour for lateral torsional buckling: a sudden large increment in lateral deflection, Δy, per increment of the vertically applied tip load, Fz. When the estimated buckling load, Fb, is present as preload, the RMx - β behaviour consistently shows a flat line for the initial increments in applied angle, β corresponding to a range of zero rotational stiffness.

The lines in the Fz - Δy graphs of figure 5.5, 5.6, 5.7 and 5.8 show a different range of applied force, Fz, and thus a different evaluated range of Fz - Δy. This indicates that the buckling load estimation process required different values for the range of the applied force, Fz, for different variation percentages to detect buckling behaviour and estimate the critical buckling load, Fb.

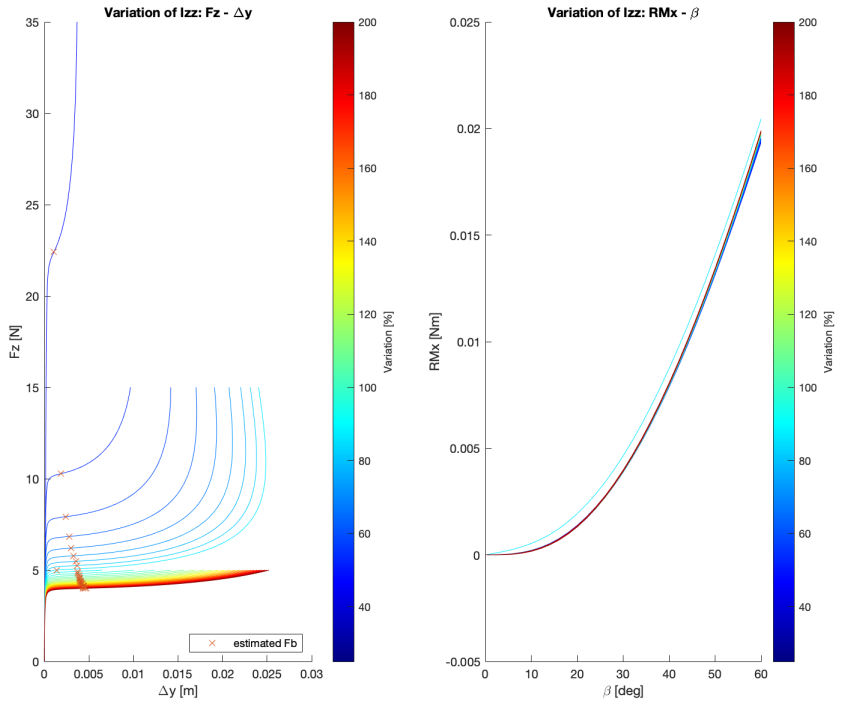

Figure 5.3: The Fz - Δy behaviour obtained in the estimation process of the critical buckling load is shown per variation percentage of the geometrical property Izz (left). The estimated critical buckling load, Fb, is indicated by an orange cross for each variation. The reaction moment, RMx, is plotted for the applied angle, β, per variation percentage of the geometrical property Izz (right).

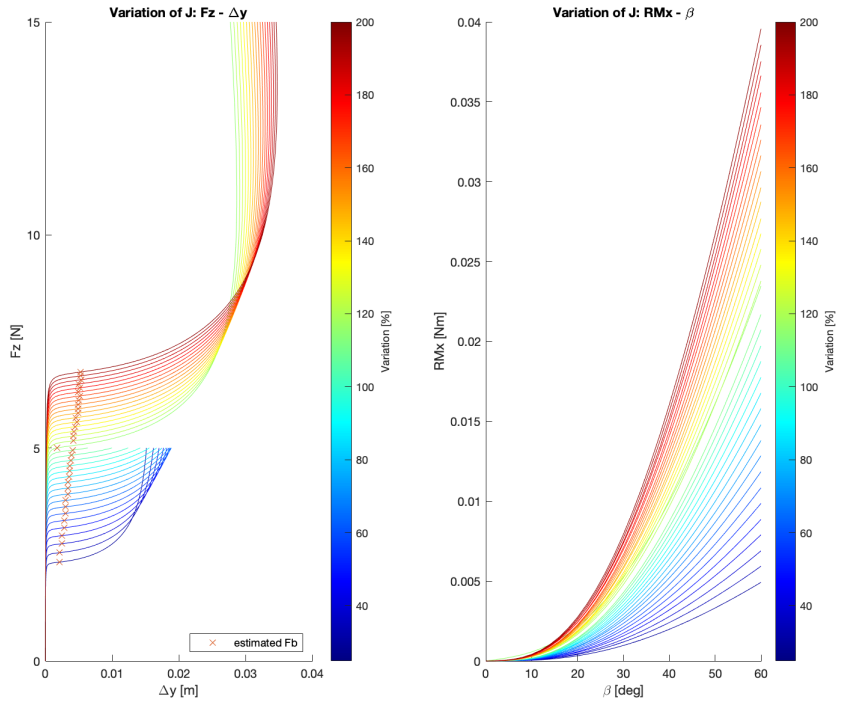

Figure 5.4: The Fz - Δy behaviour obtained in the estimation process of the critical buckling load is shown per variation percentage of the geometrical property J (left). The estimated critical buckling load, Fb, is indicated by an orange cross for each variation. The reaction moment, RMx, is plotted for the applied angle, β, per variation percentage of the geometrical property J (right).

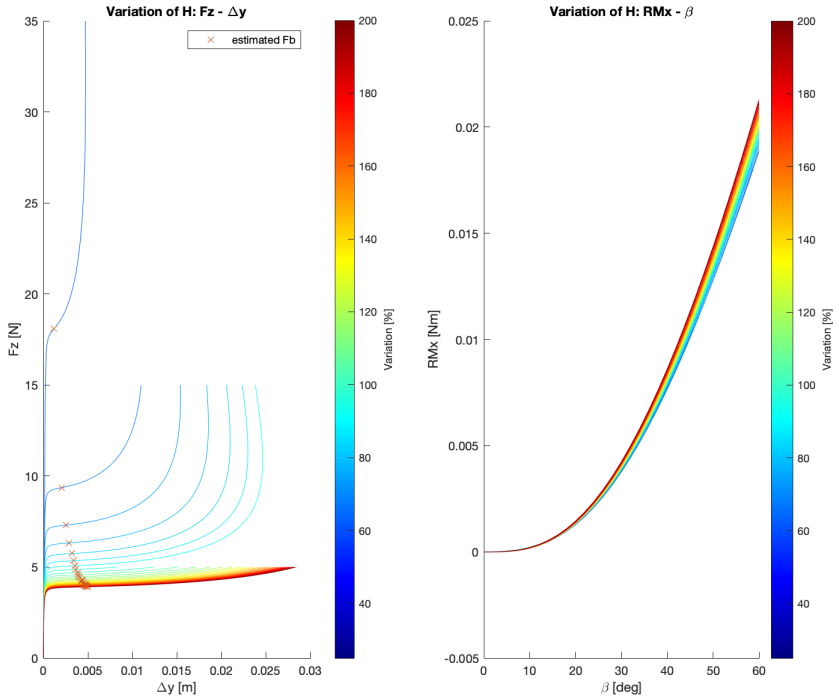

Figure 5.5: The Fz - Δy behaviour obtained in the estimation process of the critical buckling load is shown per variation percentage of the web height, H (left). The estimated critical buckling load, Fb, is indicated by an orange cross for each variation. The reaction moment, RMx, is plotted for the applied angle, β, per variation percentage of the web height, H (right).

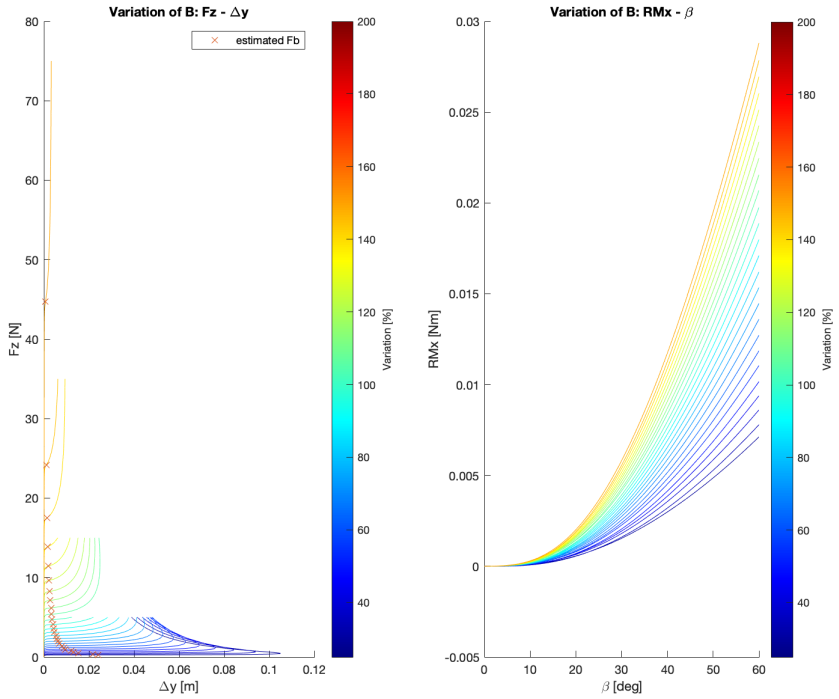

Figure 5.6: The Fz - Δy behaviour obtained in the estimation process of the critical buckling load is shown per variation percentage of the flange width, B (left). The estimated critical buckling load, Fb, is indicated by an orange cross for each variation. The reaction moment, RMx, is plotted for the applied angle, β, per variation percentage of the flange width, B (right).

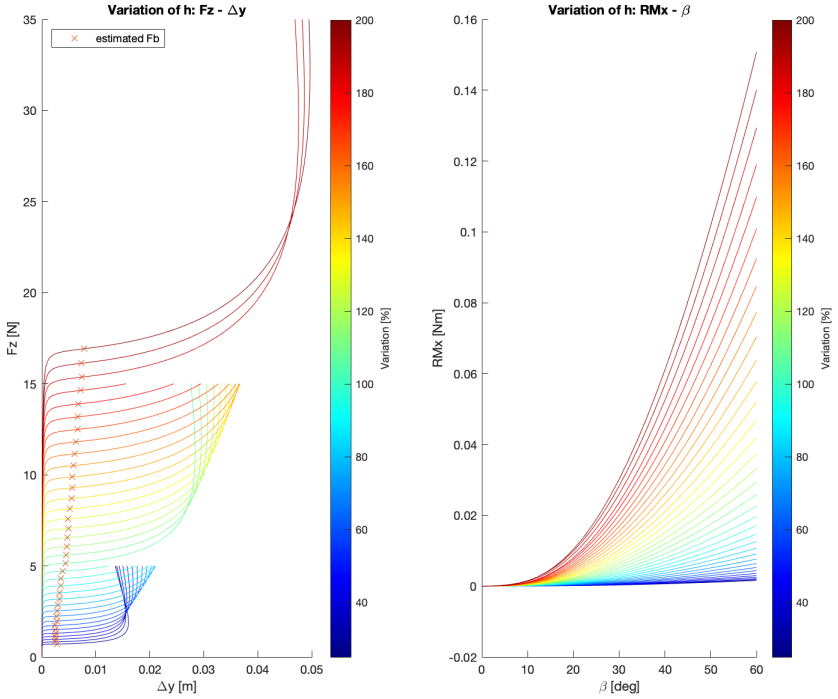

Figure 5.7: The Fz - Δy behaviour obtained in the estimation process of the critical buckling load is shown per variation percentage of the flange thickness, h (left). The estimated critical buckling load, Fb, is indicated by an orange cross for each variation. The reaction moment, RMx, is plotted for the applied angle, β, per variation percentage of the flange thickness, h (right).

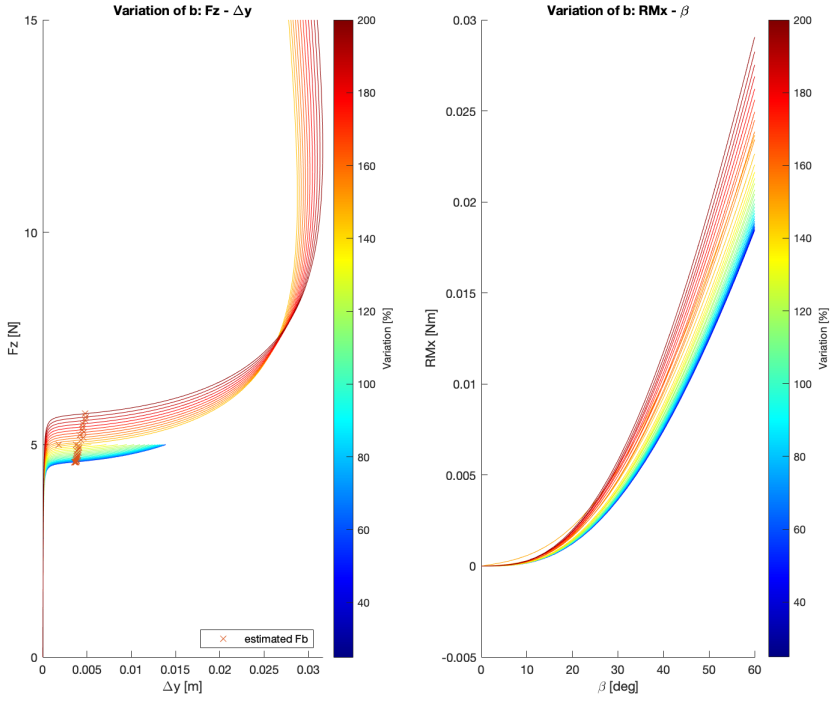

Figure 5.8: The Fz - Δy behaviour obtained in the estimation process of the critical buckling load is shown per variation percentage of the web thickness, b (left). The estimated critical buckling load, Fb, is indicated by an orange cross for each variation. The reaction moment, RMx, is plotted for the applied angle, β, per variation percentage of the web thickness, h (right).

6

Supplementary Material: Optimisation Scheme

This chapter provides a detailed explanation of the optimisation scheme used to obtain a beam with minimal lateral deflection and a significantly reduced rotational stiffness.

6.1. Optimisation objective

The aim of the optimisation is to find an I-beam that has minimal lateral deflection and a significantly lower longitudinal rotational stiffness when subjected to lateral torsional buckling with respect to an unbuckled beam in pure torsion. Therefore the objective function that is to be minimised is defined as the lateral deflection, Δy. This value should be as low as possible while the beam is in a buckled state. Meanwhile a preload equal to at least the critical buckling load, causing the beam to be in the buckled state, should significantly reduce the rotational stiffness of the beam in the buckled state compared to the unbuckled state.

6.2. Optimisation constraints

To ensure the condition of a buckled state and a significant reduction of longitudinal rotational stiffness between the unloaded beam and the preloaded, buckled, beam, the following constraints are implemented:

1. The applied preload should have at least the magnitude of the buckling load.

2. The resulting longitudinal secant rotational stiffness of the beam in the buckled state should be at least 50% lower than the longitudinal secant rotational stiffness of the same beam in the neutral, unloaded and thus non-buckled, state in pure torsion for a fixed applied angle of 60.

The longitudinal secant rotational stiffness, k, is defined by the magnitude of the net difference of the reaction moment for the applied rotation, ΔM, divided by the magnitude of the net difference of the applied rotation, $\Delta\beta$, $k = \Delta M/\Delta\beta$.

If the buckling load does not result in at least a 50% decrease in longitudinal rotational stiffness, the applied load is iteratively increased by 10% until the applied force results in at least 50% decrease in longitudinal rotational stiffness about the final beam element. This can result in the optimised I-beam having an absolute applied load that is larger than the critical buckling load. This means the optimised I-beam may be loaded beyond the critical buckling load.

The constraint is illustrated by figure 6.1 showing the reaction moment - rotation, RMx - β graph for a buckled and unbuckled beam. The secant rotational stiffness is shown for the buckled and unbuckled configuration indicated respectively by k sec rot, buckled and k sec rot unbuckled. The constraint ensures that the buckled rotational stiffness should be at most 50% of the unbuckled secant rotational stiffness to ensure a minimal stiffness reduction of 50%.

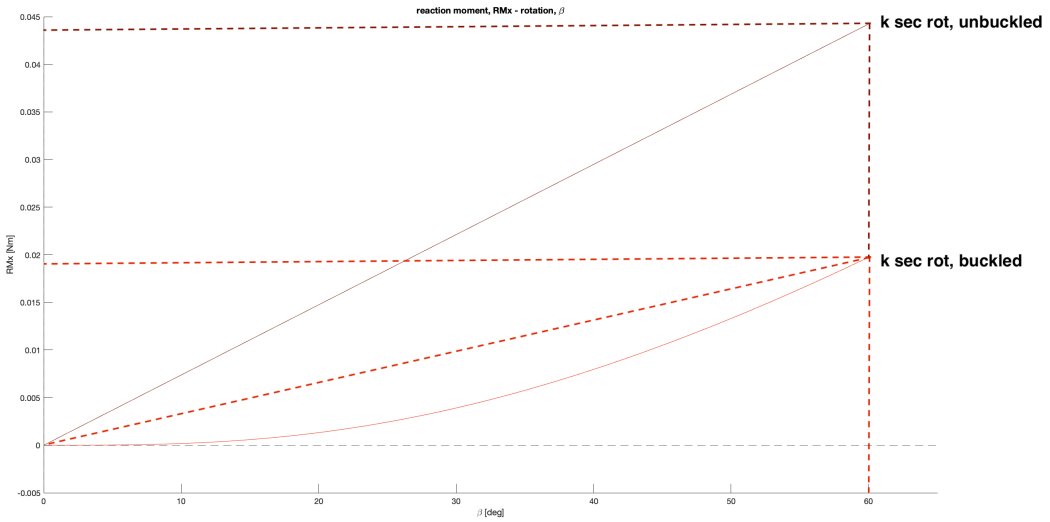

Figure 6.1: The determination of the longitudinal secant rotational stiffness is illustrated for the buckled beam, indicated by 'k sec rot buckled', and the unbuckled beam, indicated by 'k sec rot unbuckled'.

6.3. Equivalent formulations of the stiffness reduction constraint

It should be noted that the constraint stating that the resulting longitudinal secant rotational stiffness in the buckled state should be at least 50% lower than the longitudinal secant rotational stiffness of the same beam in the neutral, unloaded and thus non-buckled, state in pure torsion for a fixed applied angle, set as 60, is in fact equivalent to having a constraint that ensures that the reaction moment at the applied angle of 60should be at most 50% of the reaction moment of a neutral unloaded to which a rotation of 60is applied.

However the final applied angle is always equal to 60and the initial value is always 0. Therefore the constraint of obtaining at least a reduction of 50% of secant rotational stiffness could be reframed as having a reaction moment at the applied angle of 60that is lower than at least 50% of the reaction moment of the unbuckled beam to which only a rotation is applied. This is how the model is set up in the Matlab® code. The applied load for which the reaction moment at 60of the buckled beam reaches a value lower than 50% of the reaction moment of the unbuckled beam is the load which is taken as the applied preload. Starting from the buckling load this applied preload is iteratively increased by 10% until the constraint of the reduction in reaction moment, or in other words the reduction in longitudinal secant rotational stiffness, is satisfied. The lateral deflection, Δ y, resulting from the rotation is set as the objective value that is to be minimised.

6.4. Final optimisation scheme

The optimisation loading scheme is similar to the loading scheme used for the parameter study, displayed in figure 6.2 and 6.3. The major addition is the constraint that ensures the beam having at least a 50% decrease in secant longitudinal rotational stiffness. The final optimisation loading scheme is as following:

1. A rotation of 60is applied about the longitudinal axis of a beam in the unloaded and thus unbuckled state. This gives the value of the longitudinal secant rotational stiffness of a neutral beam in pure torsion.

2. the 3 step loading scheme as used for the parameter study is applied (fig. 6.2 and fig. 6.3): The critical buckling load is estimated, the buckling load is applied, the orientation of the beam and applied load are realigned to have a horizontal final beam element, a rotation of 60is applied about the longitudinal axis of the final beam element and the reaction moment and resulting longitudinal secant rotational stiffness are computed.

3. The constraint is implemented and if necessary the preload is increased incrementally to ensure a 50% reduction of secant rotational stiffness in the buckled state with respect to the unbuckled beam subject purely to an equal rotation of 60. Finally once the constraint is satisfied the resulting lateral deflection, Δy, is taken as the value for the error that is to be minimised.

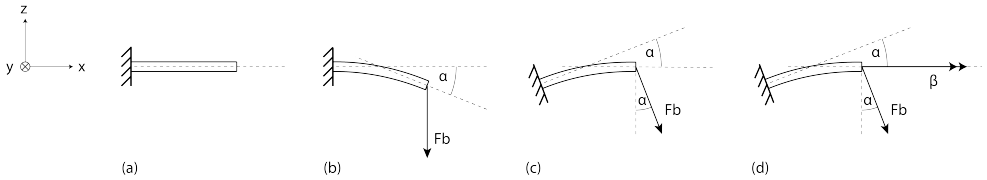

Figure 6.2: The cantilever beam (a) is loaded by the buckling load, Fb, at its free end (b). The beam is realigned by rotation about the y-axis (c). The rotation is applied about the local longitudinal axis at the free end of the beam which coincides with the global x-axis

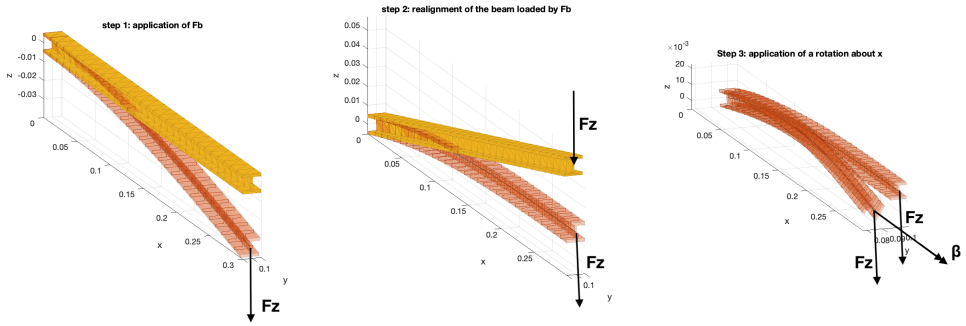

Figure 6.3: The cantilever beam is loaded by the critical buckling load, Fz in this figure, at its free end (left). The beam is realigned by rotation about the y-axis such that the longitudinal axis of the free end is parallel to the x-axis (middle). The rotation β is applied about the local longitudinal axis at the free end of the beam which coincides with the global x-axis (right) while the critical buckling load, Fz in this figure, is present as preload

7

Supplementary Material: Experimental Verification

This chapter serves to provide more insight and details on the experimental verification through additional images and illustrations.

7.1. Modelling dependencies

The experimental verification aims to:

1. validate the magnitude of the critical buckling loads
2. validate the reduction of longitudinal rotational stiffness through LTB
3. validate the reduction in lateral deflection through optimisation.

These objectives are investigated for the base beam, the best performing beam of the parameter study (the beam with the lowest lateral deflection for an applied rotation of 60with the critical buckling load as preload) and the optimised beam.

Throughout the simulations a 3-step loading scheme, as elaborated on in chapter **??**, was applied. This loading scheme forms the backbone of the experimental validation of the simulation results. It should be noted that the 3-step loading scheme has a FEM solving process for each of the 3 steps. This means that the simulation based numerically obtained solution of the previous step influences the result of the next step. More specifically the estimated value of the critical buckling load in step 1 determines the clamping angle, α, which is used to realign the beam and the orientation of the critical load in step 2. Next, the application of the rotation in step 3 determines the value for the secant rotational stiffness about the x-axis. Thus, to ensure that the rotation applied in the third step is about the global x-axis in the experimental setup, the critical load and the corresponding clamping angle need to be obtained experimentally, since only then the conditions for which the rotation is applied to a critically loaded beam are equivalent for the simulation and the experiment. Only then the conditions are such that the stiffness reduction of the beam and the co-occurring lateral deflection in the buckled state can be evaluated.

7.2. Validation of the magnitude of the critical buckling loads

For the validation of critical loads each beam is clamped as a cantilever and loaded at the free end by an attached weight that forms a pure tip load (figure 7.1). The applied load is varied by varying the amount of weight.

Thereby the beam is loaded to different states of deformation. To determine the magnitude of the critical load, for each applied load a frontal and side image is taken and the images are processed using the ‘imageJ’ software package. The frontal image serves to determine the in plane angle of twist, ϕ. The side view image serves to determine the clamping angle, α, at the critical load, which is needed

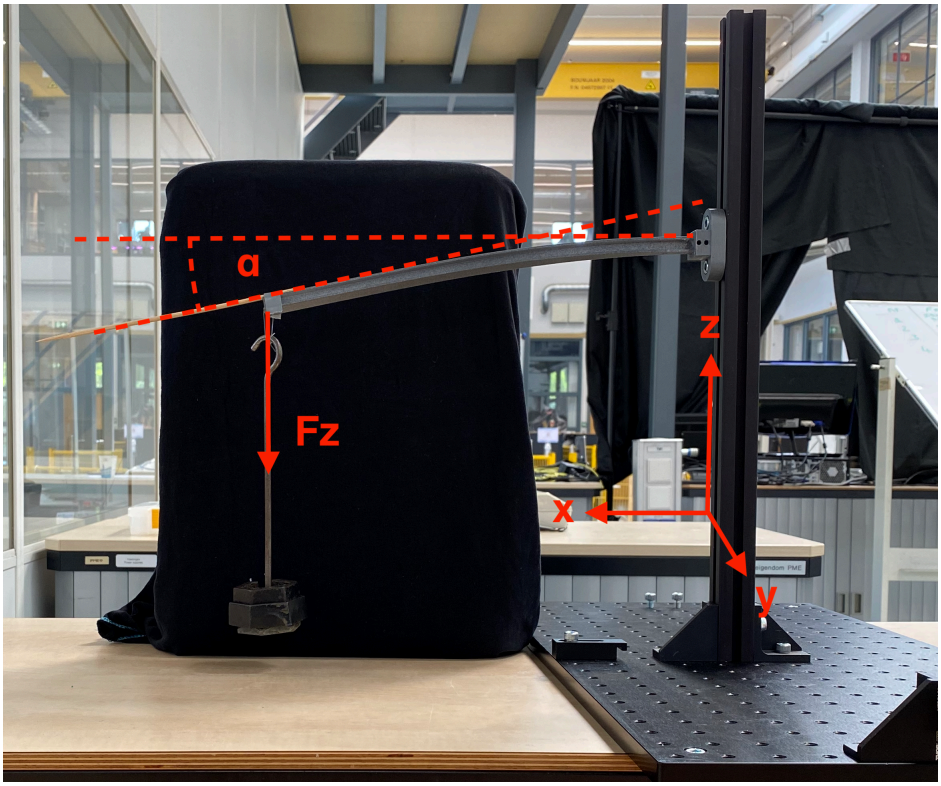

Figure 7.1: A weight is applied resulting in an applied pure tip load, Fz, at the free end. The bending angle, α, is determined by image processing, since its value is needed for the clamping angle later on.

for the second experiment on the validation of stiffness reduction. Figure 7.1 shows an example image of the side view and the bending angle α that will be used as the clamping angle for the validation of the stiffness reduction.

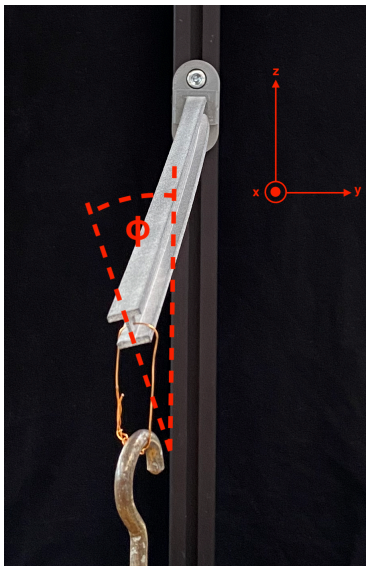

Figure 7.2: The in plane twist angle ϕ is determined and kept track off to determine the critical load

The in plane angle of twist is traced by image processing. Figure 7.2 shows an example image of how the in plane angle ϕ is determined. It is expected that for loads equal to or larger than the critical load a sudden increase in the angle of twist will occur with respect to loads lower than the critical load. The lateral deflection was not selected as a variable to determine the critical load as the optimised

beam is optimised to have a minimal lateral deflection. Therefore a less obvious sudden increase in lateral deflection is expected for loads equal to or larger than the critical load, making this a less suitable metric to determine the critical load based on image processing.

7.3. Validation of the stiffness reduction and optimisation based reduced lateral deflection

For the validation of the reduction of rotational stiffness each beam is loaded by an applied moment in the neutral unbuckled state with zero preload and an applied moment in the unstable, buckled state, with a preload equal to the critical buckling load, of which the magnitude was found in the first experiment.

The beam without preload is subjected to a pure moment by placing a moment arm through the center line of the cross-section of the beam at the free end of the beam. The setup for the application of a pure moment is displayed in figure 7.3. At both ends of the moment arm an equal but opposite load is applied to ensure that a pure moment is applied with a net zero tip load. A weight is hung directly on end of the moment arm. At the other end of the moment arm a string is attached which is connected to a weight and hung around a pulley.

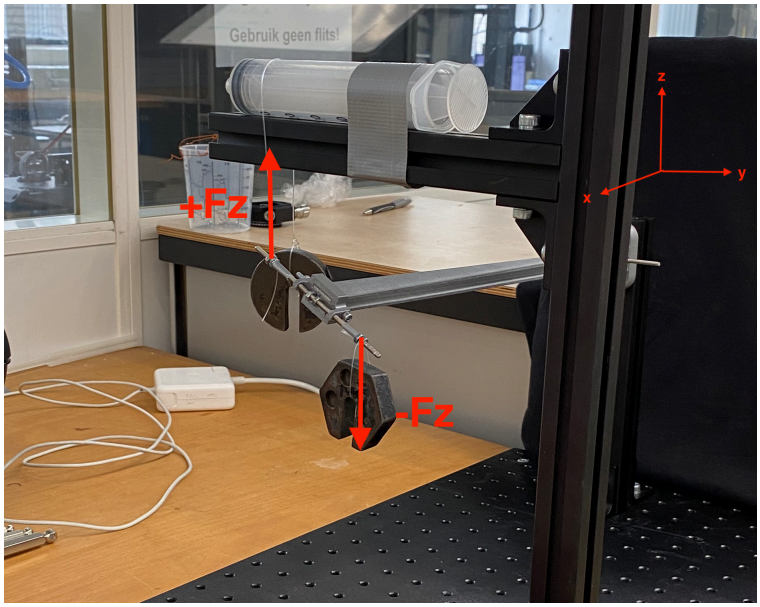

Figure 7.3: A pure moment is applied to the beam by applying an equal but opposite force in z-direction at an equal distance from the centre of the cross-section of the beam.

For the application of the moment to a beam with preload equal to the critical load, the load case is based on step 2 of the 3-step loading scheme presented in chapter 4 (figure 4.1). The beam is clamped at an angle, α, and the critical buckling load, Fb, is applied as a preload at an angle α with respect to the vertical axis such that the free end of the beam has a longitudinal axis parallel to the horizontal global x-axis.

The value for α (the clamping angle and the angle of the preload) are set by the bending angle for the vertically applied critical load obtained in the first experiment.

The values of the critical load that are to be applied as preload are also taken from the first part of the experiment to ensure that the moment is applied for a preload that is true to the real world critical load rather than a simulation based value.

Figure 7.4 displays the experimental setup of applying a moment to a beam that is held unstable by the critical load that is present as preload. The setup works as following:

To apply the preload at an angle α, it is decomposed in a horizontal (+x direction) and vertical (-z direction) component. The vertical component is applied as a weight attached directly at the free end of the beam. The horizontal component is applied through a horizontal string attached to the the free end of the beam and routed around a pulley with a weight attached on the other end of the string.

The moment is applied about the horizontal x-axis by placing the weight, representing the vertical

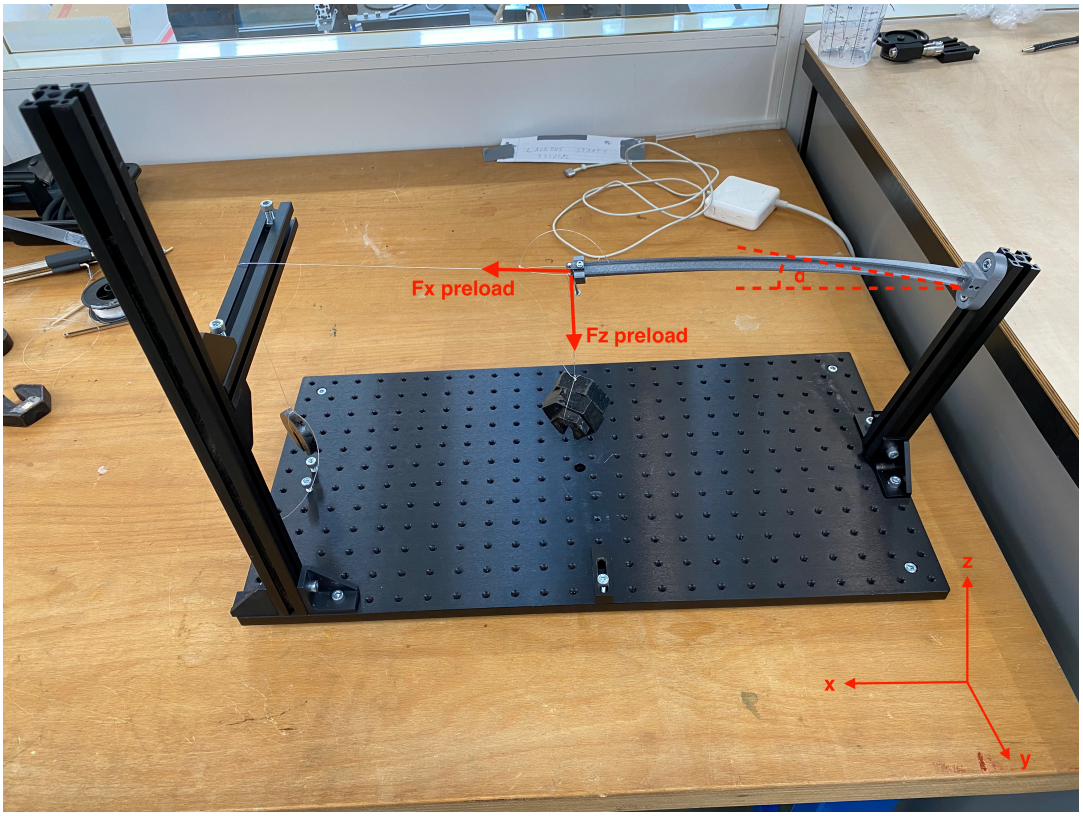

Figure 7.4: The beam is clamped at an angle α. The preload is decomposed in a horizontal component in x-direction and a vertical component in negative z-direction. The net magnitude of the preload is equal to the critical buckling load

component of the preload hung directly at the free end of the beam, at a distance from the exact centre of the beam cross-section on a moment arm. This ensures that the beam is subjected to a vertical preload component, a moment about the horizontal x-axis and a horizontal preload by a second string without additional parasitic force components that are absent in the simulation.

The magnitude of the applied moment is based on the magnitudes found in the simulation at the end of the fixed applied rotation of 60.

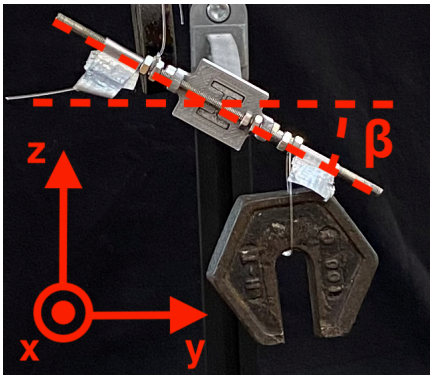

Figure 7.5: For the beam without preload the applied moment causes the rotation β, of which the value is obtained through image processing of the orientation of the moment arm indicated by the red dashed lines.

For both the cases of an applied moment with and without preload a rotation occurs. For the beam subjected to a preload an additional lateral deflection occurs due to the beam being subjected to LTB. The values of the rotation, β, and lateral deflection, Δy, are determined through image processing of a frontal image of the beam without preload and an applied pure moment (figure 7.5) and the beam with preload equal to the critical buckling load and an applied moment (figure 7.6).

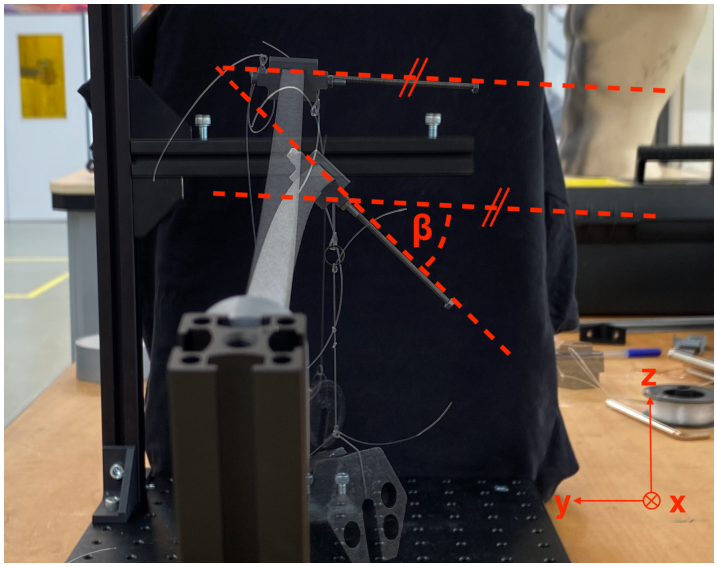

Figure 7.6: For the beam with preload the applied moment causes the rotation β, of which the value is obtained through image processing of the orientation of the moment arm indicated by the red dashed lines. The unloaded and preloaded beam are overlaid in Photoshop to determine the angle β

The lateral deflection is determined by the taking the diagonal AB of the cross-section and taking the net displacement in y-direction of the centre of AB, which corresponds to the centre of the cross-section. This method is displayed in figure 7.7.

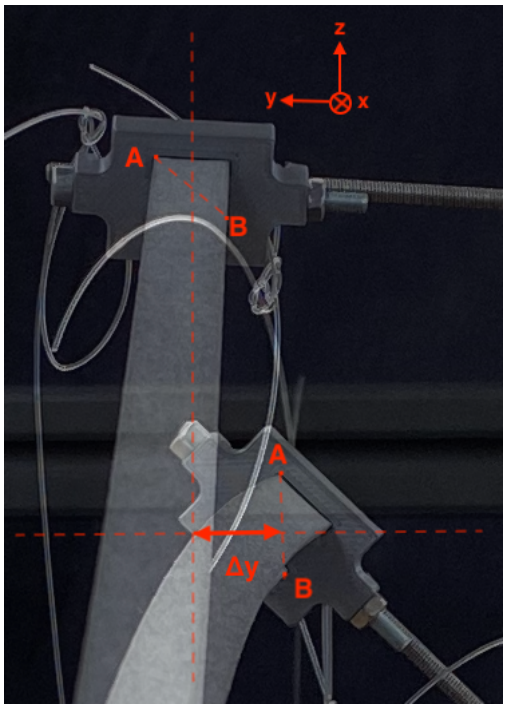

Figure 7.7: The lateral deflection, Δy, is determined by the net displacement of the centre of diagonal AB.

The applied moment and corresponding rotation present a value for the secant rotational stiffness for the beam with and without preload. The values for the secant rotational stiffness are compared to to estimate the reduction in secant rotational stiffness that is expected due to the preload causing a state of LTB.

8

Discussion

The optimisation case showed that optimal performance in terms of a minimal lateral deflection can be obtained that was undiscovered through the parameter study. However, it is fair to note that even though a reduction in lateral deflection from 0.0028 to 0.0018, which could be presented as reduction of 36%, may, in reality, be invisible on the scale of an unstable beam with a length of 0.297 due to modelling inaccuracies and limitations of the 1D FEM model. Nonetheless with respect to the base beam with a deflection of $\Delta y = 0.01574$ the optimised beam showed a significant reduction of 88%.

Regarding potential modelling inaccuracies, a remark is to be made with respect to the selected method of applying a rotation about an axis that is always parallel to the global x-axis to obtain the reaction moment, rotation behaviour of the cantilever beam. Before the application of the rotation, the beam, in its preloaded and realigned state (fig. 4.1c), has a longitudinal axis normal to the cross-section at the free end that is initially parallel to the global x-axis. However, throughout the incremental application of the rotation, the orientation of the longitudinal axis normal to the cross section of the free end changes, since the beam deflects laterally and twists longitudinally due to LTB.

Thereby the resultant moment - rotation behaviour and corresponding stiffness profile is also determined about this fixed orientation axis instead of an axis that is always normal the cross-section at free end of the beam. However, for future work or the design of applications an orientation specific stiffness profile may be more difficult to use than a stiffness profile about a fixed axis.

For the optimisation case it should be noted that the magnitude of the buckling load was not considered as part of the constraints or objective function. The magnitude of the buckling load was free as long as the load was at least equal to the buckling load of the beam at hand such that the beam would become unstable. For applications aimed at exploiting reduced rotational stiffness of beams by LTB this may be different and the magnitude of the buckling load may in fact become a relevant constraint.

On the outlook of the simulation results it should be noted that the applied angle significantly affects the values for the performance metrics of the secant rotational stiffness and the reduction of secant rotational stiffness. Especially for relatively small angles near the region of zero rotational stiffness, the secant rotational stiffness may be much lower and thus the stiffness reduction percentage would become much higher.

The applied angle is also influencing the outlook of the results of the optimisation, since a smaller applied angle would result in a much lower secant rotational stiffness and higher values for the corresponding stiffness reduction. This would allow the constraint of a minimal stiffness reduction of 50% to be satisfied more easily. Alternatively, by using a smaller fixed value for the applied angle, the stiffness reduction constraint can easily be increased to larger values.

Another aspect that influences the outlook of the results for the secant rotational stiffness and the reduction of the secant rotational stiffness is the selected method of applying the approximated critical buckling load as preload before application of the rotation for the parameter variation and the optimisation case. As was shown in this work, whenever LTB is detected application of the buckling load consistently shows an initial moment - rotation behaviour with zero stiffness regardless of the exact beam dimensions.

From section **??** it was observed that the if the applied load is increased beyond the magnitude of the absolute critical load the initial increments in rotation show negative stiffness behaviour. This

means that the reaction moment for the final value of the same applied angle is lower for a beam loaded by a force larger than the critical load than the reaction moment for a beam loaded by the exact critical load. Consequently the secant rotational stiffness would be lower and the stiffness reduction higher. The behaviour of beams becoming unstable due to LTB could even be tuned to have a secant rotational stiffness of zero if the reaction moment for the final value of the applied angle results in a reaction moment of zero.

The experimental validation results showed different values for the critical loads, stiffness reductions and the lateral deflections with respect to the simulation. However the results showed a significant reduction in secant rotational stiffness by 49% for the base beam and 35% for the optimised beam. Thereby the stiffness reduction through a beam subject to LTB is validated.

The differences between the observed critical loads in the experiment and the model are much larger for the best parameter study beam and the optimised beam than the critical load obtained for the base beam. For beams with wide flanges the beam model appears to be less reliable as for wider cross-sections effects of cross-sectional distortion become more prevalent in the overall force deformation behaviour of the beam. Especially for less slender beams with wider flanges simulation with shells or solids may provide more accurate results.

The observed reduction in lateral deflection in the experimental results between the base beam and the optimised beam are to be taken with consideration as they are based on different magnitudes of applied moments applied to different beams. In the simulation all beams are preloaded, subjected to a fixed rotation and then the resulting angle and lateral deflection are obtained. To keep the experiment simple a moment, rather than a rotation, is applied to a beam subjected to preload and the resulting rotation is observed. These moments are not identical for all beams as they are based on the reaction moments obtained in the simulation for a fixed applied angle.

Additionally the application of a moment by hanging weights on strings resulted in a moment that was dependent of the resulting rotation as the rotation caused shortening of the effective moment arm. Since the lateral deflections are now experimentally obtained for different angles of rotation and different moments, the lateral deflection of the base beam and the optimised beam cannot be directly be compared to one another.

However it was observed that the rotation resulting from the applied moment are fairly close, 27 for the base beam and 25 for the optimised beam, whereas the lateral deflection is 90% less for the optimised beam. Therefore it is considered plausible that the optimised beam results in significantly lower lateral deflection than the base beam if an identical angle were to be applied to both beams.

Furthermore the differences between the simulation and model can also be attributed to manufacturing inaccuracies as well as inaccuracies in the experimental setup. Manufacturing of the prototype beams resulted in a slight beam curvature in the xy-plane. Also the experimental setup presented additional forces to the system because of friction of the string on the pulleys and the orientations of the string not always being exactly parallel to the global x-axis.

9

Conclusion

Inspired by the need for a wrist support capable of having low rotational stiffness for pronation and supination while supporting the weight of a hand, this work proposes an investigation of the potential of exploiting lateral torsional buckling to reduce the longitudinal rotational stiffness with minimal co-occurring lateral deflection for cantilever I-beams through: (i) a verification of negative rotational stiffness behaviour in the buckled state, (ii) a parameter study of both cross-sectional geometrical properties and cross-sectional dimensions and (iii) an optimisation case for a straight cantilever I-beam with minimal lateral deflection and reduced secant rotational stiffness.

The procedure to numerically estimate the buckling load proved to be consistent as the applied force - lateral deflection behaviour and the moment - applied rotation for the approximated value of the critical load consistently showed very similar results for a wide variety of I-beams.

Simulations showed that for an applied load equal to the critical load a region of zero stiffness occurred for the initial range of the applied rotation. For an applied load larger than the critical load a symmetric negative rotational stiffness behaviour occurred.

The parameter study showed insight in potential tradeoffs between the magnitude of the secant rotational stiffness about the longitudinal beam axis and the lateral deflection of the free end of the beam due to LTB as well as which beam parameters contribute to significantly lower values of the lateral deflection and how the buckling load changed along with the variation of the beam parameters.

The optimisation resulted in a beam with lower lateral deflection than any of the beams in the parameter study. The dimensions of the optimised beam are similar to the best performing beam of the parameter study as both have relatively wide flanges. Simulation of the optimised beam showed a significant reduction of lateral deflection of 36% with respect to the best beam in the parameter study and a reduction of 99% with respect to the base beam.

The experimental validation showed different values for the critical loads and applied moment - rotation behaviour. However the experiment confirmed that the secant rotational stiffness reduces significantly by subjecting the beam to lateral torsional buckling and that the optimisation resulted in a beam with significantly lower lateral deflection.

Overall this work forms an initial step towards the use of reduced rotational stiffness of beams by exploiting the phenomenon of lateral torsional buckling. It was shown that rotational stiffness can be significantly decreased by applying the buckling load to a cantilever I-beam. In addition to the case of wrist support for DMD patients having a strongly reduced rotational stiffness may be beneficial for the application of compliant mechanisms or variable stiffness applications for which a simple method, the application of a bending load, to reduce rotational stiffness on demand is desired.

For future work the results of this study can be expanded by tailoring the performance towards specific applications of for example the wrist support that inspired this thesis. Also it may be interesting to look into beam optimisation of additional beam parameters as shape and cross-section variation, as they may even further minimise the lateral deflection by application of the critical buckling load

deflection when implemented in an optimisation procedure similar to the optimisation presented in this work.

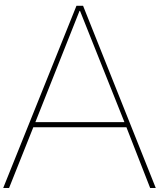

Appendix: Literature review on methods of controllable stiffness for structures

Preceding the thesis project on lateral torsional buckling a literature review was performed on methods of controllable stiffness for structures. The motivation for this review was to look for inspiration that could result in a wrist support that could support the wrist in flexion/extension but also turn off this support for pronation/supination, in other words inspiration for a variable stiffness structure.

Review on methods of controllable stiffness for structures

Laurens Staats

***Abstract*—Variable or controllable stiffness structures are structures that can stiffen or soften on demand. The shared desired characteristic of changing stiffness on demand is of interest across the fields of aerospace engineering, medical devices and soft robotics. So far reviews on variable stiffness have been done tailored to the needs of these different fields. The aim of this work is to form a cross-disciplinary review through a more fundamental classification based on four main branches that influence the stiffness of a structure and four main types of stiffness. Additionally this work aims to provide an indication, comparison and overview of the performance characteristics of existing concepts though evaluation of maximum to minimum stiffness ratios, the amount of stiffness modes and technology readiness levels as well as the main drawbacks of existing concepts. The classification shows that there is a clear focus on variable bending stiffness through the application of prestress exploiting stimuli as pressurisation, fluidisation and electrostatic fields. Another clear focus in the field of variable stiffness structures is the use of smart materials such as shape memory polymers and shape memory alloys. Overall technology readiness of the concepts is low and concepts showing the most promising characteristics are mostly on the fundamental side of the technology readiness scale. More technologically advanced concepts present less ideal values and still show various drawbacks for real life applications.**

***Index Terms*—Variable stiffness, controllable stiffness, material properties, shape, prestress, boundary conditions.**

I. Introduction

Variable stiffness structures are a topic of interest across various fields of research. Major examples are the fields of aerospace engineering, medical devices and soft robotics. Although their applications are vastly different, the shared desired characteristic is that these structures can change their stiffness on demand with minimal actuation power.

In aerospace engineering the topic of variable stiffness structures finds presence in the field of shape morphing applications [1]. Current aircraft designs are not optimised for all the different phases in flight. Through shape morphing the aircraft and, often more specifically, the wings can change shape such that the wing is more efficient across various flight conditions resulting in greater fuel efficiency. Morphing through traditional mechanical and hydraulic actuators is often not viable due to the additional weight of these actuators. Therefore solutions are sought that need low energy to change shape. Lowering the stiffness, changing the shape and then increasing the stiffness again results in low power requirements for changing shapes and easy optimisation of flight efficiency across the different phases of flight. Kuder et al. [2] review concepts for variable stiffness with a focus on shape morphing for aerospace applications through a classification based on four categories: material engineering, mechanism-driven variable stiffness, semi-active variable stiffness solutions and structural elasticity-related variable stiffness. Sun et al. [3] review smart materials and structures for varying stiffness in the context of aerospace morphing applications. Their perspective is that such applications are systems which consist of smart materials and structures that fulfil the functions of sensing, control and actuation. Smart materials and structures were reviewed and classified based on these three functions.

In medical applications variable stiffness applications are a topic of interest for minimally invasive surgery procedures. Surgical equipment needs to be stiff for procedures such as cutting, grasping or support of other surgical equipment [4]. Yet it also needs to be compliant to be less harmful to surrounding tissue especially when manoeuvring through the tissue to reach the location where the surgical procedure is to be performed. Blanc et al. [5] reviewed controllable stiffness mechanisms for the application of medical devices with controllable stiffness using a classification based on three categories: geometrical properties, elastic properties and actuator-like solutions. Blanc et al. [5] also quantitatively compared performance of the concepts found on criteria relevant to medical devices with controllable stiffness.

Another application of variable stiffness in the medical field is the field of wearable orthotics and exoskeletons. Traditionally these are made of heavy rigid parts and actuators to be able to carry load and support body function. Structures that can become stiff or compliant on demand could reduce actuation requirements, resulting in more lightweight and low profile solutions that are more comfortable and more versatile in function to the user.

Additionally variable stiffness solutions are explored in the field of soft robotics. Manti et al. [6] reviewed concepts for variable stiffness for the application in the field of soft robotics. The focus is on the use of variable stiffness elements for interaction of soft robots with natural environments. Their review proposes a classification of concepts based on active antagonistic actuators focussed on changing stiffness through their coupling with each other or with passive structures, and concepts based on semi active actuators focussed on changing elastic properties intrinsically.

As a result of this cross disciplinary interest in variable stiffness applications, McEvoy et al. [7] review the field of research focussed on materials with programmable properties such as stiffness by integrating material science and computer science. The review investigates solutions for the integration of sensing, actuation, computation, and communication to create materials with programmable properties. These programmable materials may then be suitable for use in variable stiffness applications in aerospace engineering, soft robotics or medical equipment.

So far prior work has reviewed variable stiffness concepts

from the perspective of specific fields of applications through various classifications. The aim of this review is to (i) form a cross disciplinary review of variable stiffness structures through a classification of the variable stiffness mode and the working principle, (ii) provide an indication, comparison and overview of the performance characteristics of these concepts for future applications.

Section II describes the method on the categorisation made to find principles and concepts of variable stiffness structures. In section III-A the concepts found in literature are examined and classified through the categorisation as established in section II. Additionally, section III-B displays an indication of performance of variable stiffness concepts for a comparison between concepts as well as an overview of some of their characteristic properties for future applications. In section IV the categorisation proposed in this review is discussed on its advantages and shortcomings in finding literature and identifying gaps in existing literature. Also the performance indication is evaluated on the insight it provides.

II. Method

In order to systematically search for literature on methods of controllable stiffness of structures the following categorisation was made. There are four factors determining the stiffness of a structural element: (1) material properties, (2) shape, (3) prestress and (4) boundary conditions. Changing the stiffness can thus be done by changing any of the four factors. Additionally four main types of stiffness of structures can be distinguished: (1) bending stiffness, (2) torsional stiffness, (3) axial stiffness and (4) shear stiffness.

Based on these four branches that can influence four major types of stiffness a solution space is set up in which existing literature can be mapped (fig. 1). The working principle of each concept in literature is appointed to one the influence branches and mapped to the type of stiffness that is varied. The solution space can be expanded by adding a third dimension which is the actuation stimulus. Unlike the four factors determining the stiffness and the four major types of stiffness the stimulus axis is not used as a search guideline. Rather, it is explored as literature is found.

In order to find concepts in literature to fit in the categorisation the search terms were used as displayed in table I.

III. Results

In section II a three dimensional categorisation is presented in which the concepts found in literature can be placed. Subsection III-A discusses the concepts found in literature based sorted by influence branch. For each concept the type of stiffness and actuation stimulus is specified. Section III-B provides an overview and comparison of the performance of the concepts.

A. Concepts classified per branch

In figure 2 an overview is presented of the number of concepts found in literature based on the classification based on the type of stiffness and influence branch. Follow up work

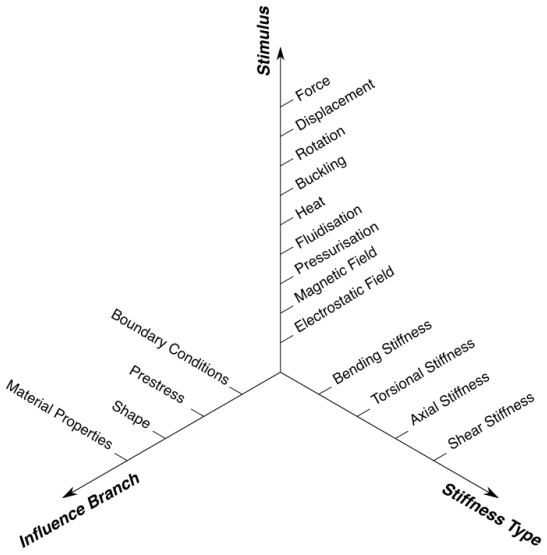

Fig. 1. The classification is illustrated as a solution space.

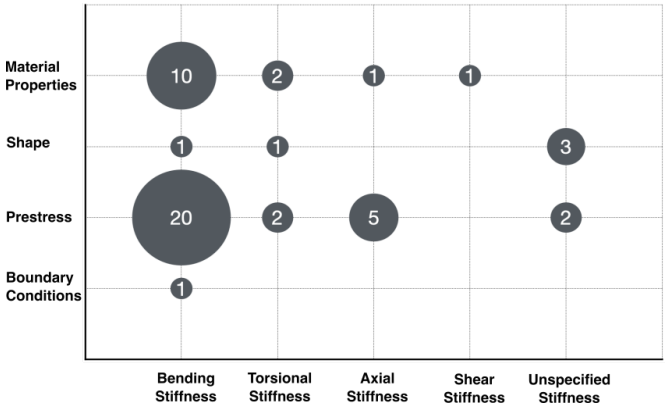

Fig. 2. The bubble chart displays the number of concepts per branch and type of stiffness.

based on the same concept was not counted twice. Articles with concepts addressing multiple types of variable stiffness are counted separately for the different types of stiffness. It should be noted that the amount of literature in the solution space should be regarded as an illustration of the number of concepts found through the classification proposed in this review rather than an exact measure of existing concepts in literature.

The scope of the classification yielded concepts from various areas of research. Overall, the majority, 28 out of 48 concepts, focussed on varying stiffness through the application of prestress. 20 of 28 concepts on prestress focussed on bending stiffness. The material branch presented 14 concepts of which 10 were focussed on bending stiffness. The shape branch yielded 5 concepts and the boundary condition branch yielded one concept. Overall 32 concepts were focussed on variable bending stiffness and a total of 16 were focussed on variable torsional, axial and shear stiffness.

TABLE I
TERMS USED FOR SEARCHING LITERATURE

Terms combined with AND operator				
variable	stiffness	compliant	structure	material
controllable	bending stiffness	soft	element	material properties
tuneable	torsional stiffness	reconfigurable	origami	shape
adjustable	axial stiffness		surface	geometry
adaptable	shear stiffness		shell	prestress
tailorable			beam	boundary conditions
			mechanism	
			shell mechanism	
			exoskeleton	
			robotics	

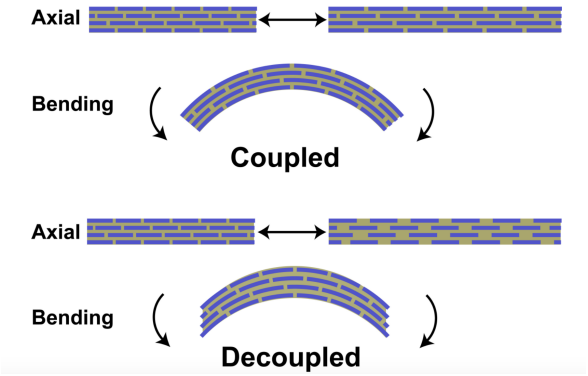

Fig. 3. The segmented beam consists of constant stiffness segments alternated by SMP. In the soft state the stiff segments decouple [8].

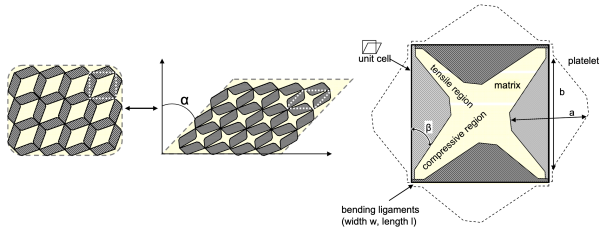

Fig. 4. Stiff grey platelets are alternated by variable stiffness matrix material [9].

*1) **Changing stiffness by changing material properties**:*

- *Bending stiffness & axial stiffness, heat*
  In [8] Mcknight et al. propose a variable stiffness beam made of a laminate consisting of constant stiffness elements made of high yield spring steel and variable stiffness elements made of a shape memory polymer (SMP) based on polyurethane. Segments of constant stiffness are separated by the variable stiffness material and these segmented layers are alternated with complete layers of the variable stiffness polymer (fig. 3). When heated above the glass transition temperature of 55 degrees Celsius the SMP, in a transition window of 20 degrees changes its E modulus from 2 GPa to 50MPa. In both the axial loading and bending the beam becomes less stiff due to shear of the variable stiffness SMP, decoupling the constant stiffness elements. Depending on the exact laminate geometry the ratio of maximum to minimum stiffness varied from 64 to 15 with lower values for the storage modulus of 0.12 GPa, 014 GPa, 0.23 GPa and 0.79 GPa to the respectively maximum values of 7.7 GPa, 10.8 GPa, 8.0 GPa, 12.3 GPa with corresponding ratios of 64, 77, 34, 15.
- *Shear stiffness, heat*
  In [9] the work of [8] is continued in the form of a variable stiffness composite capable of accounting for large shear strains by means of constant stiffness platelets and a matrix made of shape memory polymer. Softening of the composite happens by heating the composite above the glass transition temperature of the matrix. The platelets are designed such that once the composite is heated the shear stiffness decreases and large shear strains can be accounted for specifically (fig. 4).
- *Bending stiffness, heat*
  In [10] the design of a robotic material is discussed. The principle behind this robotic material is that its properties are more customisable and controllable than smart materials such as shape memory polymers or shape memory alloys. The robotic material consists of discrete polycaprolactone (PCL) elements with each element containing a sensor, controller and actuator in the form of a heating component. By local heating the stiffness of the element changes. Having multiple elements forming a beam allows for a variable stiffness beam that can be programmed into different configurations under the same load (fig. 5). The current rate of change for stiffness is in the range of minutes which may be a disadvantage for applications. Also because of all the electronics involved, larger scale applications will require careful power routing and analysis of local heating and cooling in order to keep this robotic material functioning as desired. A prototype was experimentally validated by selectively heating and softening of the beam and gravity being the vertical load that caused deformation.
- *Bending stiffness, heat*
  In [11] a variable stiffness carbon fibre composite is proposed aimed at morphing wing applications in aerospace. The composite is designed to have variable bending

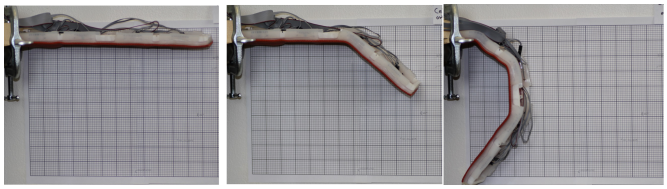

Fig. 5. Heating in different locations and in different order of activation results in different structures when subjected to the same gravitational load of its mass [10].

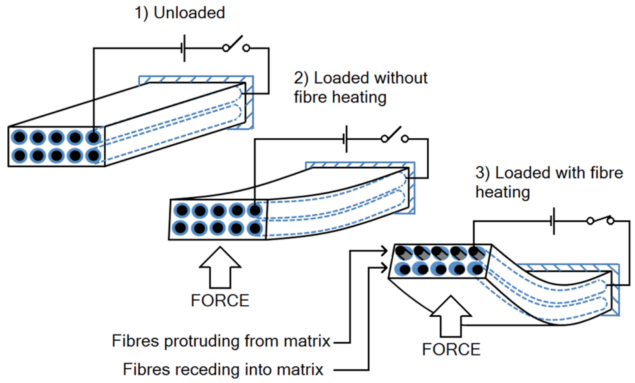

Fig. 6. The composite softens when a current is applied to the SMP fibre coating [11].

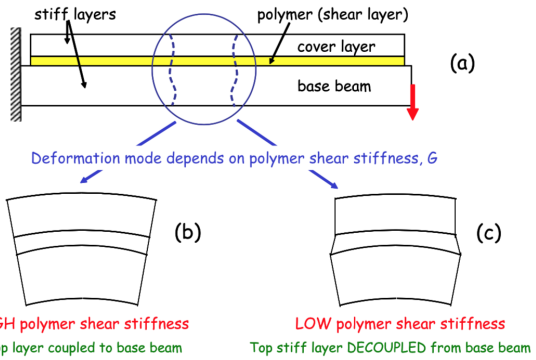

Fig. 7. The beam consists of a base beam, polymer layer and cover layer (a). The beam is stiff when the base beam and cover layer are coupled (b). The beam is soft when the base beam and cover layer are decoupled (c) [12].

stiffness. The unique property lies in the fact that only the coating of the fibres is made of the shape memory polymer rather than the entire matrix. Current is fed through the coating of the fibres, resulting in heating of the coating above the SMP glass transition temperature and thereby softening of the composite (fig. 6). Softening of the composite through softening the fibre coating leads to quicker softening than composites in which the entire matrix material needs to be heated above the glass transition temperature as in [8] and [9]. A stiffness reduction of 88% was obtained from 69 +- 8 GPa in the stiff state to 8 +-5 GPa in the soft state.

- *Bending stiffness, heat*
  In [12] a variable stiffness multilayer beam is described. The beam consists of a stiff aluminium base beam that is clamped. On the top and bottom of the base beam is a shape memory polymer layer with a variable shear stiffness. On the outer side of the polymer layer is a stiff aluminium cover layer. By heating the variable stiffness layer above its glass transition temperature the shear stiffness lowers decoupling the stiff base and cover layer (fig. 7). In the stiff state the base and cover layer are coupled resulting in a beam that is stiff in bending. After heating the polymer and the stiff layers decouple resulting in a low bending stiffness of the base beam. The heating is actuated by an electric heating element fitted in the polymer layer. Two lengths of the beam were tested as well as two different polymers, cast acrylic material and PVC type I, and two polymer layer thicknesses. Longer beams gave higher maximum to minimum stiffness ratios for cast acrylic cast material, 2.83 to 3.2, and shorter beams in lower maximum to minimum stiffness ratios, 2.03 to 2.6. For PVC type I longer beams also resulted in higher maximum to minimum stiffness ratios, 2.84 to 4 and shorter beams in lower maximum to minimum stiffness ratios, 2.1 to 2.25. Beam thickness mostly influenced the time needed to transition from the stiff to the soft state.
  In [13] the work of [12] on variable stiffness beams based on coupling and decoupling of SMP layers is continued. In [13] a numerical analysis and experimental validation on the optimal parameters of the beam are performed in order to estimate parameters that maximise the maximum to minimum stiffness ratio in bending. It is concluded that the Young's modulus of the cover layer should be as high as possible, the higher the Young's modulus of the cover layer, the thinner the cover layer should be and that the polymer should be relatively stiff in its stiff state. When applying the optimal parameters simulations show a maximum to minimum bending stiffness ratio for the clamped beam of 70 and a ratio of 130 for a pinned-pinned beam.
  In [14] the work in [12] and [13] on a variable stiffness multilayer beam is continued further. In [14] the energy requirements are investigated to deform a stiff beam with force compared to the heat actuation energy needed to soften the beam such that it becomes compliant and easy to bend. For less slender beams the actuation energy needed to decrease the stiffness outweighs the energy needed for an actuation force that results in the same deformation of a non variable stiffness rigid beam.
- *Bending & torsional stiffness, heat*
  The concept described in [15] is a laminate consisting of layers of constant stiffness alternated by layers with variable shear stiffness. The aim is to have a laminate with variable stiffness in bending and torsion. Stiff layers made of carbon fiber-reinforced polymer are alternated

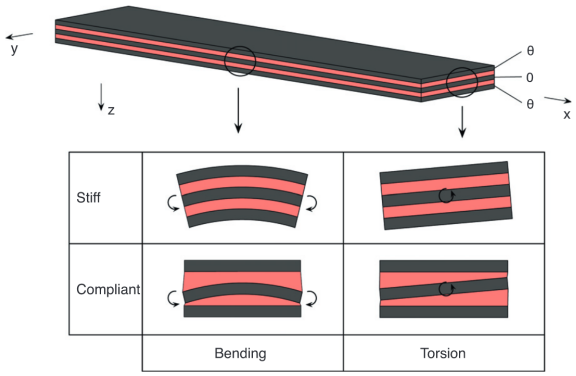

Fig. 8. The laminate softens through decoupling of the variable stiffness layer (red) [15].

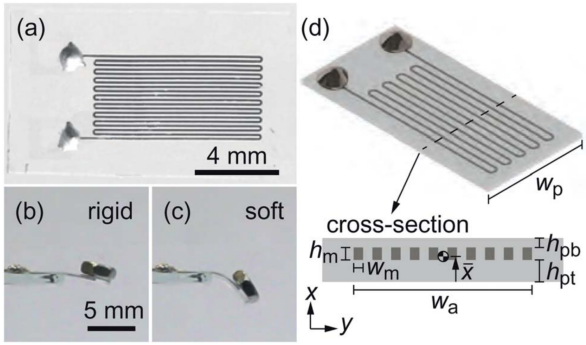

Fig. 9. The structure softens the heating of the LMPA channels. The prototype is tested on mm scale [16].

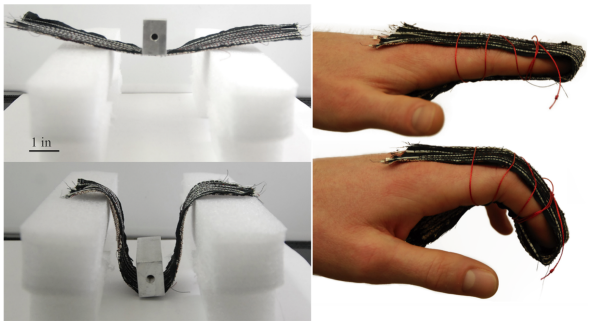

Fig. 10. The fabric is loaded in bending in the stiff state (left, top) and soft state (left, bottom). The fabric is wrapped around a human finger (right) to allow or resist bending of the finger [17].

with variable shear stiffness layers made of the elastomer "Soundcoat Dyad 609". The variable stiffness layers can couple or decouple the stiff layers making the laminate as a whole softer or stiffer on demand (fig. 8). The resulting laminate has variable bending stiffness as well as variable torsional stiffness. In the stiff state the variable and the stiff layers have a shear stiffness of similar magnitude thereby coupling the layers and forming a stiffer laminate. In the soft state the layers are decoupled due to the variable stiffness layers allowing large shear strains. The elastomer changes stiffness by being heated above its glass transition temperature of of 44 degrees Celsius. The transition window from the stiff state to the soft state is 20 degrees. Heating is done through the application of current through the carbon fibre in the stiff layers. Heat is generated by electrical resistance. A heating period of 10 minutes was needed to heat the laminate above the glass transition temperature of the elastomer layers.

- *Bending stiffness, heat*
  In [16] a material is presented aimed at applications with controllable bending stiffness. The material consists of a microstructure of low-melting-point alloy (LMPA) channels in a PDMS (poly(dimethylsiloxane)) structure. The change of stiffness is based on heating the LMPA channels above their glass transition temperature through applying current. When applying current to the LMPA, the channels heat up and become soft, making the entire material more compliant (fig. 9). The main benefits of this material are its high maximum to minimum stiffness ratio of 25 and the stiff to soft transition time of less than a second. The Young's modulus has an upper bound of 40 MPa and a lower bound of 1.5 MPa. The material is also designed specifically to have high resistance to failure in bending. Experiments were performed with small loads.
- *Bending stiffness, heat*
  In [17] a variable stiffness fabric is presented for applications in medical braces and orthotics. The variable stiffness is obtained by creating variable stiffness fibers and sewing this into a fabric. The fibers consist of SMA (nickel titanium) wire coated by SMP (polylactic acid). The SMA forms the heat actuator and the SMP provides the variable stiffness properties. A current is fed through the SMA wire heating the SMP coating by electrical resistance of the SMA. Once the SMP reaches its glass transition temperature the fibre becomes compliant resulting in a soft state of the fabric. A prototype fabric was made and tested around a human finger (fig. 10). It successfully resisted bending motion in the stiff state and allowed movement in the soft state. The temperature at skin was 48 degrees Celsius which limited the soft state operating window to 40 seconds. The transition from the stiff to the soft state takes 15 seconds for the prototype fabric. When tested in a three point bending test the fabric had a maximum to minimum stiffness ratio of 10.
- *Bending & torsional stiffness, heat*
  In [18] the concept of variable stiffness profile beams is explored through shifting of the shear centre location. Making the shear stiffness lower on one side than the other results in a torsionally more compliant beam in the clockwise direction, decreasing the shear stiffnes of the other side results in the beam being more compliant in the anticlockwise direction (fig. 11). It is suspected that apart from varying torsional stiffness the adaptive profile beam can also be used for varying bending stiffness by changing the shear stiffness of both sides simultaneously.

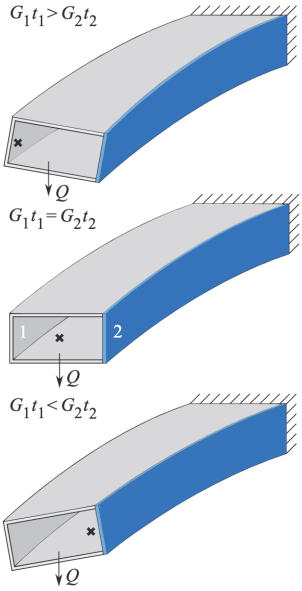

Fig. 11. The shift of the shear centre from left (top) to right (bottom) results in a shift of torsional compliance from the clockwise direction to the anti-clockwise direction [18].

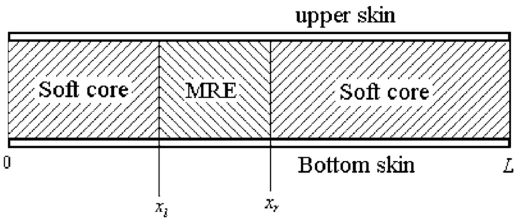

Fig. 12. The sandwich beam consists of a soft core made of MRE and non MRE parts. The faces are made of a non magnetically conductive skin [19].

- *Bending stiffness, magnetic field*
  In [19] a controllable stiffness beam is proposed based on a sandwich construction with magnetorheological elastomer (MRE). MRE is a composite consisting of rubber matrix material with ferrous chain structures inside. When exposed to a magnetic field applied in the direction of the ferrous chains, the chains will interact such that the shear modulus of the MRE increases. The beam is a sandwich beam with a soft core made of a MRE part, non MRE parts and a non magnetic conductive skin (fig. 12). The ferrous chains are oriented perpendicularly to the outer skin, such that the increase of shear modulus results in the horizontal beam becoming stiffer in bending. In continued work [20] it was concluded that for long slender beams the entire core of the beam should be made of MRE for greater controllability of stiffness.
  Bending stiffness, heat
  In [21] a neural probe with tuneable stiffness is proposed. For the implantation process the probe needs to be stiff in order to be inserted and implanted in the brain tissue without buckling. However once implanted the probe needs to be flexible in order to not cause damage in the surrounding brain tissue. The tuneable probe presented contains a channel with gallium. Upon implanting the Gallium is cooled and thereby in a solid state. During the implantation process the brain tissue is kept below the melting temperature of Gallium. Once implanted the cooling is taken away and the Gallium becomes liquid by reaching the body temperature which is above its melting temperature (fig. 13). The probe is now flexible. The concept was successfully tested in brain phantom and rat brains. Stiffness could be tuned by 5 orders of magnitude.

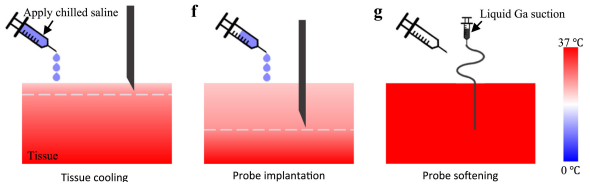

Fig. 13. The probe is stiff when inserted while cooled and becomes flexible after the cooling is removed [21].

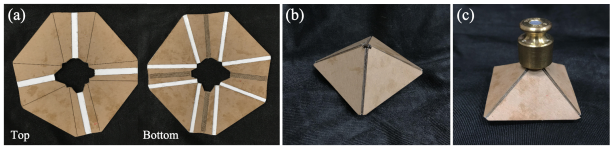

Fig. 14. When heated the origami folds into a predefined shape [22].

2) ***Changing stiffness by changing shape:***

- *Unspecified stiffness type, heat*
  In [22] a design method is described to create origami like structures from a flat sheet by using hinges made of SMP. Designs with positive, negative and a combination of positive and negative Gaussian curvature were successfully created from actuating a flat design with SMP hinges by uniform heating (fig. 14). No direct stiffness characteristics are mentioned regarding variable stiffness structures, however due to the range of obtainable shapes and their shape specific load carrying characteristics, this concept holds potential for variable stiffness applications. The folding process takes around 4 minutes depending on the exact shape.
- *Unspecified stiffness type, displacement*
  Origami also forms the base of the principle presented in [23]. Multiple designs of tubes consisting of coupled origami Miura-ior sheets are discussed. Coupled origami tubes can result in deployable structures that once deployed have one compliant deformation mode while the other deformation modes are stiff. The stiffness characteristics result from an eigenmode analysis in which the band gaps between the eigenvalues corresponding to these eigenmodes are increased through specific coupling of the origami tubes. Thereby the energy needed to go from one eigenmode to the next is large, which results in a structure that is stiff in any other direction other than the

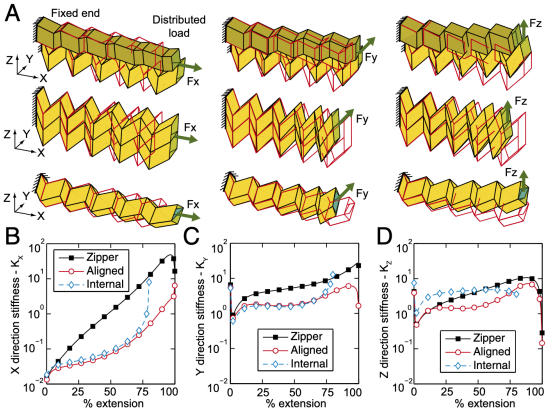

Fig. 15. Different structures can all be deployed from a flat sheet with each structure having a specific stiffness profile. The sheets can be coupled in the configuration of a zipper (A, top row), aligned (A, middle row) or internal (A, bottom row) The stiffness also varies greatly for each configuration in the x-direction (B), y-direction (C) and z-direction (D) [23].

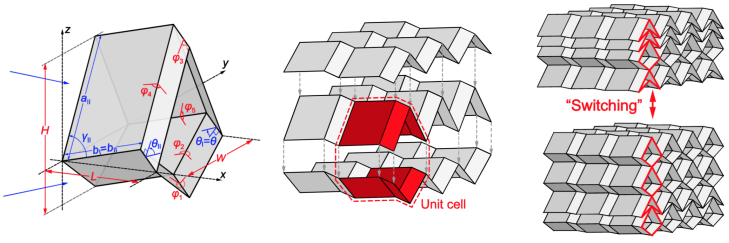

Fig. 16. A unit cell of which the stacked Miura-ori sheets consist (left), the configuration of a unit cell in the stack of sheets (middle), folding a sheet results in mode switching of the structure (right) [24]. Each mode has its specific stiffness characteristics

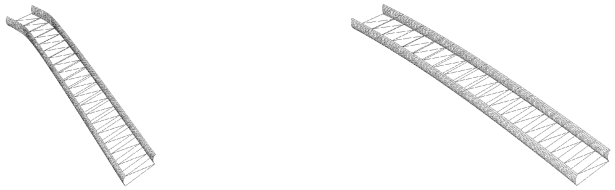

(a) Swept configuration (b) Straight configuration

Fig. 17. Simulation shows that aerodynamic load causes buckling and creates a zero stiffness-like hinge [25]. The wing in the buckled swept configuration (a). The wing in the straight configuration

eigenmode it finds itself in. Depending on the configuration and the coupling of the tubes different stiffness characteristics can be obtained. All configurations can be deployed from a deployable sheet (fig. 15).

- *Unspecified stiffness type, folding*
  In [24] the fundamentals of kinematics and design parameters for variable stiffness stacked origami structures are proposed. Stacking two Miura-ori sheets results in a multistable structure with the unique property of having a large elastic range of deformation within both stable states (fig. 16). The transition between the states occurs when a force folds the sheet. The folding causes almost no change in external dimension. Also the change between states happens at almost maximum folding which makes it hard to accidentally switch between states. The authors also indicate that internal pressurisation could be used for switching between states. By tuning the design parameters of the stacked sheets the stiffness profiles for both states can be created with great tuneability for the different stiffness modes. The stiffness variability of the concept is discrete. The stacked sheet concept has two states of stiffness. However, the authors indicate that future work could expand this principle of variable stiffness by multistability to structures with more stacked sheets and thereby more stable states. The ratio between the maximum and minimum stiffness was mostly influenced by the ratio of the crease lengths.
- *Bending stiffness, aerodynamic load*
  In [25] a concept is proposed for a variable sweep morphing wing based on multistable structures. The two outer edges of the wing consist of a tape loop-like longitudinally straight and transversely curved shell connected by a truss-ribs. When reaching a certain flight speed threshold the aerodynamic drag load causes the shell edges to buckle and become a zero stiffness hinge like wing structure that adapts to the variations in flight speed as long as the flight speed is above the threshold required for buckling (fig. 17). Below the threshold flight speed the wing acts as conventional stiff wing. A model was numerically simulated and experimentally validated. The simulation and experiment showed matching behaviour of the buckling location and the configuration of the wing after buckling.
- *Torsional stiffness, displacement*
  In [26] a wing box is presented with variable torsional stiffness for morphing wings. Mechanical actuators change the location of the front and rear spar webs (fig. 18). Lowering the cross-sectional area lowers the torsional stiffness and allows the aerodynamic loads to change the shape of the wing for more efficient flight. Bending stiffness is maintained in the span wise direction. The front and rear spar webs can be moved separately or simultaneously to change the cross-sectional area. This influences the location of the shear centre and thereby the flight properties. Changing the cross-sectional area by moving the front and rear webs separately or simultaneously present the same change in torsional stiffness.

*3) **Changing stiffness by changing prestress**:*

- *Bending stiffness, form closure*
  Henke et al. [27] propose a variable stiffness beam through the change of the area moment of inertia. When transitioning from a stack of sliding layers to a single layer rigid beam with equal dimensions as the entire stack the area moment of inertia scales up quadratically with the number of layers (fig. 19). Thereby the ratio of maximum to minimum bending stiffness also scales

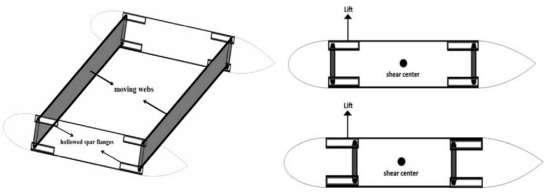

Fig. 18. Moving webs allow for variation of the cross-sectional area of the wing box (left). The cross-sectional area in its largest (top, right) and smallest configuration (bottom, right) [26].

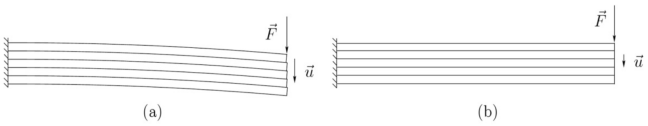

Fig. 19. A stack of sliding layers (a) is more compliant than a rigid beam with the same dimensions as the stack (b) [27].

quadratically with the number of layers. The conversion from a multi layer to a single layer beam is done by inducing friction between the layers. The prototype has two layers that can be converted to a single layer by form closure actuated by electroactive polymers (EAPs) (fig. 20). When a current is applied the EAPs shrink pulling the structure teeth of the edges in the form-closed configuration. The ratio of maximum to minimum stiffness was 5.6, which was in fact higher than anticipated. This was attributed to approximations for the area moments of inertia of the layers.

- *Bending stiffness, heat*
  In [28] the concept of varying beam stiffness through changing the area moment of inertia presented in [27] is continued but with the use of shape memory alloy (SMA) wire to contract the layers allowing for a smaller design with more layers that is less prone to failure. The SMA is wired around a stack of layers and contracts by heat actuated through electrical resistance heating. Thereby the friction between the layers increases and the multilayer beam is transformed to a large single layer beam resulting in an increased area moment of inertia and bending stiffness (fig. 21). As in [27] the bending stiffness scales

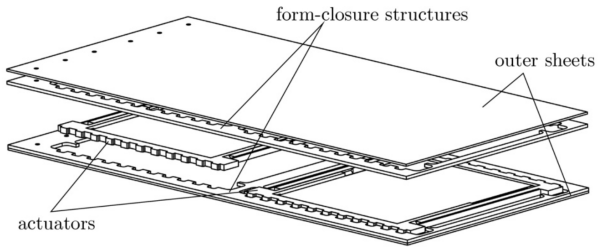

Fig. 20. Layers can connect to form a rigid stack through form closure at the edges between the layers [27].

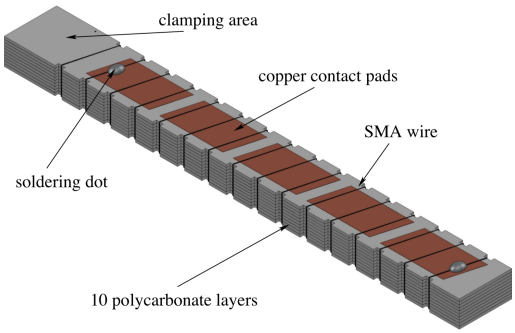

Fig. 21. SMA wires tighten the stack of layers [28].

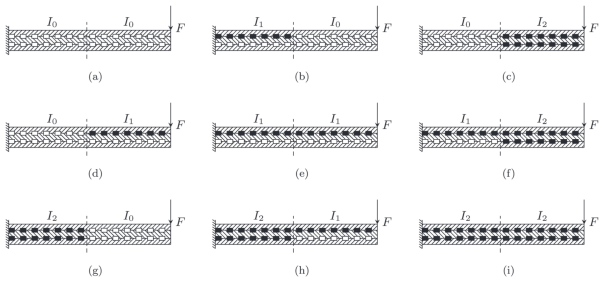

Fig. 22. The structure can be stiffened selectively by locking of segments. This is illustrated by the dark rectangles. Nine different configurations are illustrated (a - i), all having different stiffness characteristics [29].

quadratically by the amount of layers. Also, the SMA wire can be attached and actuated such that it allows for selective contraction of segments of the layers allowing local, selective stiffness increase. The expected maximum to minimum stiffness ratio from simulation of 100 for 10 layers was not achieved experimentally. Only a ratio of 18.5 was obtained. This was attributed to manufacturing difficulties of the prototype. Especially tight wiring of the SMA around the stack proved to be difficult causing a discrepancy between analytical models and the physical prototype.

In [29] the work on variable stiffness multilayer beams through variation of the area moment of inertia is continued. Like in [27] form closure between layers is used to lock the layers to form a single layer rigid beam. Here a prototype with 3 layers and 2 actuators between each layer is experimentally validated. This allows selective softening of the beam (fig. 22). A maximum to minimum stiffness ratio of 14.6 was realised in bending which was lower than 3.18 as was predicted from simulations.

- *Bending stiffness, fluidisation*
  In [30] a variable stiffness composite based on fluidic flexible matrix composites (FFMCs) is presented (fig. 23). The variable stiffness property is obtained by implementing filament wound tubes as fibers in the composite which can be filled with fluid and controlled by a valve. The composite is stiff when the the tube is filled with fluid and

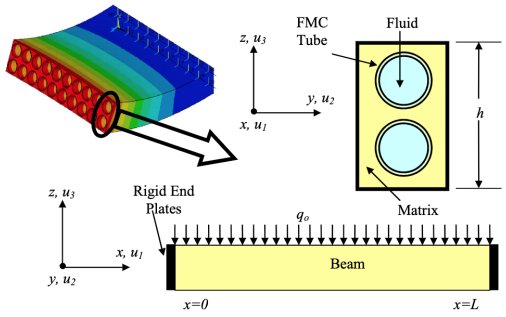

Fig. 23. Fluidisable tubes are embedded in the matrix material, resulting in a variable stiffness composite [30].

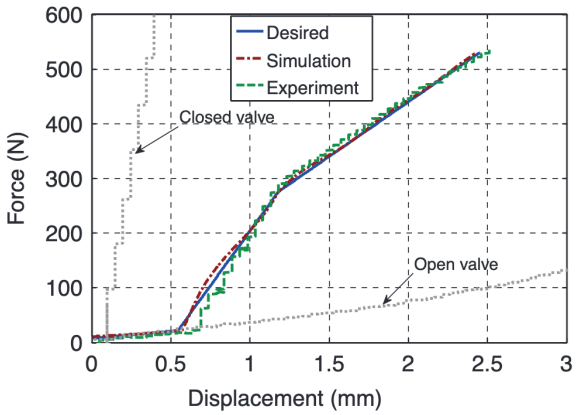

Fig. 24. Theory, simulation and experiment show resemblance in stiffness behaviour [33].

Fig. 25. The pneumatic fibres are embedded in soft matrix material to form a variable stiffness composite (left). A prototype is loaded in bending for both the soft (right, a) and stiff state (right, b) [34].

the valve is closed due to high bulk modulus of the fluid and soft when the fluid can flow freely when the valve is open. Between the closed state and the open state the stiffness can be controlled by controlling the fluid inlet with the valve.

In [31] the work from [30] is continued by experimental validation of analytical models. For a single tube the maximum to minimum stiffness ratio of 56, 27 MPa to 1.5 GPa was obtained experimentally. For a sheet of FMC composite a ratio of 21.8, 2.4 MPa to 52.4 MPa was obtained experimentally versus a ratio of 22.6, 1.9 MPa to 43 MPa, that was predicted analytically for tensile loading in the tube direction. Also all design parameters are discussed that influence the stiffness ratio and what values can be obtained based on variables as bulk modulus of the fluid, Poission's ratio, composite layup, thickness of liner around the tubes. In [32] different tube designs for FFMCs are explored. For different configurations the maximum to minimum stiffness ratios varied from 12.39 (92.538 MPa to 7.4686 MPa) to 15.178 (92.493 MPa to 6.0937 MPa) when tested in tension.

In [33] the work on fluidic flexible matrix composites of [30] and [31] is continued by investigating the active control of stiffness through control of the valves of a FFMC tube. Actively managing the fluid flow of the composite results in a variable stiffness composite with more states of stiffness than stiff or compliant. The closed loop control system was simulated and experimentally validated. The simulation and experiment showed similar results and the system could create a desired force displacement behaviour (fig. 24). Thus variable and controllable stiffness in a more custom form was obtained rather than a discrete system that is either stiff or compliant. In the experiment the tensile stiffness was varied from 20,000 N/m to 300,000 N/m to 150,000 N/m with a 2 second time span for each stiffness value.

- *Bending stiffness, pressurisation*

  In [34] a variable stiffness pneumatic morphing skin is presented for the application in aerospace applications. The concept is based on the idea of the variable stiffness composite presented in [30]. However in this case pneumatic variable stiffness fibers are used. The skin consists of a silicone rubber matrix with custom designed pneumatic muscle fibres which are connected by silk thread within the matrix (fig. 25). The silk thread keeps the distance between the fibres constant. The pneumatic fibres consist of a latex inner bladder surrounded by a braided sleeve. When pressurised the composite stiffens. The stiffness can be varied by controlling the pressure valve.The pressure value was varied from 0 to 0.4 MPa. Three distributed loads were applied: 560 Pa, 1640 Pa, 4239 Pa. The corresponding maximum to minimum stiffness ratios for transverse stiffness were respectively: 120, 19 and 5.83

- *Bending stiffness, fluidisation*

  In [35] a variable stiffness sandwich panel is presented. The panel consists of an aluminium honey comb core and outer layers consisting of a composite of FFMC tubes embedded in a soft matrix material (fig. 26). Control of the stiffness is regulated by the valve. A prototype beam was experimentally validated with a aluminium honeycomb core and a single tube on top of the honeycomb structure. For this prototype a maximum to minimum transverse stiffness ratio of 3.64 was obtained. The use of segmented tubes is also investigated through simulation. According to the theoretical analysis the use of segmented tubes can increase the maximum to minimum stiffness ratio to 60. The use of segmented beams would also allow for better control of multiple stiffness states.

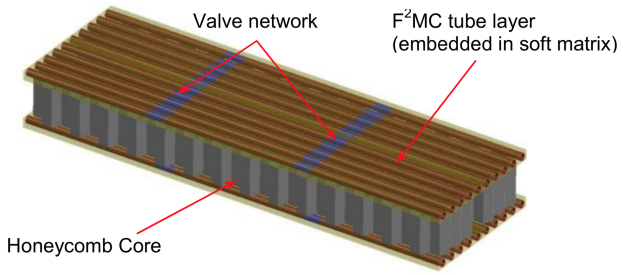

Fig. 26. An aluminium honey comb core is covered by face layers of a FFMC composite [35].

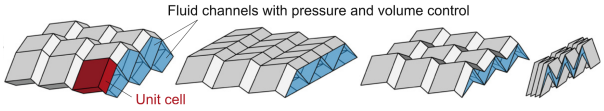

Fig. 27. Fluidisation can be done in any configuration of the origami structure [36].

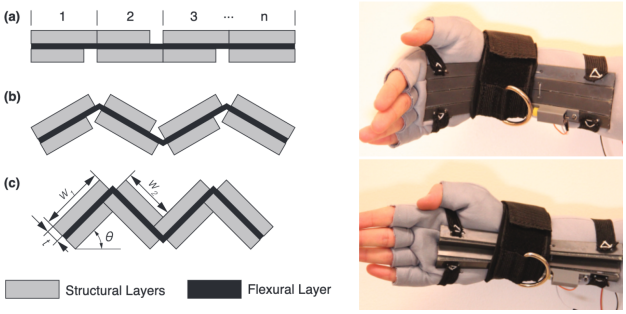

Fig. 28. The structure is pulled from the soft state (left, a) to the stiff state (left c). The structure embedded in a wrist support can allow (right, top) or resist (right, bottom) flexion of the wrist [37].

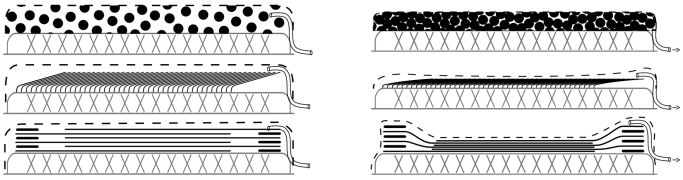

Fig. 29. The unjammed (left) vs. jammed configuration (right) is illustrated for a granular jamming beam (top), layer jamming beam with overlapping fish scales design (middle) and layer jamming beam with flat interleaved layers design (bottom) [38].

- *Unspecified stiffness, fluidisation*
  In [36] the concept of fluidic origami is presented. This concept is inspired by the fluidic flexible matrix composite tubes and the corresponding variable stiffness concepts. The novelty is to have origami Miura-Ori sheets that are connected at their creases such that the structure has chambers that can be fluidised (fig. 27). By fluidisation and valve control the stiffness can be varied and controlled as well as the shape. Therefore this concept has potential in variable stiffness as well shape morphing applications. Fluidic origami is also promising because the Miura-Ori sheets can take many different shapes while still containing chambers that can be fluidised. From simulation it was obtained that for various parameters could be tweaked such that the maximum to minimum stiffness ratio can reach up to a factor 1000. However the simulation showed that these larger order ratios are obtainable for design parameters with a relatively small lower bound stiffness.
- *Bending stiffness, tensile force*
  In [37] a design is presented for an origami based variable stiffness wrist support capable of switching from a stiff support in which the wrist cannot flex or extend to a compliant support which allows for flexion and extension. A three layer laminate consisting of 2 stiff segmented outer layers and a flexible inner layer can be pulled into a locked stiff corrugated configuration by pulling a tendon with an actuator (fig. 28). A maximum to minimum stiffness ratio of 44.9 was realised.
- *Bending stiffness, pressurisation*
  In [38] five prototype beam designs are explored with variable stiffness properties based on jamming. The underlying principle for the change in stiffness in jamming is the increase of internal friction through packing of the material particles caused by vacuum pressure (fig. 29). As a result a pressurised jammed structure is stiffer than the non pressurised configuration. All beams consist of a base beam to provide initial rigidity and a compartment with the jammable material inside. Two concepts were based on granular jamming with grounded coffee as the granular material. One has a cylindrical chamber for the jammable material and one has a conical compartment to provide more material near the base. Three concepts were based on layer jamming in which layers are packed together rather than particles. Three different layering patterns were used: a design based on overlapping fish scales, flat interleaved layers clamped on one end and horizontal layers with additional vertical closure segments. The layer jamming designs resulted in the best maximum to minimum stiffness ratios with a factor of 8 for the beam with interleaved horizontal layers and additional vertical closure segments. The worst ratio was obtained for the granular jamming beam with a cylindrical material chamber with a value of 2.2.
- *Bending stiffness, pressurisation*
  In [39] and [40] the concept of a variable stiffness joint is proposed for application in a variable stiffness snake-like manipulator through layer jamming. A stack of flaps on each side of the joint allows for stiffening of the joint in bending by being packed through a vacuum pressure (fig. 30). Apart from the variable stiffness joint a steerable snake-like manipulator is also proposed for the purpose of minimally invasive surgery. The layer jamming principle is applied in the skin of a steerable manipulator and serves

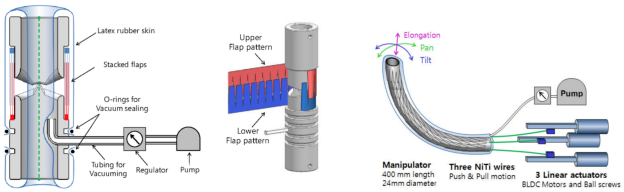

Fig. 30. Section view of the variable stiffness joint (left). Through pressurisation of the stacked flaps the joint can stiffen. The stacked flaps fully circumference the joint (middle). Application of stacked flaps in the skin of a steerable manipulator allows for stiffness control on demand (right) [39].

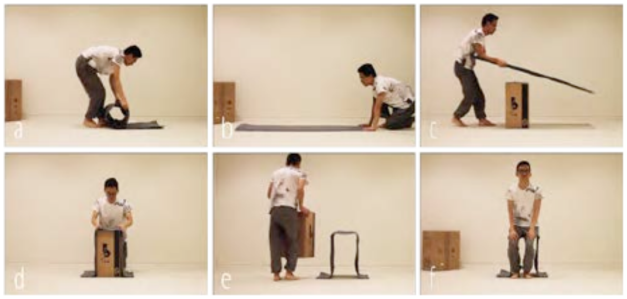

Fig. 31. A stool is set up from a reconfigurable surface that stiffens through the principle of jamming [41].

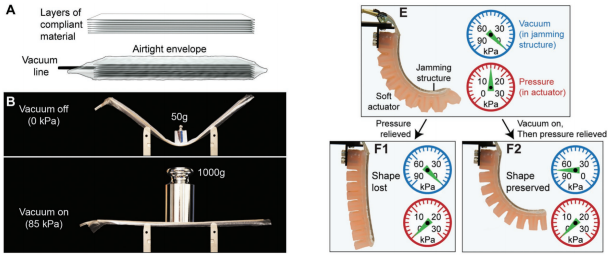

Fig. 32. The layer jamming envelope is tested in bending (left, bottom). The shape of the grasper can be actuated by positive pressure, while the stiffening is performed through application of a vacuum (right) [42].

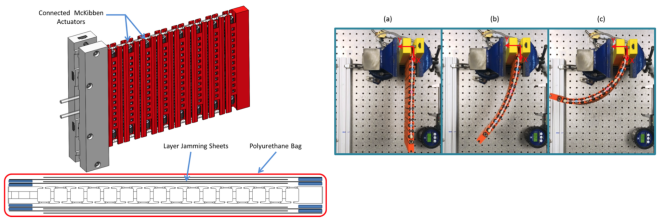

Fig. 33. The sheet contains McKibben actuators for morphing and layer jamming sheets for stiffening (left). The sheet is morphed from a straight state (right, a) to a curved state (right, c) [43].

to stiffen the entire manipulator on demand. In the soft mode the snake structure can be steered with 3 cables attached to linear actuators. The layer jamming capability of the skin allows for stiffening of the snake structure in any given configuration. The skin fully encloses the steerable manipulator.

- *Unspecified stiffness, pressurisation*
  In [41] applications of layer jamming in thin sheets are presented. Thin jamming sheets for variable stiffness allow for a variety of applications. Four concepts are experimentally tested: a variable stiffness display that can switch from open to private viewing mode, reconfigurable furniture (fig. 31) and shoes with variable stiffness cushioning by layer jamming in the insole. Additionally the option of memorising shapes through saving the required actuation pressure for the specific layer jamming application in software is explored. This allows for storage and reproduction of the preferred configuration of the application.
- *Bending stiffness & torsional stiffness, pressurisation*
  In [42] the principle of layer jamming is applied to a two finger grasper. The gripper consists of two fingers which each contain a layer jamming envelope and a positive pressure air chamber. The shape of the gripper is actuated by inflating the positive air chamber and the shape. The shape is then locked by increasing the stiffness through applying a vacuum to the jamming envelope (fig. 32). After applying the vacuum the bending stiffness of the finger became 32 times as large and the torsional stiffness became 2.7 times as large.
- *Bending stiffness, pressurisation*
  In [43] a concept is proposed for a structure with both variable stiffness as well as shape morphing properties through the use of layer jamming and McKibben actuators. The structure is a variable stiffness morphing sheet. Integrated McKibben actuators allow for shape morphing while the layer jamming allows for variable stiffness. The structure can be stiffened in any of the morphed configurations (fig. 33). The sheet can obtain multiple state of stiffness through the level of vacuum pressure. In the non-morphed state the largest maximum to minimum stiffness ratio was 57.04 which occurred at the strongest vacuum pressure tested. In the morphed state the structure was morphed and then stiffened. Two scenarios were tested: one with the pneumatic morphing McKibben actuators left on and one with the actuators left off. The highest maximum to minimum stiffness ratio was obtained with the actuators on and was 75.01. The maximum ratio obtained with non-active actuators was 63.05. Also the effect of the number of layers, either 4 or 6, was tested. It was found that for 6 layers the maximum loading force was higher, but that the maximum to minimum stiffness ratio was lower, which was attributed to a higher initial stiffness of the 6 layer structure.
- *Bending stiffness, pressurisation*
  In [44] the concept of granular jamming is applied to a finger support. A granular jamming beam is attached to a finger (fig. 34). In the soft state the finger can move as normal. When a vacuum pressure is applied the beams stiffen. This also reinforces the grip of the hand. However,

Fig. 34. A one finger prototype was made to resist motion of the finger in bending [44].

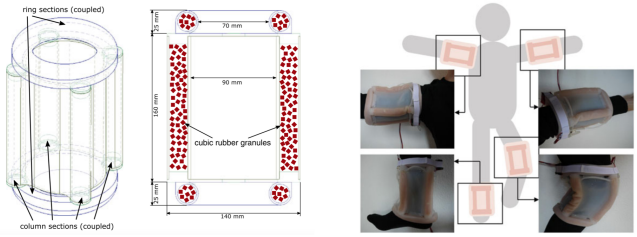

Fig. 35. The joint support has 4 column and 2 circuler jamming chamber (left). The support is designed for use at the ankle, knee, shoulder and elbow joint [45].

the one finger prototype proved to still deform when the finger performed slight motion on purpose.

- *Bending & torsional stiffness, pressurisation*
  In [45] a wearable variable stiffness body support for human joints is proposed for rehabilitation or "daily assistance of chronic biomechanical impairment" [45, p. 850]. The concept consists of a wearable silicone sleeve with six granular jamming chambers: four columns and two rings (fig. 35). The granular particles are made from rubber. The elastic silicone sleeve and soft rubber particles were selected to comfortably adapt to the anatomy of the user even in the stiff state. The shape is designed such that the device is suitable for different joints such as ankles, knees, shoulders and elbows. A small wearable pump and battery make for a fully wearable device. By applying a vacuum the ring and columns can stiffen on demand. By regulating the pressure the stiffness mode, bending or torsion, as well as the stiffness value can be controlled. The prototype system is connected to a smartphone which can be used for stiffness control. In bending the the maximum to minimum stiffness ratio was 4 with respective stiffness values of 0.0514 Nm/deg and 0.0134 Nm/deg. In torsion the maximum to minimum stiffness ratio was 1.4 with respective stiffness values of 0.0089 Nm/deg to 0.0064 Nm/deg.
- *Bending stiffness, pressurisation*
  In [46] a variable stiffness actuator based on granular jamming is proposed for application in a snake-like robot.

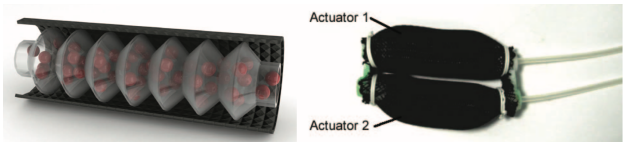

Fig. 36. The bellowed chamber (left) applied antagonistically (right) to allow for both stiffening and shape morphing [46].

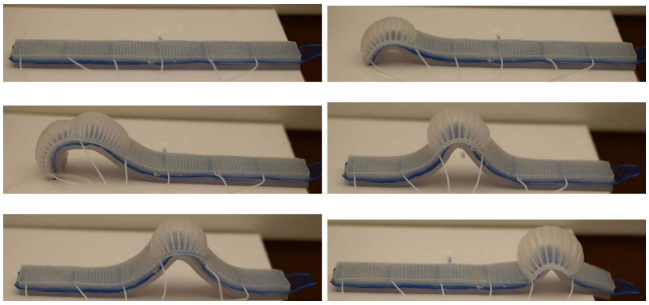

Fig. 37. From left to right, top to bottom: the structure is inflated on on the top side resulting in locomotion [47].

The actuator consists of two bellowed chambers filled with particles (fig. 36). By applying vacuum pressure to the bellowed chamber the actuator can stiffen, because of the particle jamming. The actuator also allows for the actuation of morphing. By applying a positive pressure to one of the bellowed chambers the actuator can bend. The actuator is alternatively subjected to both positive and negative pressure depending on the desired function of either morphing or stiffening. Morphing and stiffening are integrated such that the bending angle and curvature can both be controlled by one actuator. The largest increase in stiffness was 65% for the vacuumed state vs the non vacuumed state. In terms of morphing the maximum strain was 35%. Loads were in the range of 0 to 0.5 N.

- *Unspecified stiffness, pressurisation*
  In [47] a soft mechanism is presented based on inflatable unit cells that is capable of locomotion by pneumatic actuation. When inflated the cell bends one way. The mechanism uses inflatable unit cells mounted on two sides of a flat strip. By selectively inflating the mechanism can propel itself forward (fig. 37). Similar to the concept in [57] inflating unit cells on both cells antagonistically allows for increase of stiffness. Control of the morphing and variable stiffness is done through the use of pumps, valves, sensors and controllers.
- *Axial stiffness, pressurisation*
  In [48] a cellular structure for morphing wings actuated by air pressure is described. The structure consists of pressurisable honeycomb shaped chamber alternated by circular voids (fig. 38). An optimisation is proposed such that the structure can achieve a maximum one-dimensional strain with a zero Poisson's ratio. Simulation resulted in a 24% one dimensional strain. In terms of

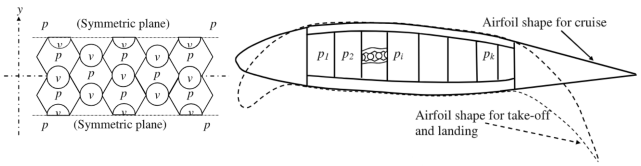

Fig. 38. The internal structure of pressurisable honeycombs alternating voids (left). Pressurisation of the structure causes the wing to morph to a shape that is tailored towards specific phases of the flight [48].

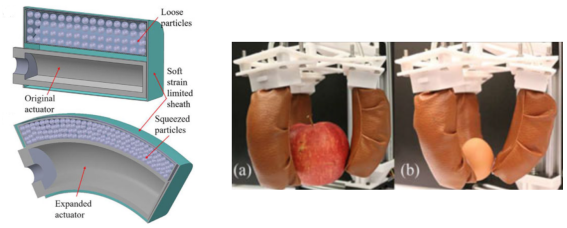

Fig. 39. Inflation of the air chamber results in jamming of the particles in the particle chamber on top (left). The concept is applied in a three finger gripper and was capable of holding objects from daily life (right) [49].

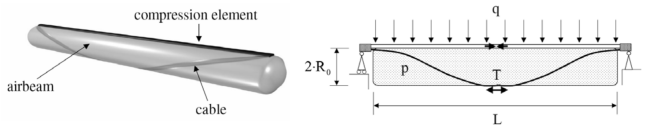

Fig. 40. The configuration of the inflatable airbeam, compression strut and cable (left) is such that the compression strut is always loaded in compression and the cable is always loaded in tension (right) [50].

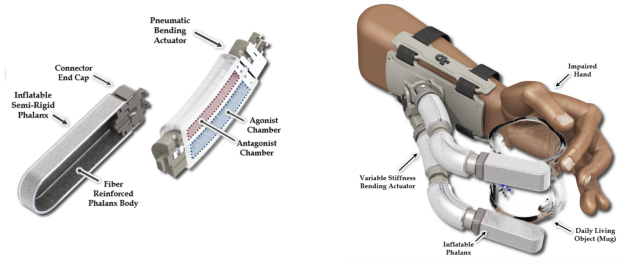

Fig. 41. Inflatable bending actuators adapt to the shape of the object and can be stiffened through further pressurisation (left). The fingertip-like phalanx is also pressurised for stiffening. The device is aimed at assisting in the task of holding objects in daily life (right) [52].

stiffness the structure is designed to carry aerodynamic loads in both the undeformed and deformed configuration. Rather than having increased or decreased stiffness when pressurised the variable stiffness in this concept lies in the property that when pressurised stiffness is decreased in tension and increased in compression.

- *Bending stiffness, pressurisation*
  In [49] the principle of particle jamming is used for the application of a gripper. Unlike other concepts based on jamming the gripper can go from a compliant state to a stiff state by applying positive pressure through inflation rather than by applying a vacuum (fig. 39). The particles are jammed by inflating of a chamber attached to the chamber in which the particles reside. When inflating from 20 kPa to 100 kPa the rotational stiffness increases from almost 0 to 1500 mNm / rad. Between 0 and 1500 mNm/rad the rotational stiffness can be varied by applying the appropriate amount of pressure.
- *Bending stiffness, pressurisation*
  In [50] the concept of tensairity is presented for structural elements and inflatable wings. Tensairity structures consists of an inflatable chamber that is supported by rigid elements which are purely loaded in compression or tension (fig. 40). This allows for deployable lightweight structures capable of much higher loads than purely inflatable structures without the weight penalty of traditional structural elements. In this article characteristics are explored for the aerospace applications of inflatable wings. In context of variable stiffness these structures have potential because they can go from practically zero stiffness in the deflated state to a structural support capable of carrying loads in the inflated state. Nowadays this concept is used in fully finalised current structural engineering applications [51].
- *Bending stiffness, pressurisation*
  In [52] a concept is proposed for a pneumatically actuated variable stiffness supernumerary grasp-assist device which helps patients with little force in their hands to perform activities in daily life. The key to the variable stiffness as well as the motion of the device lies in the pneumatic bending actuator. The bending actuator consists of an agonist and antagonist chamber (fig. 41). This allows for stiffening of the actuator but also the control of allowed motions. Additional variable stiffness is actuated by the semi-rigid phalanx which is an air chamber shaped like a finger which can be pressurised and thereby stiffened. The concept was experimentally validated with a prototype device being tested on its performance in stiffening as well its capability of grasping objects from daily life. Inflation of the phalanx showed only slight variability of stiffness when the pressure was varied from 0.0 kPa to 68.95 kPa. The stiffness of 5 N/cm to hold a mug was only obtained for certain phalanx dimensions. The order of magnitude for the different stiffnesses was around 5 N/cm for all different phalanx dimensions.
- *Axial stiffness, fluidisation and pressurisation*
  In [53] the concept of a variable stiffness McKibben actuator is proposed. The variable stiffness is obtained through filling the actuator with liquid to increase the stiffness. The system is soft in the pneumatic state and stiff in the hydraulic state. Because a full exchange of air and hydraulic fluid can be a challenge the system is designed such that it behaves fully compliant even

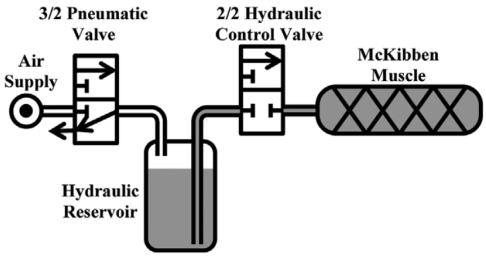

Fig. 42. A controlled system with valves and reservoirs allows for switching between the compliant and stiff mode whithout the need for a full exchange of air and hydraulic fluid [53].

when liquid is present (fig. 42). This is done by having a reservoir of air and a hydraulic reservoir. When in the compliant state the hydraulic valve is fully open. This allows the air to displace the hydraulic liquid freely in and out of the hydraulic reservoir. When in the hydraulic mode the valves are controlled such that all the air is vented or pushed out of the actuator, resulting in a fully hydraulic muscle. The actuator has two stiffness modes. It is either compliant when filled with air or stiff when filled with liquid. A prototype actuator was tested in both pneumatic as well as the hydraulic mode for 4 different tensile loads of 9.8 N, 19.6 N, 29.4 N, 39.2 N with respective pneumatic mode stiffness of 10.694 N/m, 12.542 N/m,11.967 N/m, 11.868 N/m and hydraulic mode stiffness values of 59.153 N/m, 69.851 N/m, 62.732 N/m, 63,593 N/m. This resulted in the respective maximum to minimum stiffness ratios of 4.53, 4.57, 4.24, 4.36.

- *Bending stiffness, electrostatic field*
  In [54] a variable stiffness sandwich beam is presented made of carbon fibre reinforced polymer (CFRP) with a dielectric layer on the inside connecting to an elastomer core. Similar to the concepts based on layer jamming the stiffness is increased by increasing the friction between the flexible layers. Unlike many jamming concepts that are actuated through pressurisation or fluidisation the friction is increased by application of an electrostatic field. When applying an electric field the shear stress between the dielectric layers and the core increases resulting in higher bending stiffness. The ratio of maximum to minimum bending stiffness is 18. Continued work in [55] found that the electrostatic forces have relatively short range which makes these less of a hazard.
- *Bending & axial stiffness, electrostatic field*
  In [56] the concept of electrostatic layer jamming is proposed for applications in soft robotics. The layers consist of electrodes surrounded by electric insulation. When applying a voltage to the electrodes the layers will attract (fig. 43). The amount of electrodes per layer allow for tuning of the variable stiffness characteristics. The amount of applied voltage allows for multiple states of stiffness rather than one compliant and one stiff state. A

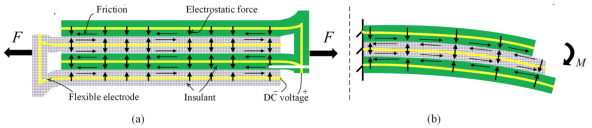

Fig. 43. The application of an electric field increases the friction between layers resulting in increased axial (a) and bending stiffness (b) [56].

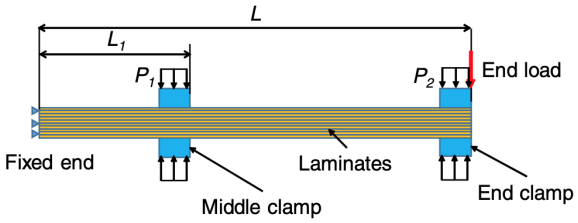

Fig. 44. Pressure clamps can control stiffness by their exerted force and their location along the beam [57].

prototype with five layers was experimentally validated and tested for both tensile and bending stiffness. The largest maximum to minimum stiffness ratio of 7 was obtained in bending at an applied voltage of 2000V. Furthermore in [56] the concept of electric layer jamming is implemented in a prototype of a soft robotic gripper. The gripper morphs through pressurisation and stiffens through electrostatic jamming. The prototype was capable of holding a cup.

- *Bending stiffness, force clamping*
  In [57] a variable stiffness layer jamming mechanism is presented based on pressure clamps. Similar to layer jamming concepts actuated by pressurisation the beam transitions from a soft to a stiff state by the increase of friction between the layers. However, the novelty is the use of pressure clamps placed at multiple spots along the beam (fig. 44). This omits issues of leakages in jamming concepts based on pressurisation or fluidisation and allows for multiple stiffness states by control the clamps. A system with two clamps and ten layers is experimentally validated and was capable of maximum to minimum stiffness ratio of 17. From numerical simulations it is expected that for a four clamp system the maximum to minimum stiffness ratio can reach a value of 46.

*4) **Changing stiffness by changing boundary conditions**:*

- *Bending stiffness, rotation*
  In [58] a variable stiffness compliant leaf hinge is proposed. The hinge allows for one degree of freedom rotation and has a different bending stiffness depending on the angle of rotation. When in bending the joint flexure becomes supported by different point contacts which results in a redefined bending stiffness of the flexure because the effective elastic length is changed (fig. 45). Compared to other variable stiffness solutions this joint is unique in the sense that its deformation when loaded

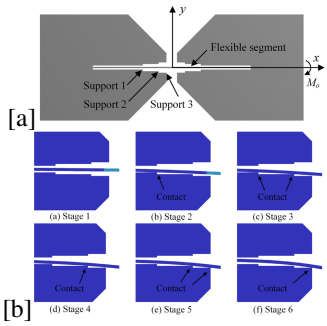

Fig. 45. The flexure has 3 supports on each side (a). The 6 total support points offer 6 stages of stiffness (b) [58].

defines the stiffness rather than an external stimulus. This omits the need for external power and actuators but also limits the controllability of the joint stiffness. A 3D model was made and the stiffness variation was simulated. The linear and non-linear simulation methods resulted in 6 different stiffness values over 6 phases of the rotation. The non linear and linear simulation method showed similar orders of magnitude for each phase of the rotation. The nonlinear analysis showed stiffness values from 222.22 Nmm/rad to 2267.32 Nmm/rad and the linear method resulted in stiffnesses between 222.22 Nmm/rad and 2248.06 Nmm/rad. For both the linear and non linear case the maximum to minimum stiffness ratio was about 10. The nonlinear method resulted in stiffnesses of respectively 222.22 Nmm/rad, 423.35 Nmm/rad, 974.19, 593.17 Nmm/rad, 2267.32 Nmm/rad, 743.76 Nmm/rad and the linear method showed similar orders of magnitude with respectively 222.22 Nmm/rad, 423.28 Nmm/rad, 972.97 Nmm/rad, 592.59 Nmm/rad, 2248.06 Nmm/rad, 740.74 Nmm/rad.

B. Performance overview and comparison

Tables II, III, IV and V present a comparison of performance for the concepts found. The maximum to minimum stiffness ratios are listed as stated by the corresponding article. When no ratios are presented the stiffness ratio is labeled as unspecified. Next the type of variable stiffness is listed as bending, torsional, axial, shear or unspecified. Each concept is labeled according to type of stiffness that is focussed on in the corresponding article. The term unspecified is used because certain articles only present concepts on variable stiffness and not the type of stiffness. The continuity of stiffness lists whether the concepts can vary its stiffness in a way that is binary, multistate or continuous. Binary concepts can adopt either a stiff or compliant state. Multistate concepts can adopt a discrete number of stiffness states that are more than two. Continuous concepts can adopt any state of stiffness between a lower and upper bound. The transition time describes the order of magnitude for the time required to transition from one state of stiffness to another. Terms with an (*) are estimations made based on similarity to other concepts that do state their transition time. When no values are presented in the article and the concept is not similar to others the transition time is labeled as unspecified. Additionally the table lists whether the concept is stiff or compliant in its non-actuated state. Several concepts are labeled as neutral because they only require actuation to change their stiffness but when non-actuated they can reside in either a compliant or stiff state depending on the exact configuration.

Next, each concept is assigned a NASA Technology Readiness Level [59]. These provide a qualitative indication on technology readiness through an internationally recognised scale. However it should be noted that these remain qualitative guidelines and therefore the exact level should be considered as the author's view rather than an absolute measure.

Finally, due to the performance comparison covering concepts across various disciplines, it may lack the comparison of essential features for certain fields of applications. The column with side notes serves to illustrate the properties that should be regarded as the major drawbacks.

*1) **Performance: Changing stiffness by changing material properties (table II)**:* Within the material branch most concepts utilised shape memory polymers and their stiff to soft transition when heated. All SMP based solutions soften by being heated above the glass transition temperature by electrical resistance heating. Bending stiffness is the most explored type of stiffness, but concepts focussed on torsional, axial and shear stiffness are present. Also most concepts are either stiff or compliant without stiffness modes in between. The transition takes several minutes for most concepts. An exception is the SMP coated carbon fibre composite which only takes several seconds due to the SMP just being used for the coating rather than for the matrix of the composite. As a result most concepts in this branch were stiff in the unactuated state and became compliant when actuated. Also the majority of concepts only had two stiffness states, either stiff or compliant, and most had a relatively long transition time in the order of minutes. All SMP based concepts are stiff when non-actuated. The variable stiffness probe is the only concept that is compliant in its non-actuated state.

*2) **Performance: Changing stiffness by changing shape (table III)**:* Within the shape branch concepts were relatively low in technology readiness. The concepts were mostly explored by simulations or were basic prototypes far from an application level. Because of most work being performed on a fundamental level little quantitative data was available on maximum to minimum stiffness ratios and exact types of variable stiffness were unspecified. Like the SMP based concepts in the material branch the SMP hinged origami takes several minutes to transition. The other concepts have transition times in the order of seconds. The concepts presented in coupled Miura-ori tubes, stacked Miura-ori sheets and the variable cross section wing box are labelled as neutral when non-actuated because they only require actuation for the change of stiffness rather than for maintaining the state of stiffness.

*3) **Performance: Changing stiffness by changing prestress (table IV)**:* The prestress branch contained the largest number

TABLE II
MATERIAL PROPERTIES BRANCH: PERFORMANCE OVERVIEW

Concept	max. to min. stiffness ratio	stiffness type	continuity	transition time	stimulus	NASA TRL	stiffness non actuated	side notes
segmented SMP beam [8]	15 - 77	bending, axial	binary	minutes	heat	2	stiff	unspecified actuation requirements
platelet SMP beam [9]	unspecified	shear	binary	minutes	heat	2	stiff	little detail of stiffness behaviour
robotic material [10]	unspecified	bending	multistate	minutes	heat	3	stiff	complex electronic systems
SMP coated fibre composite [11]	8	bending	binary	seconds	heat	3	stiff	purely a material
SMP shear coupling beam [12], [13], [14]	2.03 - 3.2	bending	binary	minutes	heat	3	stiff	large heating requirements
SMP laminate [15]	10	bending, torsional	binary	minutes	heat	4	stiff	large heating requirements
LMPA channel composite [16]	25	bending	binary	seconds	heat	4	stiff	small scale
SMP fibre fabric [17]	10	bending	binary	seconds	heat	4	stiff	high temperature at skin
shear centre shifting [18]	unspecified	bending, torsional	binary	unspecified	heat	3	stiff	unspecified actuation requirements
MRE beam [19]	unspecified	bending	binary	unspecified	magnetic field	2	compliant	magnetic interference
gallium probe [21]	5	bending	binary	minutes	heat	5	compliant	use of gallium

TABLE III
SHAPE BRANCH: PERFORMANCE OVERVIEW

Concept	max. to min. stiffness ratio	stiffness type	continuity	transition time	stimulus	NASA TRL	stiffness non actuated	side notes
SMP origami [22]	unspecified	unspecified	binary	minutes	heat	3	stiff	no specific guideline towards stiffness design
coupled tubes Miura-ori [23]	unspecified	unspecified	multistate	seconds*	displacement	3	neutral	complex switching between stiffness states
stacked sheets Miura-ori [24]	unspecified	unspecified	multistate	seconds*	folding	2	neutral	far from application level
multistable wing [25]	unspecified	bending	binary	seconds*	aerodynamic load	3	stiff	lower stiffness bound is zero stiffness
wing box variable cross-section [26]	unspecified	torsional	continuous	seconds*	displacement	2	neutral	large displacement required

of concepts of all four branches. Within the branch clear clusters of topics can be observed. A first sub class can be distinguished by concepts based on layer jamming to increase stiffness by increasing the moment on inertia. A second class can be formed by the concepts on fluidic flexible matrix composites and pneumatics. A third class can be formed by all concepts based on layer jamming and granular jamming through pressurisation. A final sub class can be formed by the two concepts based on layer jamming through the application of an electric field. All concepts are compliant in the non-actuated state. 9 out of 25 concepts were specified as requiring seconds to transition to a stiff state. The other 16 concepts were estimated to transition in a number of seconds because their working principle resembled concepts that did specify these values. Most concepts based on prestress offer various states of stiffness.

*4) **Performance: Changing stiffness by changing boundary conditions (table V)**:* The branch of boundary conditions yielded one result. Unlike concepts in the other branches the concept does not require separate actuation for the change in stiffness like heat, pressurisation, fluidisation or application of magnetic or electric fields. However its variable stiffness depends on the angle of rotation. Thus the hinge cannot be stiffened in any configuration. In terms of transition time it takes several seconds to rotate the hinge and obtain increased bending stiffness.

TABLE IV
PRESTRESS BRANCH: PERFORMANCE OVERVIEW

Concept	max. to min. stiffness ratio	stiffness type	continuity	transition time	stimulus	NASA TRL	stiffness non actuated	side notes
variable moment of inertia layer beam form closure [27] [29]	5.6	bending	multistate	seconds*	form closure	3	compliant	form closure requires thick structure
variable moment of inertia layer beam SMA control [28]	18.5	bending	multistate	seconds*	heat	3	compliant	complex manufacturing
FFMC tube [30], [31]	56	bending	continuous	seconds	fluidisation	3	compliant	fluid leakage, pump required
FFMC composite [32], [33]	21.8	bending	multistate	seconds	fluidisation	4	compliant	fluid leakage, pump required
pneumatic morphing skin [34]	120	bending	multistate	seconds*	pressurisation	4	compliant	air tightness, pump required
FFMC sandwich beam [35]	3.64	bending	binary	seconds*	fluidisation	3	compliant	fluid leakage, pump
fluidic origami [36]	1000	unspecified	continuous	seconds*	fluidisation	2	compliant	only fundamentally developed
origami wrist support [37]	44.9	bending	binary	seconds	tensile force	4	compliant	cable pulling required
granular & layer jamming beams [38]	2.2 - 8	bending	binary	seconds*	pressurisation	3	compliant	vacuum, air tightness pump required
layer jamming joint snake manipulator [39], [40]	unspecified	bending	binary	seconds*	pressurisation	3	compliant	vacuum, air tightness pump required
thin sheets layer jamming [41]	unspecified	unspecified	multistate	seconds*	pressurisation	4	compliant	vacuum, air tightness pump required
jamming gripper [42]	32 (bending) 7 (torsion)	bending, torsional	multistate	seconds*	pressurisation	3	compliant	vacuum, air tightness pump required
layer jamming McKibben panel [43]	30.67 - 75.01	bending	multistate	seconds	pressurisation	4	compliant	vacuum, air tightness pump required
jamming finger support [44]	unspecified	bending	binary	seconds*	pressurisation	3	compliant	vacuum, air tightness pump required
jamming joint support [45]	4 (bending) 1.4 (torsion)	bending, torsional	multistate	seconds	pressurisation	4	compliant	vacuum, air tightness pump required
antagonistic jamming integrated actuator [46]	1.65	bending	multistate	seconds*	pressurisation	3	compliant	positive and negative pressure required
antagonistic inflatable strip [47]	unspecified	unspecified	multistate	seconds	pressurisation	3	compliant	air tightness pump required
cellular wing structure [48]	unspecified	axial	multistate	minutes	pressurisation	3	neutral	air tightness pump required
jamming gripper positive pressure [49]	6	bending	continuous	seconds*	pressurisation	5	compliant	air tightness pump required
tensairity [50]	unspecified	bending	binary	seconds*	pressurisation	9	compliant	no stiffness in deflated state
antagonistic grasp assist [52]	unspecified	bending	continuous	seconds	pressurisation	4	compliant	small scale
hydraulic pneumatic McKibben actuator [53]	4.24 - 4.53	axial	binary	seconds	pressurisation, fluidisation	3	compliant	air tightness pump required
dielectric stiffening [54], [55]	18	bending	binary	seconds*	electrostatic field	3	compliant	requires voltage of 3000V
electrostatic jamming [56]	7	bending, axial	multistate	seconds*	electrostatic field	4	compliant	requires voltage of 2000V
clamp jamming [57]	17	bending	multistate	seconds*	compressive force	3	compliant	mechanical clamps required

TABLE V
BOUNDARY CONDITIONS BRANCH: PERFORMANCE OVERVIEW

Concept	max. to min. stiffness ratio	stiffness type	continuity	transition time	stimulus	NASA TRL	stiffness non actuated	side notes
filleted leaf hinge [58]	10	bending	multistate	seconds	rotation	2	compliant	stiffness depends on angle of rotation

IV. Discussion

The first aim of this literature review is to form a cross disciplinary review of variable stiffness structures through a classification of the variable stiffness mode and the working principle. For researchers of future applications in a certain scientific field this cross disciplinary review allows for easy identification of relevant concepts in other fields. These concepts may otherwise be overlooked because of unfamiliarity with these other fields of research.

Additionally the classification on the major stiffness modes of bending, torsional, axial and shear stiffness allows for easy identification of relevant concepts for the preferred mode of variable stiffness.

The solution space resulting from the categorization shows which types of variable stiffness are heavily explored and which ones are not. The emphasis on these stiffness types can trigger the extrapolation of concepts meant for variation of one type of stiffness to a different type of stiffness.

A disadvantage of the broad classification adopted in this review is that many concepts end up being packed in the same influence branch. When screening the concepts within the influence branch it can be observed that classification through additional sub categories may be suitable. For example the prestress branch contains several concepts based on layer jamming. When searching literature having additional sub categories could result in the discovery of more concepts through the exploitation of these sub categories in the search strategy.

Due to its broadness the classification proposed in this review does not clearly identify gaps in literature that are physically impossible or gaps that are possible but not explored. Classifications can be made such that they provide insight on the characteristics of concepts that could fill these gaps. Rather, the classification in this review globally identifies which types of variable stiffness are more heavily investigated and through which main influence factor.

The second aim of this review is to provide an indication, comparison and overview of the performance characteristics of these concepts for future applications. The comparison presented does provide global insight in design properties. However these are defined such that they could be derived for a large number of articles that all have various ways of presenting their performance stats. As a result the performance comparison does not show more in depth stats essential to researchers and designers of variable stiffness applications. For example the scale of the variable stiffness range is essential for future applications and could be a desired first filter to find relevant concepts. Due to the different definitions and experimental methods across articles it is a challenge to score them all with the same performance characteristic. The same holds for properties as energy actuation requirements or coupling behaviour between stiffness modes.

Also, due to the performance comparison being a broad comparison across various disciplines, it may lack essential features for certain fields of applications. The column with side notes serves to illustrate the properties that should be regarded as the major obstacles to overcome, it should be noted that the side notes remain a global indication of drawbacks.

Also from the the comparison it can be observed that maximum to minimum stiffness ratios vary a lot. However the larger values generally belong to concepts that are more fundamental with corresponding lower levels of technology readiness. Articles discussing these more fundamental concepts generally only present results based on simulations with many different parameters. The performances that are most heavily emphasised are often valid for a specific optimal case. In the form of a more advanced prototype the concept may be capable of only slightly achieving the performance of the presented optimal values. The more technologically advanced concepts present performances in the lower end of the value range for the stats presented in the performance comparison. However these lower end values are more realistic for the actual applications.

Also, many concepts are still far from the maximum NASA technology readiness level of 9 which means the majority of concepts are far from a fully functioning application. This implies that the field of variable stiffness research is still in a fairly conceptual phase. Therefore it is expected that many practical issues are yet unsolved and long term testing is often yet to be performed.

V. Conclusion

The aim of this review is to (i) form a cross disciplinary review of variable stiffness structures through a classification of the variable stiffness mode and working principle, (ii) provide an indication, comparison and overview of the performance characteristics of these concepts for future applications. A classification is proposed based on four factors that when varied result in a varied stiffness of a structure: (1) material properties, (2) shape, (3) prestress and (4) boundary conditions and four types of stiffness: (1) bending stiffness, (2) torsional stiffness, (3) axial stiffness and (4) shear stiffness. A third dimension of actuation stimulus is filled out through the literature found and is not a classification method itself.

The scope of the classification yielded concepts from various areas of research. The majority, 28 out of 48 concepts, focussed on varying stiffness through the application of prestress of which 20 focussed on bending stiffness. 14 concepts were appointed to the material branch, 5 to the shape branch and 1 to the boundary conditions branch. Overall 32 concepts were focussed on variable bending stiffness and a total of 16 were focussed on variable torsional, axial and shear stiffness.

Within the material branch most concepts utilised shape memory polymers and their stiff to soft transition by being heated above their glass transition temperature. The majority of concepts had two stiffness states, either stiff or compliant, and most had a relatively long transition time in the order of minutes.

Within the shape branch concepts were relatively low in technology readiness and provided data based on simulations or experiments on a fundamental level far from an application

level. This resulted in little quantitative data for maximum to minimum stiffness ratios.

The prestress branch contained the largest number of concepts. Within the branch clear clusters of topics could be observed: layer jamming to change stiffness by increasing the moment on inertia, fluidic flexible matrix composites, pneumatics and layer jamming and granular jamming based on pressurisation.

The branch of boundary conditions yielded one result which had a variable stiffness that, unlike most other concepts, is not dependent on an external stimulus.

Overall most work appeared to be in a rather fundamental phase of development. The concepts with most promising properties are mostly on the fundamental side of the technology readiness scale. The concepts that are further advanced present less ideal values and bring various drawbacks that need to be tackled before the concepts are fully ready for application.

Future work could focus on the classification of sub categorisations such that gaps in literature are not just identified but are suitable for providing perspective on how they can be filled. Also more universal scoring factors to review and compare the performance of the concepts in literature could help in presenting a more refined overview of performance for those seeking to use variable stiffness concepts in new applications.

REFERENCES

[1] S. Barbarino, O. Bilgen, R. M. Ajaj, M. I. Friswell, and D. J. Inman, "A review of morphing aircraft," *Journal of intelligent material systems and structures*, vol. 22, no. 9, pp. 823–877, 2011.

[2] I. K. Kuder, A. F. Arrieta, W. E. Raither, and P. Ermanni, "Variable stiffness material and structural concepts for morphing applications," *Progress in Aerospace Sciences*, vol. 63, pp. 33–55, 2013.

[3] J. Sun, Q. Guan, Y. Liu, and J. Leng, "Morphing aircraft based on smart materials and structures: A state-of-the-art review," *Journal of Intelligent material systems and structures*, vol. 27, no. 17, pp. 2289–2312, 2016.

[4] Y.-J. Kim, S. Cheng, S. Kim, and K. Iagnemma, "A stiffness-adjustable hyperredundant manipulator using a variable neutral-line mechanism for minimally invasive surgery," *IEEE transactions on robotics*, vol. 30, no. 2, pp. 382–395, 2013.

[5] L. Blanc, A. Delchambre, and P. Lambert, "Flexible medical devices: review of controllable stiffness solutions," in *Actuators*, vol. 6, no. 3. Multidisciplinary Digital Publishing Institute, 2017, p. 23.

[6] M. Manti, V. Cacucciolo, and M. Cianchetti, "Stiffening in soft robotics: A review of the state of the art," *IEEE Robotics & Automation Magazine*, vol. 23, no. 3, pp. 93–106, 2016.

[7] M. A. McEvoy and N. Correll, "Materials that couple sensing, actuation, computation, and communication," *Science*, vol. 347, no. 6228, p. 1261689, 2015.

[8] G. McKnight and C. Henry, "Variable stiffness materials for reconfigurable surface applications," in *Smart Structures and Materials 2005: Active Materials: Behavior and Mechanics*, vol. 5761. International Society for Optics and Photonics, 2005, pp. 119–126.

[9] ——, "Large strain variable stiffness composites for shear deformations with applications to morphing aircraft skins," in *Behavior and Mechanics of Multifunctional and Composite Materials 2008*, vol. 6929. International Society for Optics and Photonics, 2008, p. 692919.

[10] M. A. McEvoy, N. Farrow, and N. Correll, "Robotic materials with controllable stiffness," in *Proceedings of the 19th International Conference on Composite Materials (ICCM)*, 2013.

[11] C. Tridech, H. A. Maples, P. Robinson, and A. Bismarck, "High performance composites with active stiffness control," *ACS applied materials & interfaces*, vol. 5, no. 18, pp. 9111–9119, 2013.

[12] F. Gandhi and S.-G. Kang, "Beams with controllable flexural stiffness," *Smart Materials and Structures*, vol. 16, no. 4, p. 1179, 2007.

[13] F. Gandhi, G. Murray, and S.-G. Kang, "Flexural stiffness control of multi-layered beams," in *49th AIAA/ASME/ASCE/AHS/ASC Structures, Structural Dynamics, and Materials Conference, 16th AIAA/ASME/AHS Adaptive Structures Conference, 10th AIAA Non-Deterministic Approaches Conference, 9th AIAA Gossamer Spacecraft Forum, 4th AIAA Multidisciplinary Design Optimization Specialists Conference*, 2008, p. 2205.

[14] G. Murray and F. Gandhi, "Multi-layered controllable stiffness beams for morphing: energy, actuation force, and material strain considerations," *Smart Materials and Structures*, vol. 19, no. 4, p. 045002, 2010.

[15] W. Raither, A. Bergamini, F. Gandhi, and P. Ermanni, "Adaptive bending-twist coupling in laminated composite plates by controllable shear stress transfer," *Composites Part A: Applied Science and Manufacturing*, vol. 43, no. 10, pp. 1709–1716, 2012.

[16] B. E. Schubert and D. Floreano, "Variable stiffness material based on rigid low-melting-point-alloy microstructures embedded in soft poly (dimethylsiloxane)(pdms)," *Rsc Advances*, vol. 3, no. 46, pp. 24 671–24 679, 2013.

[17] T. P. Chenal, J. C. Case, J. Paik, and R. K. Kramer, "Variable stiffness fabrics with embedded shape memory materials for wearable applications," in *2014 IEEE/RSJ International Conference on Intelligent Robots and Systems*. IEEE, 2014, pp. 2827–2831.

[18] W. Raither, A. Bergamini, and P. Ermanni, "Profile beams with adaptive bending–twist coupling by adjustable shear centre location," *Journal of intelligent material systems and structures*, vol. 24, no. 3, pp. 334–346, 2013.

[19] G. Y. Zhou and Q. Wang, "Magnetorheological elastomer-based smart sandwich beams with nonconductive skins," *Smart Materials and Structures*, vol. 14, no. 5, p. 1001, 2005.

[20] G. Zhou and Q. Wang, "Use of magnetorheological elastomer in an adaptive sandwich beam with conductive skins. part i: Magnetoelastic loads in conductive skins," *International Journal of Solids and Structures*, vol. 43, no. 17, pp. 5386–5402, 2006.

[21] X. Wen, B. Wang, S. Huang, M.-S. Lee, P.-S. Chung, Y. T. Chow, I.-W. Huang, H. G. Monbouquette, N. T. Maidment, P.-Y. Chiou *et al.*, "Flexible, multifunctional neural probe with liquid metal enabled, ultra-large tunable stiffness for deep-brain chemical sensing and agent delivery," *Biosensors and Bioelectronics*, vol. 131, pp. 37–45, 2019.

[22] M. R. Garza, E. A. Peraza-Hernandez, and D. J. Hartl, "Self-folding origami surfaces of non-zero gaussian curvature," in *Behavior and Mechanics of Multifunctional Materials XIII*, vol. 10968. International Society for Optics and Photonics, 2019, p. 109680R.

[23] E. T. Filipov, T. Tachi, and G. H. Paulino, "Origami tubes assembled into stiff, yet reconfigurable structures and metamaterials," *Proceedings of the National Academy of Sciences*, vol. 112, no. 40, pp. 12 321–12 326, 2015.

[24] G. Park, S. Sengupta, and S. Li, "Multi-stability and variable stiffness of cellular solids designed based on origami patterns," in *SPIE Proceedings*, vol. 10164, 2017.

[25] F. Mattioni, P. M. Weaver, K. D. Potter, and M. I. Friswell, "The application of thermally induced multistable composites to morphing aircraft structures," in *Industrial and Commercial Applications of Smart Structures Technologies 2008*, vol. 6930. International Society for Optics and Photonics, 2008, p. 693012.

[26] R. Ajaj, M. Friswell, W. Dettmer, A. Isikveren, and G. Allegri, "Conceptual modeling of an adaptive torsion wing structure," in *52nd AIAA/ASME/ASCE/AHS/ASC Structures, Structural Dynamics and Materials Conference 19th AIAA/ASME/AHS Adaptive Structures Conference 13t*, 2011, p. 1883.

[27] M. Henke, J. Sorber, and G. Gerlach, "Multi-layer beam with variable stiffness based on electroactive polymers," in *Electroactive Polymer Actuators and Devices (EAPAD) 2012*, vol. 8340. International Society for Optics and Photonics, 2012, p. 83401P.

[28] M. Henke and G. Gerlach, "On a high-potential variable flexural stiffness device," in *Smart Sensors, Actuators, and MEMS VI*, vol. 8763. International Society for Optics and Photonics, 2013, p. 876312.

[29] ——, "A multi-layered variable stiffness device based on smart form closure actuators," *Journal of Intelligent Material Systems and Structures*, vol. 27, no. 3, pp. 375–383, 2016.

[30] M. Philen, Y. Shan, C. Bakis, K.-W. Wang, and C. Rahn, "Variable stiffness adaptive structures utilizing hydraulically pressurized flexible matrix composites with valve control," in *47th*

AIAA/ASME/ASCE/AHS/ASC Structures, Structural Dynamics, and Materials Conference 14th AIAA/ASME/AHS Adaptive Structures Conference 7th, 2006, p. 2134.

[31] Y. Shan, M. Philen, A. Lotfi, S. Li, C. E. Bakis, C. D. Rahn, and K.-W. Wang, "Variable stiffness structures utilizing fluidic flexible matrix composites," *Journal of Intelligent Material Systems and Structures*, vol. 20, no. 4, pp. 443–456, 2009.

[32] Y. Chen, J. Sun, Y. Liu, and J. Leng, "Experiment and analysis of fluidic flexible matrix composite (f2mc) tube," *Journal of intelligent material systems and structures*, vol. 23, no. 3, pp. 279–290, 2012.

[33] M. Philen, "Force tracking control of fluidic flexible matrix composite variable stiffness structures," *Journal of Intelligent Material Systems and Structures*, vol. 22, no. 1, pp. 31–43, 2011.

[34] Y. Chen, W. Yin, Y. Liu, and J. Leng, "Structural design and analysis of morphing skin embedded with pneumatic muscle fibers," *Smart Materials and Structures*, vol. 20, no. 8, p. 085033, 2011.

[35] S. Li, A. Lotfi, Y. Shan, K. Wang, C. D. Rahn, and C. E. Bakis, "A variable transverse stiffness sandwich structure using fluidic flexible matrix composites (f2mc)," in *Active and Passive Smart Structures and Integrated Systems 2008*, vol. 6928. International Society for Optics and Photonics, 2008, p. 69280M.

[36] S. Li and K. Wang, "Fluidic origami: a plant-inspired adaptive structure with shape morphing and stiffness tuning," *Smart Materials and Structures*, vol. 24, no. 10, p. 105031, 2015.

[37] M. B. Oliveira, C. Liu, M. Zhao, and S. M. Felton, "Design of a variable stiffness wrist brace with an origami structural element," in *ASME 2018 Conference on Smart Materials, Adaptive Structures and Intelligent Systems*. American Society of Mechanical Engineers Digital Collection, 2018.

[38] V. Wall, R. Deimel, and O. Brock, "Selective stiffening of soft actuators based on jamming," in *2015 IEEE International Conference on Robotics and Automation (ICRA)*. IEEE, 2015, pp. 252–257.

[39] Y.-J. Kim, S. Cheng, S. Kim, and K. Iagnemma, "Design of a tubular snake-like manipulator with stiffening capability by layer jamming," in *2012 IEEE/RSJ International Conference on Intelligent Robots and Systems*. IEEE, 2012, pp. 4251–4256.

[40] ——, "A novel layer jamming mechanism with tunable stiffness capability for minimally invasive surgery," *IEEE Transactions on Robotics*, vol. 29, no. 4, pp. 1031–1042, 2013.

[41] J. Ou, L. Yao, D. Tauber, J. Steimle, R. Niiyama, and H. Ishii, "jamsheets: thin interfaces with tunable stiffness enabled by layer jamming," in *Proceedings of the 8th International Conference on Tangible, Embedded and Embodied Interaction*, 2014, pp. 65–72.

[42] Y. S. Narang, J. J. Vlassak, and R. D. Howe, "Mechanically versatile soft machines through laminar jamming," *Advanced Functional Materials*, vol. 28, no. 17, p. 1707136, 2018.

[43] C. Mikol and H.-J. Su, "An actively controlled variable stiffness structure via layer jamming and pneumatic actuation," in *2019 International Conference on Robotics and Automation (ICRA)*. IEEE, 2019, pp. 7555–7561.

[44] E. Thompson-Bean, O. Steiner, and A. McDaid, "A soft robotic exoskeleton utilizing granular jamming," in *2015 IEEE International Conference On Advanced Intelligent Mechatronics (AIM)*. IEEE, 2015, pp. 165–170.

[45] S. Hauser, M. Robertson, A. Ijspeert, and J. Paik, "Jammjoint: A variable stiffness device based on granular jamming for wearable joint support," *IEEE Robotics and Automation Letters*, vol. 2, no. 2, pp. 849–855, 2017.

[46] A. Jiang, S. Adejokun, A. Faragasso, K. Althoefer, T. Nanayakkara, and P. Dasgupta, "The granular jamming integrated actuator," in *2014 International Conference on Advanced Robotics and Intelligent Systems (ARIS)*. IEEE, 2014, pp. 12–17.

[47] N. Correll, Ç. D. Önal, H. Liang, E. Schoenfeld, and D. Rus, "Soft autonomous materials—using active elasticity and embedded distributed computation," in *Experimental Robotics*. Springer, 2014, pp. 227–240.

[48] Q. Luo and L. Tong, "Adaptive pressure-controlled cellular structures for shape morphing i: design and analysis," *Smart materials and structures*, vol. 22, no. 5, p. 055014, 2013.

[49] Y. Li, Y. Chen, Y. Yang, and Y. Wei, "Passive particle jamming and its stiffening of soft robotic grippers," *IEEE Transactions on Robotics*, vol. 33, no. 2, pp. 446–455, 2017.

[50] J. Breuer, W. Ockels, and R. Luchsinger, "An inflatable wing using the principle of tensairity," in *48th AIAA/ASME/ASCE/AHS/ASC Structures, Structural Dynamics, and Materials Conference*, 2007, p. 2117.

[51] "Lighter, stronger, better!" [Online]. Available: http://www.tensairitysolutions.com/

[52] L. Tiziani, A. Hart, T. Cahoon, F. Wu, H. H. Asada, and F. L. Hammond, "Empirical characterization of modular variable stiffness inflatable structures for supernumerary grasp-assist devices," *The International Journal of Robotics Research*, vol. 36, no. 13-14, pp. 1391–1413, 2017.

[53] C. Xiang, M. E. Giannaccini, T. Theodoridis, L. Hao, S. Nefti-Meziani, and S. Davis, "Variable stiffness mckibben muscles with hydraulic and pneumatic operating modes," *Advanced Robotics*, vol. 30, no. 13, pp. 889–899, 2016.

[54] A. Bergamini, R. Christen, B. Maag, and M. Motavalli, "A sandwich beam with electrostatically tunable bending stiffness," *Smart materials and structures*, vol. 15, no. 3, p. 678, 2006.

[55] A. Bergamini, R. Christen, and M. Motavalli, "Electrostatically tunable bending stiffness in a gfrp–cfrp composite beam," *Smart materials and structures*, vol. 16, no. 3, p. 575, 2007.

[56] T. Wang, J. Zhang, Y. Li, J. Hong, and M. Y. Wang, "Electrostatic layer jamming variable stiffness for soft robotics," *IEEE/ASME Transactions on Mechatronics*, vol. 24, no. 2, pp. 424–433, 2019.

[57] Y. Zhou, L. M. Headings, and M. J. Dapino, "Discrete layer jamming for variable stiffness co-robot arms," *Journal of Mechanisms and Robotics*, vol. 12, no. 1, 2020.

[58] Z. Xie, L. Qiu, and D. Yang, "Analysis of a novel variable stiffness filleted leaf hinge," *Mechanism and Machine Theory*, vol. 144, p. 103673, 2020.

[59] J. C. Mankins, "Technology readiness levels," *White Paper, April*, vol. 6, p. 1995, 1995.

B

Appendix: Matlab Code

B.1. Main file: simulation of LTB for a user defined I-beam

```
% MASTER 3 STEP SOLVING FILE for variable parameters
%% Clear the workspace and command window
close all;
clear all;
clc;

% start the timer
 tic
%%
% N1, N2, N3 help start the loops later on
N1 = 1; % loop parameter to run different values for the variable that is
   to be varied
N2 = 1;
N3 = 1;
% allocation variable to store displacements and rotations for each
   variable
timesteps = 30; % 30 is my standard
iterations = 500; % 500 is my standard
convergence_err = 1e-8;
N_nodes = 32; % needs to be a factor of 4

% range of factors that the original parameter value is miltiplied by
Variation_factor = [1]; % [0.75:0.25:1.25]; % [0.25:0.05:2];
   %[0.25:0.25:2]; etc.
% optimised beam result loaded below for verification
% optimised_beam = load('5 point multistart MAY 14 PA12');


% initial guess of force by which you expect the buckling to have happened
% at least, an educated guess, for which I know some order of magnitude by
% iteration trial and error.
% the timesteps-est are a separate number of timesteps, because they give
% much more accurate results when this number is fairly high compared to
% the number of time steps used for the application of a rtoation on the
% beam at its instability point.
F_initial_guess = -7;
F_perturb_y = (1/1000)*F_initial_guess;
timesteps_est = 1000; % 1000 is my standard
```

```
applied_angle = pi/3;
% I may want to add the number of iterations used in the buckling load
% estimation



% presizing the matrix that contains all the displacement in y to later on
% show the buckling process
% old line below below
% all_def_y_est = zeros(timesteps_est,length(Variation_factor));
% new line for automatic buckling load estimation which may happen in
% different numbers of timesteps for different variation factors
all_def_y_est = cell(1,length(Variation_factor));
all_Force_history_est = cell(1,length(Variation_factor));


% presizing the matrices with all deformations and all rotations for
% plotting purposes
% for load step 1, mostly unused
all_deformations_step1 = zeros(timesteps, 3*length(Variation_factor));
all_rotations_step1 = zeros(timesteps, 3*length(Variation_factor));
all_clamping_angles_deg = zeros(1,length(Variation_factor));
F_M_end_rot_hor_x_div_F_M_end_rot_ver_z =  zeros(1,length(Variation_factor
    ));
all_Fx = zeros(1,length(Variation_factor));
all_Fz = zeros(1,length(Variation_factor));

% for load step 2
all_deformations_per_timestep_step2_pos_rot = zeros(timesteps+1, 3*length(
    Variation_factor));
all_rotations_per_timestep_step2_pos_rot = zeros(timesteps+1, 3*length(
    Variation_factor)); % timestep + 1 to include a timestep 0 for plotting
     purposes later

% for load step 2
All_RF_RM_per_timestep_step2_pos_rot = zeros(timesteps+1,6*length(
    Variation_factor));

% All reaction moments for the unbuckled beam configuration
All_RMx_unbuck = zeros(1,length(Variation_factor));
All_avg_rot_stiffness_unbuck = zeros(1,length(Variation_factor));
% All buckling loads will be stored in the vector below
All_buckling_loads = zeros(1,length(Variation_factor));
% All buckling time steps will be stored in the vector below
All_buckling_timesteps = zeros(1,length(Variation_factor));
% All buckling point have a certain displacment in y, those are stored in
% the vector below
All_buckling_def_y = zeros(1,length(Variation_factor));

for N1 = 1: length(Variation_factor)


% DEFINE LOAD ON THE FINAL NODE BELOW, THIS IS INDEPENDENT OF SELECTED
    GEOMETRY
```

```
% variation of independent beam parameters

H_factor = Variation_factor(N1);
B_factor = 1; % Variation_factor(N1);
h_factor = 1; % Variation_factor(N1);
b_factor = 1; % Variation_factor(N1);

% variation of dependent beam parameters
Iyy_factor = 1; % Variation_factor(N1);
Izz_factor = 1; % Variation_factor(N1);
J_factor = 1; % Variation_factor(N1);
A_factor = 1; % Variation_factor(N1);




% H beam cross section parameters
H = 0.00705; % original value of plastic prototype
B = 0.010; % original value of plastic prototype
h = 0.0017; % original value of plastic prototype
b = 0.0010; % original value of plastic prototype
% dims = [H B h/H b/B];


CSD = [H B h b];
% CSD = [optimised_beam.dims(1,1) optimised_beam.dims(1,2) optimised_beam.
    dims(1,3)*optimised_beam.dims(1,1) optimised_beam.dims(1,4)*
    optimised_beam.dims(1,2)];

% This H profile is based on the real life plastic beam that shows some
% instability

% BASED ON BEAM PARAMETERS THE BUCKLING LOAD IS ESTIMATED


% beam shape:
beam_length = 0.3; % dims(1,5);% default was 0.4;
% beam_length = optimised_beam.dims(1,5);
d_nodes = beam_length/N_nodes; % probably unused when non straight beam is
     used



% STRAIGHT BEAM

% straight pure horizontal beam
 nodal_coordinates = [linspace(0,beam_length,N_nodes)',0.1*ones(N_nodes,1)
    ,zeros(N_nodes,4)];

% % straight tilted upwards beam
% x = linspace(0,beam_length,N_nodes)';
% y = 0.1*ones(N_nodes,1);
% z = 0.1*x;
% angles_orientations = zeros(N_nodes,3);
% nodal_coordinates = [x, y, z, angles_orientations];
%
```

```
% OR

% % CURVED BEAM
% % theta_end = (1/25)*pi; % angle that defines the curvature of the beam

% % here you define the initial shape as a beam with circular curvature in
% % the xz plane
% % to investigate a beam that is oriented upwards we introduce a
    curvature
% % radius
% % here. NB nodes are spaced with equal angle of curvature along the
% % circular arc
%
% thetatest = linspace(0,theta_end,N_nodes);
% R = beam_length/theta_end; % radius of curvature for the curved beam
% xtest = R*sin(thetatest);
% ztest = (R-R*cos(thetatest));
% nodal_coordinates = [xtest',0.1*ones(N_nodes,1),ztest',zeros(N_nodes,3)
    ];
%
% % The y-coordinates are all at 0.1, because if you set them all as 0 the
% % code does not converge


% PARABOLICALLY SHAPED BEAM

% x = linspace(0,beam_length,N_nodes)';
% y = 0.1*ones(N_nodes,1);
% z = 0.25*x.^2;
% angles_orientations = zeros(N_nodes,3);
% nodal_coordinates = [x, y, z, angles_orientations];


% % for the fun SINUSOID
% x = linspace(0,beam_length,N_nodes)';
% y = 0.1*ones(N_nodes,1);
% z = 0.25*sin(4*pi*x);
% angles_orientations = zeros(N_nodes,3);
% nodal_coordinates = [x, y, z, angles_orientations];


% F_buckling = some function that finds the buckling load
% [Fz_estimated_buckling_y_based, buckling_timstep,def_y,Force_history_est
    ,yes_no_buckling] = buckling_load_estimator(F_initial_guess,F_perturb_y
    ,timesteps_est,CSD,H_factor, B_factor, h_factor, b_factor, Iyy_factor,
    Izz_factor, J_factor, A_factor,nodal_coordinates,N_nodes,beam_length);

% revamped version of the buckling load estimator that should be automatic
    !
[Fz_estimated_buckling_y_based, buckling_timstep,def_y,Force_history_est,
    yes_no_buckling,loopcount,t] = V2_buckling_load_estimator(
    F_initial_guess,timesteps_est,iterations,CSD,H_factor, B_factor,
    h_factor, b_factor, Iyy_factor, Izz_factor, J_factor, A_factor,
    nodal_coordinates,N_nodes,beam_length);
```

```
% [Fz_estimated_buckling_y_based, buckling_timestep,all_def_y,
    Force_history_est,yes_no_buckling,loopcount,t] =
    V2_buckling_load_estimator(F_guess,timesteps_est,iterations,CSD,
    H_factor, B_factor, h_factor, b_factor, Iyy_factor, Izz_factor,
    J_factor, A_factor,nodal_coordinates,N_nodes,beam_length)

%%

% disp(yes_no_buckling);




% [Mcr,Fcr_estimate] = Mcr_Eurocode3(CSD, H_factor, B_factor, h_factor,
    b_factor, Iyy_factor, Izz_factor, J_factor, A_factor, nodal_coordinates
    , iterations, convergence_err,N_nodes);
% disp(Mcr)
% disp(Fcr_estimate)

% old line below
% all_def_y_est(:,N1) = def_y;
% new line to store the deformations for each variation factor, but we
    need
% a cell array because not each variation factor resulted in buckling in
% the initial range with a ccertain amount of timesteps
% all_def_y_est{:,N1} = def_y;
%
%
% all_Force_history_est{:,N1} = Force_history_est;
% % show the F-y plot
% figure
% plot(def_y,Force_history_est')
% xlabel('change in displacement [m]')
% ylabel('applied force [N]')
% title('first deformation step force Fz - displacement y graph')
% legend('delta y')



% The estimated load is stored:
All_buckling_loads(1,N1) = Fz_estimated_buckling_y_based;

% The estimated buckling timesteps are stored:
All_buckling_timesteps(1,N1) = buckling_timstep;

% All_buckling_def_y(1,N1) = def_y(buckling_timstep,1);


% here the reaction moment for the unbuckled beam is calculated


% process to find the reaction moment for an unbuckled beam
ep1_unbuck    = [0 0 0];      ep2_unbuck    = [nan nan nan];
theta1_unbuck = [0 0 0];      theta2_unbuck = [applied_angle nan nan];
```

```
F_M_end_unbuck = zeros(6,1); % [Fx, Fy, Fz, Mx, My, Mz]' are all zero,
    since only a rotation is applied here

% m_beams is created for the undeformed beam for the unbuckled case
[m_beams_unbuck, dofs_unbuck, par_unbuck, Fe_unbuck] =
    m_beam_generate_CSD_IyyIzzJA (CSD, H_factor, B_factor, h_factor,
    b_factor, Iyy_factor, Izz_factor, J_factor, A_factor, nodal_coordinates
    , F_M_end_unbuck, ep1_unbuck, theta1_unbuck, ep2_unbuck, theta2_unbuck,
    timesteps, iterations, convergence_err,N_nodes);

% implement m_beams, dofs, par, Fe structures to create the deformed beam
% no need for the solver with pre force yet, since we are only applying a
% rotation
[history_unbuck, m_beams_unbuck2] = solveNONLINstaticCOR(m_beams_unbuck,
    dofs_unbuck,par_unbuck,Fe_unbuck);
% m_beams_unbuck2 is unused.
% the reaction moment for the initial rotation only case
reaction_forces_moments_per_timestep_unbuck = zeros(timesteps,6);
for n_unbuck = 1:timesteps
reaction_forces_moments_per_timestep_unbuck(n_unbuck,:) =
    reaction_RF_RM_generate(history_unbuck,n_unbuck, ep2_unbuck,
    theta2_unbuck)';
end
All_RF_RM_per_timestep_unbuck =
    reaction_forces_moments_per_timestep_unbuck;
Reaction_moment_x_final_unbuck = All_RF_RM_per_timestep_unbuck(timesteps
    ,4);
RMx_unbuck = Reaction_moment_x_final_unbuck;
% only the final reaction moment is currenty stored in a row vector. This
% is purely for the computation of the average rotational stiffness for an
% unbckled beam
All_RMx_unbuck(1,N1) = RMx_unbuck;
All_avg_rot_stiffness_unbuck(1,N1) = RMx_unbuck/applied_angle;
% disp(RMx_unbuck)



if isnan(Fz_estimated_buckling_y_based) == 1
% the matrices storing all data for multiple parameter values are filled
% out by NaN below:
all_def_y_est{:,N1} = NaN; % def_y;
all_Force_history_est{:,N1} = NaN; % Force_history_est;

All_buckling_def_y(1,N1) = NaN; % def_y(buckling_timstep,1);

all_deformations_step1(:,N2:N2+2) = nan(size(all_deformations_step1(:,N2:
    N2+2))); % deformation_per_timestep_step1;
all_rotations_step1(:,N2:N2+2) = nan(size(all_rotations_step1(:,N2:N2+2)))
    ; % rotation_per_timestep_step1;
all_deformations_per_timestep_step2_pos_rot(2:timesteps+1,N2:N2+2) = nan(
    size(all_deformations_per_timestep_step2_pos_rot(2:timesteps+1,N2:N2+2)
    )); % deformation_per_timestep_step2;
all_rotations_per_timestep_step2_pos_rot(2:timesteps+1,N2:N2+2) = nan(size
    (all_rotations_per_timestep_step2_pos_rot(2:timesteps+1,N2:N2+2))); %
    rotation_per_timestep_step2;
```

```
All_RF_RM_per_timestep_step2_pos_rot(2:timesteps+1,N3:N3+5) = nan(size(
    All_RF_RM_per_timestep_step2_pos_rot(2:timesteps+1,N3:N3+5))); %
    reaction_forces_moments_per_timestep_step2;



else % do the normal process of applying the buckling load

% buckling behaviour
all_def_y_est{:,N1} = def_y;
% all_def_x_est{:,N1} = def_x;
% all_def_z_est{:,N1} = def_z;



all_Force_history_est{:,N1} = Force_history_est;
All_buckling_def_y(1,N1) =  def_y(buckling_timstep,1);


% the estimation is set as the buckling load
F_buckling = Fz_estimated_buckling_y_based;
% OR
% line below can be used to run the code for a given load. This saves time
% when checking the code below
% F_buckling = -5;


F_end_x = 0;
F_end_y = 0; % -0.01; % -0.01; %-0.01; %-0.01; %0.01;
F_end_z = F_buckling;%-2.7295; % -2.4850; %%0; % -3.35; %-2; % -2.1:
% moments more essential in second load step
M_end_x = 0; % 0.02
M_end_y = 0;
M_end_z = 0;

ep1    = [0 0 0];      ep2    = [nan nan nan];
theta1 = [0 0 0];      theta2 = [nan nan nan];

F_M_end = [F_end_x F_end_y F_end_z M_end_x M_end_y M_end_z]'; % F_M_end =
    [Fx, Fy, Fz, Mx, My, Mz]';

% The perturbation ratio defines how much big the load is compared to the
% horizontal perturbation (only useful when applying forces):
Perturbation_ratio = abs(F_M_end(3)/F_M_end(2));


% m_beams is created for the undeformed beam
[m_beams, dofs, par, Fe] = m_beam_generate_CSD_IyyIzzJA (CSD, H_factor,
    B_factor, h_factor, b_factor, Iyy_factor, Izz_factor, J_factor,
    A_factor, nodal_coordinates, F_M_end, ep1, theta1, ep2, theta2,
    timesteps, iterations, convergence_err,N_nodes);
```

```
% Here the force/moment or displacment/angle is placed and the deformation
    of the beam is modelled

% implement m_beams, dofs, par, Fe structures to create the deformed beam
% no need for the solver with pre force yet
[history, m_beams2] = solveNONLINstaticCOR(m_beams, dofs,par,Fe);

% Finding the deformations of the end node for each time step using the
% function 'deformations' (which I designed), they are all relative to the
% initial coordinates xyz
deformation_per_timestep_step1 = deformations(timesteps,N_nodes,history);

% Finding the rotations of the end node for each time step using a
% function 'rotations'  (which I designed)
rotation_per_timestep_step1 = rotations(timesteps,N_nodes,history);

% end node net rotations; just the last values in the vector
theta_x_end_node_step1 = rotation_per_timestep_step1(timesteps,1);
theta_y_end_node_step1 = rotation_per_timestep_step1(timesteps,2);
theta_z_end_node_step1 = rotation_per_timestep_step1(timesteps,3);
% the displacements and rotations of the final node are shown
displ =[m_beams2.D(N_nodes,1);m_beams2.D(N_nodes,2);m_beams2.D(N_nodes,3);
   theta_x_end_node_step1;theta_y_end_node_step1;theta_z_end_node_step1]

all_clamping_angles_deg(N1) = theta_y_end_node_step1*(180/pi);
% saving all deformations and rotations for each beam structure
% NB these will be the same as deformation_per_timestep_step1 and
% rotation_per_timestep_step1 if you don't have multiple values for
   certain
% parameters in this loop. In other words they are the same when the loop
% only runs once.

all_Fx(N1) = sin(theta_y_end_node_step1)*abs(F_buckling); % NB orientation
    is always positive (horizontal +) by this definition
all_Fz(N1) = -1*cos(theta_y_end_node_step1)*abs(F_buckling); % NB
   orientation is always negative (downward) by this definition

all_deformations_step1(:,N2:N2+2) = deformation_per_timestep_step1;
all_rotations_step1(:,N2:N2+2) = rotation_per_timestep_step1;


% vector with all displacements xyz of the end node for each timestep
% also better to put in a function perhaps? YES and it works!

% the applied force per time and the applied moment per time step data is
   created in vector Force_history
Force_history_step1 = linspace(0,Fe(6*m_beams.numberNodes-3),par.nTimestep
   ); % Fz
Moment_history_step1 = [linspace(0,Fe(6*m_beams.numberNodes-2),par.
   nTimestep);linspace(0,Fe(6*m_beams.numberNodes-1),par.nTimestep);
   linspace(0,Fe(6*m_beams.numberNodes),par.nTimestep)];
% this was the first load step
```

```
%% determination the required rotation to solve load step 1 to a beam with
    flat final element
% coordinates of deformed beam resulting from load step 1
nodal_coordinates_def = [nodal_coordinates(:,1:3) + history(timesteps).m.D
   (:,1:3)]; % x, y, z coordinates
final_element_vector_def = [nodal_coordinates_def(N_nodes,:) -
   nodal_coordinates_def(N_nodes-1,:)]';
unit_vector_final_element_def = final_element_vector_def* (1/sqrt(
   final_element_vector_def'*final_element_vector_def));

% coordinates of deformed and then rotated beam
[x2, y2, z2, phi, R_y] = beam_orientation_rotation(N_nodes,
   nodal_coordinates,history,timesteps);
nodal_coordinates_def_rot = [x2 y2 z2];
final_element_vector_def_rot = [nodal_coordinates_def_rot(N_nodes,:) -
   nodal_coordinates_def_rot(N_nodes-1,:)]';
% the unit vector is computed again and should be [1 0 0]'
unit_vector_final_element_def_rot = final_element_vector_def_rot* (1/sqrt(
   final_element_vector_def_rot'*final_element_vector_def_rot));

%% ILLUSTRATION GRAPH
% % This sub section is just for illustration purpose that the rotation as
% % calcularted before should give the deformed beam
%
%
% % plots of undeformed, deformed and the deformed & rotated beam
% figure
% hold on
% grid on
% axis equal
% xlabel('x')
% ylabel('y')
% zlabel('z')
%
% % original parabolic beam
% plot3(nodal_coordinates(:,1),nodal_coordinates(:,2),nodal_coordinates
   (:,3))
% %   deformed beam
% plot3(nodal_coordinates_def(:,1),nodal_coordinates_def(:,2),
   nodal_coordinates_def(:,3))
% %   unit vector normal to final cross section of deformed beam
% plot3([nodal_coordinates_def(N_nodes,1) nodal_coordinates_def(N_nodes,1)
   +unit_vector_final_element_def(1,1)],[nodal_coordinates_def(N_nodes,2)
   nodal_coordinates_def(N_nodes,2)+unit_vector_final_element_def(2,1)],[
   nodal_coordinates_def(N_nodes,3) nodal_coordinates_def(N_nodes,3) +
   unit_vector_final_element_def(3,1)],'--')
%
%
% % deformed & rotated beam
% plot3(nodal_coordinates_def_rot(:,1),nodal_coordinates_def_rot(:,2),
   nodal_coordinates_def_rot(:,3))
% % unit vector normal to final cross section of deformed and rotated beam
% plot3([nodal_coordinates_def_rot(N_nodes,1) nodal_coordinates_def_rot(
   N_nodes,1)+unit_vector_final_element_def_rot(1,1)],[
   nodal_coordinates_def_rot(N_nodes,2) nodal_coordinates_def_rot(N_nodes
```

```
    ,2)+unit_vector_final_element_def_rot(2,1)],[nodal_coordinates_def_rot(
    N_nodes,3) nodal_coordinates_def_rot(N_nodes,3)+
    unit_vector_final_element_def_rot(3,1)],'--')
% legend('undeformed','deformed','unit vector last element deformed beam
    ','deformed and rotated','unit vector last element deformed and rotated
     beam')
% hold off


%% solving step 2, load step 1 redone but in a rotated configuration
% redoing the first load step on an initially rotated beam by the angle
    that we now know
% this entire section that redoes the first load step is done, becasue I
% could not figure out where to implement the coordinates of the deformed
% and rotated beam as starting coordinates for the second load step
% rotating the undeformed beam
nodal_coordinates_ini_rot = [ [R_y*[nodal_coordinates(:,1:3)]']' [R_y*[
    nodal_coordinates(:,4:6)]']'];
% also rotating the applied load
F_M_end_rot = [R_y*F_M_end(1:3,1) ; R_y*F_M_end(4:6,1)];

% test without the horizontal component
% F_M_end_rot = [0; R_y(2,:)*F_M_end(1:3,1); R_y(3,:)*F_M_end(1:3,1) ; R_y
    *F_M_end(4:6,1)];


F_M_end_rot_hor_x_div_F_M_end_rot_ver_z(N1) = F_M_end_rot(1,1)/F_M_end_rot
    (3,1);
% line below is an attempt to fit the model to a potential experiment
% F_M_end_rot = [0 0 F_buckling 0 0 0]';;

% line below only F_M is rotated because I don't apply a rotation or
% displacement here! NOT rotated are ep1, theta1, ep2, theta2, because
    they
% are all 0 or NaN

% 1 m_beam_generate_CSD for variable H, B, h, b
% [m_beams_rot, dofs, par, Fe_rot] = m_beam_generate_CSD (CSD,
    nodal_coordinates_ini_rot, F_M_end_rot, ep1, theta1, ep2, theta2,
    timesteps, iterations, convergence_err, N_nodes) ;
[m_beams_rot, dofs, par, Fe_rot] = m_beam_generate_CSD_IyyIzzJA (CSD,
    H_factor, B_factor, h_factor, b_factor, Iyy_factor, Izz_factor,
    J_factor, A_factor, nodal_coordinates_ini_rot, F_M_end_rot, ep1, theta1
    , ep2, theta2,timesteps, iterations, convergence_err,N_nodes);

% OR

% % 2 m_beam_generate_IyyIzzJA for variable Iyy, Izz, J, A
%  [m_beams_rot, dofs, par, Fe_rot] = m_beam_generate_IyyIzzJA (IyyIzzJA,
    CSD, nodal_coordinates_ini_rot, F_M_end_rot, ep1, theta1, ep2, theta2,
    timesteps, iterations, convergence_err,N_nodes) ;



% Here the force/moment or displacment/angle is placed and the deformation
     of the beam is modelled
```

```
% implement m_beams_rot, dofs, par, Fe_rot structures to create the
    deformed beam
% no need for the solver with pre force yet
[history_rot, m_beams2_rot] = solveNONLINstaticCOR(m_beams_rot, dofs,par,
    Fe_rot);


%% check of the final element unit vector!

% coordinates of deformed beam calculated from a rotated load on a rotated
% undeformed beam
nodal_coordinates_def1 = [nodal_coordinates_ini_rot(:,1:3) + history_rot(
    timesteps).m.D(:,1:3)]; % same as nodal_coordinates_def_rot, as it
    should be!
final_element_vector_def1 = [nodal_coordinates_def1(N_nodes,:) -
    nodal_coordinates_def1(N_nodes-1,:)]';
unit_vector_final_element_def1 = final_element_vector_def1* (1/sqrt(
    final_element_vector_def1'*final_element_vector_def1));

unit_vector_final_element_def1
% if this unit vector is [1 0 0] the model is working as I want it to,
% becasue then the last element is aligned with the global x-axis

%% Start of load step 2
% Step 2.1: positive rotation about x
%Setting the buckling load as a preforce

F_M_pre_end_node_step2 = F_M_end_rot;

% % line below purely as a test:
% F_M_pre_end_node_step2 = [0 0 F_M_end_rot(3,1) 0 0 0]';



% placing it in a vector with all loads on all nodes
% PreFe2 = force_end_node_generate(F_pre_end2,m_beams2);
PreFe2 = force_end_node_generate(F_M_pre_end_node_step2,m_beams2_rot); %
    here m_beams or

% option to apply a force or moment besides the already present preforce
F_end_x2 = 0;
F_end_y2 = 0;
F_end_z2 = 0;

M_end_x2 = 0;
M_end_y2 = 0;
M_end_z2 = 0;

% placing it in a vector
F_M_end2 = [F_end_x2 F_end_y2 F_end_z2 M_end_x2 M_end_y2 M_end_z2]'; %
    F_M_end = [Fx, Fy, Fz, Mx, My, Mz]';


% constraints imposed in this step besides the already present pre force
```

```
ep1_step2    = [0 0 0];
theta1_step2 = [0 0 0];

ep2_step2    = [nan nan nan];
theta2_step2 = [applied_angle nan nan];

% creating Fe2 using m_beams generate function, which also gives
% m_beams4_unnec. However m_beams4_unnec is not needed itself.

% SELECT


% 1, m_beam_generate_CSD for variable H, B, h, b

[m_beams4_unnec, dofs2, par, Fe2] = m_beam_generate_CSD_IyyIzzJA (CSD,
    H_factor, B_factor, h_factor, b_factor, Iyy_factor, Izz_factor,
    J_factor, A_factor, nodal_coordinates, F_M_end2, ep1_step2,
    theta1_step2, ep2_step2, theta2_step2,timesteps, iterations,
    convergence_err,N_nodes);


% solve step 3, aka load step 2: here the rotation is applied on a beam
% kept at the unstable equilibrium by having the pre force equal to the
% buckling load
% different solver than the previous solving steps 2 due to PRESENCE of
    pre force
[history2_rot, m_beams3_rot] = solveNONLINstaticCOR_w_PreF(m_beams2_rot,
    dofs2,par,Fe2,PreFe2);

% % nodal coordinates of the final beam
% nodal_coordinates_final_orientation = [nodal_coordinates_ini_rot(:,1:3)
    + history2_rot(timesteps).m.D(:,1:3)]; % same as
    nodal_coordinates_def_rot, as it should be!




%% create the 3D figure

% solve step 1: application of the buckling load
% Here the deformed beam is plotted
figure
hold on
% Solve step 1, aka load step 1
% PlotBeamsCrossSections(m_beams,par, 'deformed')
% PlotBeamsCrossSections(m_beams2,par, 'undeformed')
% PlotBeamsCrossSections(m_beams2,par, 'deformed')
%
% % solve step 2, rotated equivalent of solve step 1 aka load step 1
% PlotBeamsCrossSections(m_beams2_rot,par, 'undeformed')
% PlotBeamsCrossSections(m_beams2_rot,par, 'deformed')

% solve step 3, applying a rotation about the local longitudinal axis of
```

```
% the final alement which is coinciding with the global x-axis
PlotBeamsCrossSections(m_beams2_rot,par, 'undeformed')
PlotBeamsCrossSections(m_beams3_rot,par, 'deformed')

xlabel('x')
ylabel('y')
zlabel('z')
title('undeformed and deformed configurations ')
legend('Step 1A: undeformed inital beam','Step 1A: deformed initial beam',
    'Step 1B: undeformed and rotated','Step 1B: deformed and rotated','Step
     2: undeformed prefroce present','Step 2: deformed preforce and
    longitudinal rotation')
hold off

% Here I may want a command that saves the 3D figure, because this script
    is now
% only showing the figure for the last iteration of the loop.

%% Finding the deformations of the end node for each time step using the

% so deformations of step 2 for the final node are
deformation_per_timestep_step2 = zeros(timesteps, 3);

% here you cannot use the deformations function because the displacement
    is
% between two beams that are both already deformed instead of one being
% simply a given set of beam coordinates for an unloaded beam
for i =1:timesteps
deformation_per_timestep_step2(i,:) = [history2_rot(i).m.D(N_nodes,1:3) -
    history_rot(timesteps).m.D(N_nodes,1:3)];
end



% Finding the rotations of the end node for each time step using a
% function 'rotations'  (which I designed)
rotation_per_timestep_step2 = rotations(timesteps,N_nodes,history2_rot);

% end node net rotations; just the last values in the vector
theta_x_end_node_step2 = rotation_per_timestep_step2(timesteps,1);
theta_y_end_node_step2 = rotation_per_timestep_step2(timesteps,2);
theta_z_end_node_step2 = rotation_per_timestep_step2(timesteps,3);


% the displacements and rotations of the final node are shown
disp_2 =[m_beams3_rot.D(N_nodes,1);m_beams3_rot.D(N_nodes,2);m_beams3_rot.
    D(N_nodes,3);theta_x_end_node_step2;theta_y_end_node_step2;
    theta_z_end_node_step2]



% storing all displacements and all rotations for load step 2

% matrix below has x y z displacement in each 3 columns, number of rows
% represents the number of time steps
```

```
all_deformations_per_timestep_step2_pos_rot(2:timesteps+1,N2:N2+2) =
    deformation_per_timestep_step2;
% matrix below has theta x, theta y, theta z rotation in each 3 columns,
    number of rows
% represents the number of time steps
all_rotations_per_timestep_step2_pos_rot(2:timesteps+1,N2:N2+2) =
    rotation_per_timestep_step2;



%% reaction forces resulting from ep2_step2 and theta2_step2 aplied
    boundary conditions


% Reaction_forces_moments_step2 = [Fx1 Fy1 Fz1 Mx2 My2 Mz2]'
Reaction_forces_moments_step2 = reaction_RF_RM_generate(history2_rot,
    timesteps, ep2_step2, theta2_step2)
% we only use the reaction force vector the pre force for a potential next
% load step can be obtained by:
% [Reaction_forces_moments_step2, Preforce_future_next_step] =
    reaction_RF_RM_generate(history2,timesteps, ep2_step2, theta2_step2)

%% force - displacement, moment angle for when you are applying a
    displacement or rotation
% % plots reaction force - displacement, moment - rotations


reaction_forces_moments_per_timestep_step2 = zeros(timesteps,6);
for n = 1:timesteps

reaction_forces_moments_per_timestep_step2(n,:) = reaction_RF_RM_generate(
    history2_rot,n, ep2_step2, theta2_step2)';


end


All_RF_RM_per_timestep_step2_pos_rot(2:timesteps+1,N3:N3+5) =
    reaction_forces_moments_per_timestep_step2;
% slight error in this matrix is that the columns representing reaction
% forces that are NaN now have a 0 value in time step 0 before becoming
% NaN. Then again I don't think this will matter for plots that I use this
% matrix for.


end % this end command is for the if loop that allows the script to
% continue running for a non buckling solution

% updating the allocating indices to allow for the next parameter value
N2 = N2 + 3;
N3 = N3 + 6;
end

%% Buckling behaviour verifcation graph
```

```
figure
hold on
for N = 1:length(Variation_factor)
plot(abs(all_def_y_est{1,N}),abs(all_Force_history_est{1,N}))
end
plot(abs(All_buckling_def_y),abs(All_buckling_loads),'x')

xlabel('\Deltay [m]')
ylabel('Fz [N]')
title('applied tip load, Fz - lateral deflection, \Deltay graph')
% legend('Fz - \Deltay', 'allocated buckling point')
legend('H = 0.25 * H og','H = 0.5 * H og','H = 0.75 * H og','H = H og','H
    = 1.25 * H og','H = 1.5 * H og','H = 1.75 * H og','H = 2 * H og', '
    approximated buckling load')

hold off
%% same graph as above but with Fz - delta x, delta y, delta z



%% Buckling behaviour verifcation graph

figure
hold on
for N = 1:length(Variation_factor)

    % Fz - delta y
    plot(abs(all_def_y_est{1,N}),abs(all_Force_history_est{1,N}))


end
plot(abs(All_buckling_def_y),abs(All_buckling_loads),'x')

xlabel('\Deltay [m]')
ylabel('Fz [N]')
title('applied tip load, Fz - lateral deflection, \Deltay graph')
legend('Fz - \Deltay', 'allocated buckling point')
hold off



%%
% insert the plotting script for the load step 2

% try to keep color consistency for the variables (eg. same 2 colors h1
    and
% h2)

% 1: rotational stiffness RM-applied angle

% the plot is correct, but the zero point needs to be included
    artificially
figure
hold on
N5 = 1; % index to find RM_x values per timestep in matrix with all
    reaction forces and moments; 1,4, 7, ...
```

```
N6 = 4; % index to find RM_x values per timestep in matrix with all
   reaction forces and moments; 4,10, 16, ...
for N4 = 1:length(Variation_factor)

%     all_rotations_per_timestep_step2_pos_rot(:,N5)
%     All_RF_RM_per_timestep_step2_pos_rot(:,N6)

    plot(all_rotations_per_timestep_step2_pos_rot(:,N5),
       All_RF_RM_per_timestep_step2_pos_rot(:,N6))


    N5 = N5 + 3;
    N6 = N6 + 6;

end

% find a way to make legend size with number of variables automatically
legend('Mx - variable 1','Mx - variable 2')
title('Step 2: reaction moment - rotation plot')
xlabel('rotation [rad]')
ylabel('Reaction moment [Nm]')
hold off



%% 2: All reaction forces - timestep OR just selectively the RM_x
figure
hold on
N7 = 4; % index to find RM_x values per timestep in matrix with all
   reaction forces and moments; 4,10, 16, ...
for N4 = 1:length(Variation_factor)

    plot([0:1:timesteps], All_RF_RM_per_timestep_step2_pos_rot(:,N7))

    N7 = N7 + 6;
end
% find a way to make legend size with number of variables automatically
legend('Mx - variable 1','Mx - variable 2')
title('Step 2: reaction moment about x - timesteps')
xlabel('timesteps')
ylabel('Reaction moment [Nm]')
hold off

%% 3: displacements - timesteps
% These 3 plots will show parasitic displacements as a result of the
% applied rotation about x

%% displacement - timesteps
% column 1, 4, 7, ...
figure

% dispacement in x-direction - timesteps
subplot(3,1,1)

hold on
```

```
N8 = 1;
for N4 = 1:length(Variation_factor)
plot([0:1:timesteps],all_deformations_per_timestep_step2_pos_rot(:,N8))

N8 = N8+3;
end

title('Step 2: development of displacements in x-direction of the final
    node over the timesteps')
xlabel('timesteps')
ylabel('displacement x direction[m]')
legend('delta x - variable 1','delta x - variable 2')
hold off

% displacement in y - timesteps
% column 2, 5, 8, ...
subplot(3,1,2)

hold on

N9 = 2;
for N4 = 1:length(Variation_factor)
plot([0:1:timesteps],all_deformations_per_timestep_step2_pos_rot(:,N9))

N9 = N9+3;
end

title('Step 2: development of displacements in y-direction of the final
    node over the timesteps')
xlabel('timesteps')
ylabel('displacement y direction [m]')
legend('delta y - variable 1','delta y - variable 2')
hold off

% displacement in z - timesteps
% column 3, 6, 9, ...
subplot(3,1,3)

hold on

N10 = 3;
for N4 = 1:length(Variation_factor)
plot([0:1:timesteps],all_deformations_per_timestep_step2_pos_rot(:,N10))

N10 = N10+3;
end


title('Step 2: development of displacements in z-direction of the final
    node over the timesteps')
xlabel('timesteps')
ylabel('displacement z direction [m]')
legend('delta z - variable 1','delta z - variable 2')
hold off
```

```
%% 4: rotations - timesteps (POSSIBILY NOT INTERESTING, eg theta x -
    timesteps = straight line)
% NB NOT SURE if I will use this. The rotations add little value to the
% story, but the plots are easy to make based on the displacement plots in
    case we want these.

% rotation about x
% column 1, 4, 7, ...
figure

% rotation about x-dorection - timesteps
subplot(3,1,1)

hold on

N8 = 1;
for N4 = 1:length(Variation_factor)
plot([0:1:timesteps],all_rotations_per_timestep_step2_pos_rot(:,N8))

N8 = N8+3;
end

title('Step 2: development of rotations about x of the final node over the
    timesteps')
xlabel('timesteps')
ylabel('rotation about x [rad]')
legend('theta x - variable 1','theta x - variable 2')
hold off

% rotation about y - timesteps
% column 2, 5, 8, ...
subplot(3,1,2)

hold on

N9 = 2;
for N4 = 1:length(Variation_factor)
plot([0:1:timesteps],all_rotations_per_timestep_step2_pos_rot(:,N9))

N9 = N9+3;
end

title('Step 2: development of rotation about y of the final node over the
    timesteps')
xlabel('timesteps')
ylabel('rotation about y [rad]')
legend('theta y - variable 1','theta y - variable 2')
hold off

% rotation about z - timesteps
% column 3, 6, 9, ...
subplot(3,1,3)

hold on

N10 = 3;
```

```
for N4 = 1:length(Variation_factor)
plot([0:1:timesteps],all_rotations_per_timestep_step2_pos_rot(:,N10))

N10 = N10+3;
end


title('Step 2: development of rotations about z of the final node over the
    timesteps')
xlabel('timesteps')
ylabel('rotation about z [rad]')
legend('theta z - variable 1','theta z - variable 2')
hold off



disp(All_buckling_loads)

%% display of CSD with respect to the lower and upper bound
%
% dims_co = H_beam_section_coordinates(dims); % replace dims_result by
   dims if you want to run the entire file at once
% % dims_co = H_beam_section_coordinates(dims);
% % lb_co = H_beam_section_coordinates(lb);
% % ub_co = H_beam_section_coordinates(ub);
%
% figure
% hold on
% plot(dims_co(:,1),dims_co(:,2))
% % plot(lb_co(:,1),lb_co(:,2),'--')
% % plot(ub_co(:,1),ub_co(:,2),'--')
% xlabel('y [m]')
% ylabel('z [m]')
% title('Scale drawing optimised cross-section shape')
% legend('optimised CSD','lower bound CSD','upper bound CSD')
% hold off

%%
runtime = toc
```

B.2. Numerical critical load estimator function

```
% Automatic numerical critical buckling load estimator



function [Fz_estimated_buckling_y_based, buckling_timestep,all_def_y,
   Force_history_est,yes_no_buckling,loopcount,t] =
   V2_buckling_load_estimator(F_guess,timesteps_est,iterations,CSD,
   H_factor, B_factor, h_factor, b_factor, Iyy_factor, Izz_factor,
   J_factor, A_factor,nodal_coordinates,N_nodes,beam_length)

% DEFINE LOAD ON THE FINAL NODE BELOW, THIS IS INDEPENDENT OF SELECTED
   GEOMETRY


    % initial value of t, the Fguess *2^t with a max of t = 6
```

```
   t = 0;
   loopcount = 1; % variable to keep track of the loop and to store values

  % start the loop as if there is no buckling detected
%   yes_no_buckling = 'No buckling observed: Initial absolute load range
    too small try larger absolute max load as input';
  yes_no_buck = 0;

  Pre_force_end_node = zeros(6,1);
  final_def_y_previous = 0;
  % parameters below are not actually used, but they allow to use a
  % function, m_beam_generate_CSD_IyyIzzJA
 F_M_end_setup = zeros(1,6);
 ep1_setup = zeros(1,3);
 theta1_setup = zeros(1,3);
 ep2_setup = zeros(1,3);
 theta2_setup = zeros(1,3);


  % standard parameters
convergence_err = 1e-8;
t_max = 5; % 5 means that the max force range is 0 to -315 N


  % m_beams structure is created. This structure is needed for the solver
[m_beams] = m_beam_generate_CSD_IyyIzzJA (CSD, H_factor, B_factor,
    h_factor, b_factor, Iyy_factor, Izz_factor, J_factor, A_factor,
    nodal_coordinates, F_M_end_setup, ep1_setup, theta1_setup, ep2_setup,
    theta2_setup,timesteps_est, iterations, convergence_err,N_nodes);



  % if t< 10? - easier to put outside while loop
  % or
  % if Fapplied< 2000?


while  yes_no_buck == 0 && t <= t_max
% if yes_no_buckling = 'No buckling observed: Initial absolute load range
    too small try larger absolute max load as input';

Fapplied = F_guess*2^t;

F_end_x = 0;
F_end_y = Fapplied*(1/1000); %-0.01; % (1/1000) standard value for
    perturbation wrt Fz
F_end_z = Fapplied;
M_end_x = 0;
M_end_y = 0;
M_end_z = 0;

% standard constraints on the first node, the clamped base, and the final
% node, the free end of the cantilever:
ep1    = [0 0 0];      ep2    = [nan nan nan];
theta1 = [0 0 0];      theta2 = [nan nan nan];
```

```
 % below the dofs and par are defined. Those remain the same for each
% iteration, but they depend on the end constraints and thus are nice to
% include here

bc          = [1:6  m_beams.eqn-5:m_beams.eqn ];
dofs.dp     = [ep1 theta1 ep2 theta2]';
dofs.all    = (1:m_beams.eqn)';
dofs.bc     = bc(~isnan([dofs.dp]));
dofs.dp     = dofs.dp(~isnan([dofs.dp]));
dofs.R      = sparse(1:length(dofs.bc),[dofs.bc],1+0*dofs.bc,length(dofs.
    bc),m_beams.eqn);

par.nTimestep   = timesteps_est; % number of time steps over which the
    load is spread. For large deflections increase this number
par.nIter       = iterations; % can always be increased to increase chance
     of convergence
par.conv        = convergence_err;
par.plots       = 'on';
par.getKend     = 0;


F_M_end = [F_end_x F_end_y F_end_z M_end_x M_end_y M_end_z]'; % F_M_end =
    [Fx, Fy, Fz, Mx, My, Mz]';




% Here Fe is defined based on m_beams, but this part of m_beams remains
% constant for each loop and thus it can be used without the
% m_beam_generate_CSD_IyyIzzJA function

Fe_est = zeros(m_beams.eqn,1);
Fe_est(m_beams.numberNodes*6-5) = F_M_end(1);
Fe_est(m_beams.numberNodes*6-4) = F_M_end(2);
Fe_est(m_beams.numberNodes*6-3) = F_M_end(3);
Fe_est(m_beams.numberNodes*6-2) = F_M_end(4);
Fe_est(m_beams.numberNodes*6-1) = F_M_end(5);
Fe_est(m_beams.numberNodes*6) = F_M_end(6);

% setting up the preforce
PreFe = force_end_node_generate(Pre_force_end_node,m_beams); % here
    m_beams or

% here a tricky thing happens, since m_beams is replaced with a new
    m_beams
[history_est, m_beams] = solveNONLINstaticCOR_w_PreF(m_beams, dofs,par,
    Fe_est,PreFe);
```

```
% Finding the rotations of the end node for each time step using a
% function 'rotations'  (which I designed)
% all_rotations_est = rotations(timesteps_est,N_nodes,history_est);

% the applied force per time step is created in vector Force_history_est
% Force_history_est = linspace(0,Fe_est(6*m_beams.numberNodes-3),par.
    nTimestep);

% each new iteration is stored in a new column
Force_history_row_iteration(1:par.nTimestep,loopcount) = linspace(0,Fe_est
    (6*m_beams.numberNodes-3),par.nTimestep)' + PreFe(m_beams.numberNodes
    *6-3)*ones(par.nTimestep,1);

% all rows are put next to one another to form an overall force history
Force_history_est = reshape(Force_history_row_iteration,[],1);

F = Force_history_est;



% Finding the deformations per time step, using deformations function
% (which) I designed
all_deformations_est = deformations(timesteps_est,N_nodes,history_est); %
    deformations gives xyz displacements in 3 columns


% each column belongs to the new force range increment
% line below was my original idea, but it seems to be incorrect
% all_def_y_iteration(1:par.nTimestep,loopcount) = all_deformations_est
    (:,2) + ones(timesteps_est,1)*final_def_y_previous; % final def_y from
    previous iterations!


% line below is the newest version and the total lateral deflection in y
    is apparently already accounted
% for in m_beams
all_def_y_iteration(1:par.nTimestep,loopcount) = all_deformations_est(:,2)
    ; % final def_y from previous iterations!
all_def_x_iteration(1:par.nTimestep,loopcount) = all_deformations_est(:,1)
    ; % final def_x from previous iterations!
all_def_z_iteration(1:par.nTimestep,loopcount) = all_deformations_est(:,3)
    ; % final def_z from previous iterations!




%column vector
all_def_y = reshape(all_def_y_iteration,[],1);
% all_def_x = reshape(all_def_x_iteration,[],1);
% all_def_z = reshape(all_def_z_iteration,[],1);
```

```
% lateral deflection y, Here I am not sure what happens when you let the
% m_beam strucutres evolve. They may already have all the
% def_y = all_deformations_est(:,2);



% % 5 lines below are from the original estimator
% % numerical first derivative
% dF_d_def_y = gradient(F,def_y);
%
% % second numerical derivative
% ddF_dd_def_y = gradient(dF_d_def_y,def_y);

% numerical first derivative
dF_d_def_y = gradient(F,all_def_y);

% second numerical derivative
ddF_dd_def_y = gradient(dF_d_def_y,all_def_y);







% input needed is and dF_d_def_y ddF_dd_def_y

% line below finds timestep for which ddF_dd_def_y switches sign, so in
   the
% real life continious scenario this is where the second derivative passes
% through zero which is the inflexion point
idx_inflx = find(diff(sign(ddF_dd_def_y)))+1;

[abs_min_dFy_dy_test, idx_abs_min_dFy_dy] = min(abs(dF_d_def_y));



N = 1;
 while N<length(idx_inflx)+1 % so it runs until the whole vector idx_inflx
                             % has been explored AKA all the inflexion
                             % points

difference = abs(idx_abs_min_dFy_dy - idx_inflx(N));


% if command below checks for the presence of an inflexion point at all

if isnumeric(idx_inflx) == 1 && difference <= 3  && dF_d_def_y(
    idx_abs_min_dFy_dy)<0.1*dF_d_def_y(0.05*timesteps_est) % This third
    condition should help avoiding fake buckling points for vague inflexion
     points that occur due to numerical computation


        buckling_timestep_test1 = idx_abs_min_dFy_dy;
        buckling_timestep_test2 = idx_inflx(N);
        buckling_timestep = max([buckling_timestep_test1
```

```
            buckling_timestep_test2]);

%         buckling_timstep_test2 = idx_inflx(N); % can be used as check,
%         the result should be exactly the same is in the line above
        Fz_estimated_buckling_y_based  = Force_history_est(
            buckling_timestep);
%         Fz_estimated_buckling_z_based  = Force_history(idx_inflx(N)); %
%         can be used as check, the result should be exactly the same is
%         in the line above

       yes_no_buckling = 'buckling load found';
           yes_no_buck = 1; % scalar value for saying that the buckling
              load was found, 1, or not found, 0.

            % Now specify N as the value for which the while loop ends
N = length(idx_inflx)+2;
else
    N = N+1;
    % Can't I just make a statemtent that says there is no buckling if it
    % isn't found here?

% end

% if loop below creates statement for when the loop has checked all the
% values for the indices of the inflexion points with the local minima
% if N == length(idx_inflx)+1
%
%         yes_no_buckling = 'No buckling observed: Initial absolute load
   range too small try larger absolute max load as input';
%         yes_no_buck = 0;
%
%     buckling_timestep = timesteps_est;
%     Fz_estimated_buckling_y_based = F_guess;
end

% if yes_no_buckling = 'No buckling observed: Initial absolute load range
   too small try larger absolute max load as input';

 end % ending of the while loop


% end

% not sure of the location in the code, but the line below sets the final
% value of the load range as the preforce present in the previous

Fend_range = Pre_force_end_node + F_M_end;
Pre_force_end_node = Fend_range;

% old line below
% Pre_force_end_node  = F_M_end;


final_def_y_previous = all_def_y(length(all_def_y)) ; % the last element
```

```
t = t +1;
loopcount = loopcount+1;

end

% the while loop stops when either buckling is detected, for which then
   yes_no_buck = 1
% OR
% the t>10 for which then Fz = NaN
if yes_no_buck == 1 % this is the command when buckling is detected
    Fz_estimated_buckling_y_based = Fz_estimated_buckling_y_based;

else % the other option causing the while loop to stop is t>10
    % when no buckling is detected the first if loop was stopped because t
    % was exceeded and thus the structure is apparently inbucklable and
    % therefore the buckling load should be set as NaN and all later
       output
    % as well such that the optimisation can move to a new point
    Fz_estimated_buckling_y_based = NaN;
    buckling_timestep = NaN;
%     all_def_y
%     Force_history_est
    yes_no_buckling = 'No buckling observed, structure potentially
       unbucklable';


end


end
```

B.3. Optimisation files

B.3.1. Optimisation main file

```
%% A first attempt on optimisation based on Ali's I beam optimisation with
    similar free variables
%% Optimisation main file
% the optimisation is performed
% the optimised result is tested

close all;
clear all
clc
% tic
%% input beam variables

% Here my variables and bounds are set as input

% H beam cross section parameters
H = 0.00705; % original value of plastic prototype
% H = Variation_factor(N1)*H;
B =  0.010; % original value of plastic prototype
% B = Variation_factor(N1) * B;
h = 0.0017; % original value of plastic prototype
% h = Variation_factor(N1) * h;
b = 0.0010; % original value of plastic prototype
```

```
% b = Variation_factor(N1) * b;
hH= h/H;
bB= b/B;



CSD_H_B_hH_bB = [H B hH bB];

% dims= [0.0051, 0.0080, 0.1000, 0.1000];% [0.006 0.007 0.2 0.2];
x0 = [CSD_H_B_hH_bB 0.3]; % the starting configuration

% Lower, lb, and upper, ub, bounds
lb = [0.5* H, 0.5 * B, 0.25*(h/H), 0.25*(b/B), 0.25]; % 0.35
ub = [2 * H, 2*B, 2*(h/H), 2*(b/B), 0.35]; % 0.45


A = [];
b = [];
Aeq = [];
beq = [];
nonlcon=[];

%% TIME TO SEND IT

% line below should be deactivated for safety that I don't accidentally
    rerun the optimisation

% options = optimoptions('fmincon','Display','iter','Algorithm','active-
    set','MaxIterations',50,'MaxFunEvals',10000,'PlotFcns',@optimplotfval);
% [dims,fval] = fmincon(@ShapeOptmultiWrist,x0,A,b,Aeq,beq,lb,ub,@
    NonlconWrist,options);
% save('optimization_results')
tic
% command line below needs some investigation
ms = MultiStart('Display','iter')
% options line below can probably be kept original for now
options=optimset('Algorithm','interior-point','GradObj','off','Hessian','
    off','tolX',1e-4,'TolFun',1e-5,'MaxIter',25,'MaxFunEvals',10000,'
    PlotFcns',@optimplotfval);

% the 2 lines below is where the magic happens!
% this is how the problem is defined
problem = createOptimProblem('fmincon','x0',x0,'lb',lb,'ub',ub,'Aeq',[],'
    beq',[],'nonlcon',nonlcon,'objective',@LTB_objective_function,'options'
    ,options);

% here you start running the optimisation I think, the 3 in
% run(ms,problem,3) is the number of multistart points and to start it is
% wise to start with 1.
% line below starts the optimisation process
[dims, Objbest,exitflag,output,solutions] = run(ms,problem,5)
% % save('optimization_results')
runtime_optimisation = toc;
% If you run the file up to this line the optimisation has already taken
% place
```

```
% previously obtained result can be loaded through command line below
load('5 point multistart MAY 14 PA12')



%% Test of the eventual dims
% here you can run the actual found dims
% dims_result = dims;

% length_of_beam = 0.5; % [m], NB many dims plotted with 0.5 m as value

% variables for plotting lower and upper bound CSD's
% CSD= [0.006 0.007 0.2 0.2];
% lb = [0.85*CSD(1,1:2) 0.1 0.1]; % lower bound on CSD values, [0.75*CSD
    (1,1:2) 0.05 0.05]
% ub = [1.15*CSD(1,1:2) 0.3 0.3]; % upper bound on CSD values
%% loading the optimisation values from previous runs
% requires the corresponding .mat files
% load('28 April optimisation with much larger bounds')
% load('May 4 successful run for PA12 with large range bounds')
% load('May 7 optimisation with constant length of 40 cm aka 0_4 m')
% load('May 7 successful run for 03m beam PA12 with large range bounds')

%% Modelling of the lateral torsional buckling of the optimisation found
    solution
tic
% length_of_beam = 0.5; % 15-4 I think this line is irrelevant, since beam
     length is stated by dims(1,5)
% FEM function
[lat_defl_y,RMx_buck, deformation_per_timestep_step2,
    final_displacements_xyz, loopcount_while_loop, remain_RMx,
    stiffness_decrease_percent,Fz_estimated_buckling_y_based,
    Fapplied_final,m_beams, m_beams2, m_beams2_rot, m_beams3_rot, par,
    rotation_per_timestep_step2, All_RF_RM_per_timestep_step2_pos_rot,
    timesteps,def_y, Force_history_est, yes_no_buckling,buckling_timstep,
    RMx_unbuck] = function_Optimization_FEM_V2(dims);

%%

% 3D plot based on m_beams

% solve step 1: application of the buckling load
% Here the deformed beam is plotted
figure
hold on
% Solve step 1, aka load step 1
PlotBeamsCrossSections(m_beams,par, 'deformed')
PlotBeamsCrossSections(m_beams2,par, 'undeformed')
PlotBeamsCrossSections(m_beams2,par, 'deformed')
view(80,10)
%% solve step 2, rotated equivalent of solve step 1 aka load step 1
PlotBeamsCrossSections(m_beams2_rot,par, 'undeformed')
PlotBeamsCrossSections(m_beams2_rot,par, 'deformed')

%% solve step 3, applying a rotation about the local longitudinal axis of
% the final alement which is coinciding with the global x-axis
```

```
PlotBeamsCrossSections(m_beams2_rot,par, 'undeformed')
PlotBeamsCrossSections(m_beams3_rot,par, 'deformed')

xlabel('x')
ylabel('y')
zlabel('z')
title('undeformed and deformed configurations ')
legend('Step 1A: undeformed inital beam','Step 1A: deformed initial beam',
    'Step 1B: undeformed and rotated','Step 1B: deformed and rotated','Step
     2: undeformed prefroce present','Step 2: deformed preforce and
    longitudinal rotation')
hold off



%% display of CSD with respect to the lower and upper bound

% test of dims


dims_co = H_beam_section_coordinates(dims); % replace dims_result by dims
    if you want to run the entire file at once
% dims_co = H_beam_section_coordinates(dims);
lb_co = H_beam_section_coordinates(lb);
ub_co = H_beam_section_coordinates(ub);

figure
hold on
plot(dims_co(:,1),dims_co(:,2))
plot(lb_co(:,1),lb_co(:,2),'--')
plot(ub_co(:,1),ub_co(:,2),'--')
xlabel('x [m]')
ylabel('y [m]')
title('Scale drawing optimised cross-section shape')
legend('optimised CSD','lower bound CSD','upper bound CSD')
hold off

%% plotting buckling behaviour

% variables needed for plot
disp(yes_no_buckling);
all_def_y_est = def_y;
all_Force_history = Force_history_est;
All_buckling_def_y = def_y(buckling_timstep,1);
All_buckling_loads = Fz_estimated_buckling_y_based;

% the buckling behaviour plot

figure
hold on
for N = 1:1%length(Variation_factor)
plot(all_def_y_est,all_Force_history)
end
plot(All_buckling_def_y,All_buckling_loads,'x') % the data points that are
     marked as the exact buckling points
```

```
xlabel('lateral deflection y [m]')
ylabel('applied force [N]')
title('first deformation step force Fz - lateral deflection delta y graph'
    )
legend('h = 0.5 * original h','h = original h', 'h = 1.5 * original h','h
    = 2 * original h','h = 3 * original h','h = 5 * original h','h = 10 *
    original h','Fb1','Fb2','Fb3','Fb4')
hold off


% the Rmx - theta x plot

figure
subplot(1,2,1)
hold on
plot([0; rotation_per_timestep_step2(:,1)],
    All_RF_RM_per_timestep_step2_pos_rot(:,4))
plot([0;rotation_per_timestep_step2(:,1)],RMx_unbuck*ones(timesteps+1,1),'
    --')
plot([0;rotation_per_timestep_step2(:,1)],0.5*RMx_unbuck*ones(timesteps
    +1,1),'--')

hold off
legend('RMx - loaded beam','RMx - unloaded beam','RMx constraint 0.5 * RMx
     - unloaded beam')
title('Step 2: reaction moment - rotation plot')
xlabel('rotation [rad]')
ylabel('Reaction moment [Nm]')

% and the RMX - timesteps plot

subplot(1,2,2)
hold on
plot([0:1:timesteps], All_RF_RM_per_timestep_step2_pos_rot(:,4))
plot([0:1:timesteps],RMx_unbuck*ones(1,timesteps+1),'--')
plot([0:1:timesteps],0.5*RMx_unbuck*ones(1,timesteps+1),'--')

hold off
legend('RMx - loaded beam','RMx - unloaded beam','RMx constraint 0.5 * RMx
     - unloaded beam')
title('Step 2: reaction moment about x - timesteps')
xlabel('timesteps')
ylabel('Reaction moment [Nm]')
hold off

%
% parasitic displacements

% 3: displacements - timesteps
% These 3 plots will show parasitic displacements as a result of the
% applied rotation about x

%% displacement - timesteps and rotation - timesteps
figure
```

```
% dispacement in x-direction - timesteps
subplot(3,2,1)

plot([0:1:timesteps],[0; deformation_per_timestep_step2(:,1)])
title('Step 2: development of displacements in x-direction of the final
    node over the timesteps')
xlabel('timesteps')
ylabel('displacement x direction[m]')

% displacement in y - timesteps
subplot(3,2,3)

plot([0:1:timesteps],[0;deformation_per_timestep_step2(:,2)])
title('Step 2: development of displacements in y-direction of the final
    node over the timesteps')
xlabel('timesteps')
ylabel('displacement y direction [m]')

% displacement in z - timesteps
subplot(3,2,5)

plot([0:1:timesteps],[0;deformation_per_timestep_step2(:,3)])

title('Step 2: development of displacements in z-direction of the final
    node over the timesteps')
xlabel('timesteps')
ylabel('displacement z direction [m]')


% parasitic rotations

% rotation about x-direction - timesteps
subplot(3,2,2)

plot([0:1:timesteps],[0;rotation_per_timestep_step2(:,1)])

title('Step 2: development of rotations about x of the final node over the
     timesteps')
xlabel('timesteps')
ylabel('rotation about x [rad]')

% rotation about y - timesteps
% column 2, 5, 8, ...
subplot(3,2,4)

plot([0:1:timesteps],[0;rotation_per_timestep_step2(:,2)])

title('Step 2: development of rotation about y of the final node over the
    timesteps')
xlabel('timesteps')
ylabel('rotation about y [rad]')
hold off

% rotation about z - timesteps
% column 3, 6, 9, ...
subplot(3,2,6)
```

```
plot([0:1:timesteps],[0;rotation_per_timestep_step2(:,3)])

title('Step 2: development of rotations about z of the final node over the
    timesteps')
xlabel('timesteps')
ylabel('rotation about z [rad]')

%
runtime_model = toc

% Total_runtime = runtime_model + runtime_optimisation;



%% new layout of figures for the paper

figure

subplot(2,2,1)

hold on
% % Solve step 1, aka load step 1
% PlotBeamsCrossSections(m_beams,par, 'deformed')
% PlotBeamsCrossSections(m_beams2,par, 'undeformed')
% PlotBeamsCrossSections(m_beams2,par, 'deformed')
%
% % solve step 2, rotated equivalent of solve step 1 aka load step 1
% PlotBeamsCrossSections(m_beams2_rot,par, 'undeformed')
% PlotBeamsCrossSections(m_beams2_rot,par, 'deformed')
%
% % solve step 3, applying a rotation about the local longitudinal axis of
% % the final alement which is coinciding with the global x-axis
PlotBeamsCrossSections(m_beams2_rot,par, 'deformed')
PlotBeamsCrossSections(m_beams3_rot,par, 'deformed')

view(70,10)

xlabel('x')
ylabel('y')
zlabel('z')
title('undeformed and deformed configurations ')
% legend('Step 1A: undeformed inital beam','Step 1A: deformed initial beam
    ','Step 1B: undeformed and rotated','Step 1B: deformed and rotated','
    Step 2: undeformed prefroce present','Step 2: deformed preforce and
    longitudinal rotation')
hold off


subplot(2,2,2)
hold on
plot(dims_co(:,1),dims_co(:,2))
plot(lb_co(:,1),lb_co(:,2),'--')
plot(ub_co(:,1),ub_co(:,2),'--')
xlabel('x [m]')
ylabel('y [m]')
```

```
title('Scale drawing optimised cross-sectional dimensions (CSD)')
legend('optimised CSD','lower bound CSD','upper bound CSD')
hold off



% the Fz - delta y plot, left from the RMx - angle diagram to stay
% consistent with the layout as for the verification graph

% subplot(1,2,1)
subplot(2,2,3)

hold on
for N = 1:1%length(Variation_factor)
plot(all_def_y_est,all_Force_history)
end
plot(All_buckling_def_y,All_buckling_loads,'x') % the data points that are
    marked as the exact buckling points

xlabel('lateral deflection y [m]')
ylabel('applied force [N]')
title('first deformation step force Fz - lateral deflection delta y graph'
   )
legend('optimised beam','Fb optimised beam')
hold off

% the RMx - angle diagram, right from theFz - delta y plot to stay
% consistent with the layout as for the verification graph

subplot(2,2,4)
% subplot(1,2,2)

hold on
plot([0; rotation_per_timestep_step2(:,1)]*(180/pi),
   All_RF_RM_per_timestep_step2_pos_rot(:,4))
plot([0;rotation_per_timestep_step2(:,1)]*(180/pi),RMx_unbuck*ones(
   timesteps+1,1),'--')
plot([0;rotation_per_timestep_step2(:,1)]*(180/pi),0.5*RMx_unbuck*ones(
   timesteps+1,1),'--')

hold off
legend('RMx beam buckled state','RMx unloaded beam','constraint RMx = 0.5
   * RMx unloaded beam')
title('Step 2: reaction moment - rotation plot')
xlabel('rotation [deg]')
ylabel('Reaction moment [Nm]')
% the section

% loading scheme
```

B.3.2. Optimisation objective function

```
% Objective function for optimisation

function [error] = LTB_objective_function(dims)
```

```
% the function name of the FEM below. This function will calculate the
% lateral deflection for the given input beam represented by H B hH bB. It
% will calculate the buckling load apply a rotation and possibly increase
% the load until the reaction moment is lower than 0.5 times the reaction
% moment for the unbuckled beam
% [lat_defl_y,RMx_buck, deformation_per_timestep_step2,
    final_displacements_xyz, loopcount_while_loop, remain_RMx,
    stiffness_decrease_percent,Fz_estimated_buckling_y_based,
    Fapplied_final,m_beams, m_beams2, m_beams2_rot, m_beams3_rot, par,
    rotation_per_timestep_step2, All_RF_RM_per_timestep_step2_pos_rot,
    timesteps,def_y, Force_history_est, yes_no_buckling, buckling_timstep,
    RMx_unbuck] = function_Optimization_FEM_V2(dims,length_of_beam);
[lat_defl_y,RMx_buck, deformation_per_timestep_step2,
    final_displacements_xyz, loopcount_while_loop, remain_RMx,
    stiffness_decrease_percent,Fz_estimated_buckling_y_based,
    Fapplied_final,m_beams, m_beams2, m_beams2_rot, m_beams3_rot, par,
    rotation_per_timestep_step2, All_RF_RM_per_timestep_step2_pos_rot,
    timesteps,def_y, Force_history_est, yes_no_buckling, buckling_timstep,
    RMx_unbuck,beam_length] = function_Optimization_FEM_V2(dims);


lat_defl_y

lat_defl_y_final_node_final_step = lat_defl_y;

error = abs(lat_defl_y_final_node_final_step);
end
```

B.3.3. Optimisation FEM 3-step solving process

```
% Optimisation FEM solving process based on the 3-step loading scheme

function [lat_defl_y,RMx_buck, deformation_per_timestep_step2,
    final_displacements_xyz, loopcount_while_loop, remain_RMx,
    stiffness_decrease_percent,Fz_estimated_buckling_y_based,
    Fapplied_final,m_beams, m_beams2, m_beams2_rot, m_beams3_rot, par,
    rotation_per_timestep_step2, All_RF_RM_per_timestep_step2_pos_rot,
    timesteps,def_y, Force_history_est, yes_no_buckling, buckling_timstep,
    RMx_unbuck,beam_length] = function_Optimization_FEM_V2(dims)


% by calling dims here I hope to show the dims that eventually cause no
% convergence in some cases
dims


tic
% technical parameters for solving process
timesteps = 100; %30
iterations = 500;
convergence_err = 1e-8;
% potential extra inputs
% fixed_theta_x = pi/3; % rotation about x-axis
% reduction_net_RMx = 0.6; % then the RMxbuck < 0.4*RMxunbuck


% buckling load estimation parameters!
```

```
F_initial_guess = -5;
timesteps_est = 500; % default was 1000
iterations_est = 500; % default was 1000

% reduction factor below states how much the RMx of the buckled beam
    should at least be lower
% than the RMx of the unbuckled beam
reduction_factor = 0.5; % default was 0.5

% conversion of dims = [H B h/H b/B] to CSD = [H B h b], because
    originally
% the script for the buckling load estimator was written around CSD
CSD = [dims(1,1) dims(1,2) dims(1,3)*dims(1,1) dims(1,4)*dims(1,2)];


% factors below are from the original model used for the parameter study.
% They don't serbe a purpose in the optimisation
H_factor = 1;
B_factor = 1;
h_factor = 1;
b_factor = 1;
Iyy_factor = 1;
Izz_factor = 1;
J_factor =1;
A_factor = 1;


% beam_length = 0.5;
beam_length = dims(1,5);
N_nodes = 32;

% the nodal coordinates below are for a straight beam with length
% beam_length
nodal_coordinates = [linspace(0,beam_length,N_nodes)',0.1*ones(N_nodes,1),
    zeros(N_nodes,4)];

%

%%

[Fz_estimated_buckling_y_based, buckling_timstep,def_y,Force_history_est,
    yes_no_buckling,loopcount,t] = V2_buckling_load_estimator(
    F_initial_guess,timesteps_est,iterations_est,CSD,H_factor, B_factor,
    h_factor, b_factor, Iyy_factor, Izz_factor, J_factor, A_factor,
    nodal_coordinates,N_nodes,beam_length);
% disp(Fz_estimated_buckling_y_based)
% as an initial value to kick off the while loop

% When there is no buckling the following variables become NaN
% Fz_estimated_buckling_y_based
% buckling_timstep
% the force history and the displacements still are vectors that can show
% the force displacement behaviour!

% Fz_estimated_buckling_y_based
```

```
%%
if  isnan(Fz_estimated_buckling_y_based) == 1
% then all the output should be NaN
% all the output is
lat_defl_y = NaN;
RMx_buck = NaN;
deformation_per_timestep_step2 = nan(timesteps, 3);
final_displacements_xyz = [NaN NaN NaN];
loopcount_while_loop = NaN;
remain_RMx = NaN;
stiffness_decrease_percent = NaN;

Fapplied_final = Fz_estimated_buckling_y_based; % = NaN in tis case
m_beams = NaN;
m_beams2 = NaN;
m_beams2_rot = NaN;
m_beams3_rot = NaN;
par = NaN;
rotation_per_timestep_step2 = NaN;
All_RF_RM_per_timestep_step2_pos_rot = NaN;
% def_y, should still be given by the buckling load estimator
% Force_history_est, should still be given by the buckling load estimator
% yes_no_buckling, should still be given by the buckling load estimator
% buckling_timstep, already set as NaN by the buckling load estimator
RMx_unbuck = NaN;
% but only the lat_defl is used in the objective function. The rest is
   just
% output that I use when I want to test and mainly plot the dims resulting
% from the optimisation. However all the other output will still have to
   be
% set as NaN otherwise the function wants to output variabels that are not
% defined...

% otherwise run the file below


else



% process to find the reaction moment for an unbuckled beam
ep1_unbuck    = [0 0 0];      ep2_unbuck    = [nan nan nan];
theta1_unbuck = [0 0 0];      theta2_unbuck = [pi/3 nan nan];

F_M_end_unbuck = zeros(6,1); % [Fx, Fy, Fz, Mx, My, Mz]' are all zero,
   since only a rotation is applied here

% m_beams is created for the undeformed beam for the unbuckled case
[m_beams_unbuck, dofs_unbuck, par_unbuck, Fe_unbuck] =
   m_beam_generate_CSD_IyyIzzJA (CSD, H_factor, B_factor, h_factor,
   b_factor, Iyy_factor, Izz_factor, J_factor, A_factor, nodal_coordinates
   , F_M_end_unbuck, ep1_unbuck, theta1_unbuck, ep2_unbuck, theta2_unbuck,
   timesteps, iterations, convergence_err,N_nodes);
```

```
% implement m_beams, dofs, par, Fe structures to create the deformed beam
% no need for the solver with pre force yet, since we are only applying a
% rotation
[history_unbuck, m_beams_unbuck2] = solveNONLINstaticCOR(m_beams_unbuck,
    dofs_unbuck,par_unbuck,Fe_unbuck);
% m_beams_unbuck2 is unused.
% the reaction moment for the initial rotation only case
reaction_forces_moments_per_timestep_unbuck = zeros(timesteps,6);
for n_unbuck = 1:timesteps
reaction_forces_moments_per_timestep_unbuck(n_unbuck,:) =
    reaction_RF_RM_generate(history_unbuck,n_unbuck, ep2_unbuck,
    theta2_unbuck)';
end
All_RF_RM_per_timestep_unbuck =
    reaction_forces_moments_per_timestep_unbuck;
Reaction_moment_x_final_unbuck = All_RF_RM_per_timestep_unbuck(timesteps
    ,4);
RMx_unbuck = Reaction_moment_x_final_unbuck;
% disp(RMx_unbuck)

RMx_buck = RMx_unbuck;
%%
Fapplied = Fz_estimated_buckling_y_based;
loopcount_while_loop = 0;
N2=1; % can be probably be removed as a parameter
N3=1;
while RMx_buck >= (1-reduction_factor) * RMx_unbuck % the 0.5 is how much
    of the original moment is allowed to occur


    % something that redoes the 3 steps with bending the beam down, then
    % rotates it to align the final element with the horizontal and then
    % apply the rotation

F_end_x = 0;
F_end_y = 0; % -0.01; % -0.01; %-0.01; %-0.01; %0.01;
F_end_z = Fapplied;%-2.7295; % -2.4850; %%0; % -3.35; %-2; % -2.1:
% moments more essential in second load step
M_end_x = 0; % 0.02
M_end_y = 0;
M_end_z = 0;

ep1    = [0 0 0];      ep2    = [nan nan nan];
theta1 = [0 0 0];      theta2 = [nan nan nan];

F_M_end = [F_end_x F_end_y F_end_z M_end_x M_end_y M_end_z]'; % F_M_end =
    [Fx, Fy, Fz, Mx, My, Mz]';

% The perturbation ratio defines how much big the load is compared to the
% horizontal perturbation (only useful when applying forces):
Perturbation_ratio = abs(F_M_end(3)/F_M_end(2));


% m_beams is created for the undeformed beam
[m_beams, dofs, par, Fe] = m_beam_generate_CSD_IyyIzzJA (CSD, H_factor,
    B_factor, h_factor, b_factor, Iyy_factor, Izz_factor, J_factor,
```

```
    A_factor, nodal_coordinates, F_M_end, ep1, theta1, ep2, theta2,
    timesteps, iterations, convergence_err,N_nodes);




% Here the force/moment or displacement/angle is placed and the
    deformation of the beam is modelled

% implement m_beams, dofs, par, Fe structures to create the deformed beam
% no need for the solver with pre force yet
[history, m_beams2] = solveNONLINstaticCOR(m_beams, dofs,par,Fe);

% Finding the deformations of the end node for each time step using the
% function 'deformations' (which I designed), they are all relative to the
% initial coordinates xyz
deformation_per_timestep_step1 = deformations(timesteps,N_nodes,history);

% Finding the rotations of the end node for each time step using a
% function 'rotations'  (which I designed)
rotation_per_timestep_step1 = rotations(timesteps,N_nodes,history);

% end node net rotations; just the last values in the vector
theta_x_end_node_step1 = rotation_per_timestep_step1(timesteps,1);
theta_y_end_node_step1 = rotation_per_timestep_step1(timesteps,2);
theta_z_end_node_step1 = rotation_per_timestep_step1(timesteps,3);
% the displacements and rotations of the final node are shown
displ =[m_beams2.D(N_nodes,1);m_beams2.D(N_nodes,2);m_beams2.D(N_nodes,3);
    theta_x_end_node_step1;theta_y_end_node_step1;theta_z_end_node_step1];

% saving all deformations and rotations for each beam structure
% NB these will be the same as deformation_per_timestep_step1 and
% rotation_per_timestep_step1 if you don't have multiple values for
    certain
% parameters in this loop. In other words they are the same when the loop
% only runs once.


all_deformations_step1(:,N2:N2+2) = deformation_per_timestep_step1;
all_rotations_step1(:,N2:N2+2) = rotation_per_timestep_step1;


% vector with all displacements xyz of the end node for each timestep
% also better to put in a function perhaps? YES and it works!

% the applied force per time and the applied moment per time step data is
    created in vector Force_history
Force_history_step1 = linspace(0,Fe(6*m_beams.numberNodes-3),par.nTimestep
    ); % Fz
Moment_history_step1 = [linspace(0,Fe(6*m_beams.numberNodes-2),par.
    nTimestep);linspace(0,Fe(6*m_beams.numberNodes-1),par.nTimestep);
    linspace(0,Fe(6*m_beams.numberNodes),par.nTimestep)];
% this was the first load step
```

```
%% determination the required rotation to solve load step 1 to a beam with
     flat final element
% coordinates of deformed beam resulting from load step 1
nodal_coordinates_def = [nodal_coordinates(:,1:3) + history(timesteps).m.D
    (:,1:3)]; % x, y, z coordinates
final_element_vector_def = [nodal_coordinates_def(N_nodes,:) -
    nodal_coordinates_def(N_nodes-1,:)]';
unit_vector_final_element_def = final_element_vector_def* (1/sqrt(
    final_element_vector_def'*final_element_vector_def));

% coordinates of deformed and then rotated beam
[x2, y2, z2, phi, R_y] = beam_orientation_rotation(N_nodes,
    nodal_coordinates,history,timesteps);
nodal_coordinates_def_rot = [x2 y2 z2];
final_element_vector_def_rot = [nodal_coordinates_def_rot(N_nodes,:) -
    nodal_coordinates_def_rot(N_nodes-1,:)]';
% the unit vector is computed again and should be [1 0 0]'
unit_vector_final_element_def_rot = final_element_vector_def_rot* (1/sqrt(
    final_element_vector_def_rot'*final_element_vector_def_rot));



%% solving step 2, load step 1 redone but in a rotated configuration
% redoing the first load step on an initially rotated beam by the angle
    that we now know
% this entire section that redoes the first load step is done, becasue I
% could not figure out where to implement the coordinates of the deformed
% and rotated beam as starting coordinates for the second load step
% rotating the undeformed beam
nodal_coordinates_ini_rot = [ [R_y*[nodal_coordinates(:,1:3)]']' [R_y*[
    nodal_coordinates(:,4:6)]']'];
% also rotating the applied load
F_M_end_rot = [R_y*F_M_end(1:3,1) ; R_y*F_M_end(4:6,1)];

% 1 m_beam_generate_CSD for variable H, B, h, b
[m_beams_rot, dofs, par, Fe_rot] = m_beam_generate_CSD_IyyIzzJA (CSD,
    H_factor, B_factor, h_factor, b_factor, Iyy_factor, Izz_factor,
    J_factor, A_factor, nodal_coordinates_ini_rot, F_M_end_rot, ep1, theta1
    , ep2, theta2,timesteps, iterations, convergence_err,N_nodes);


% implement m_beams_rot, dofs, par, Fe_rot structures to create the
    deformed beam
% no need for the solver with pre force yet
[history_rot, m_beams2_rot] = solveNONLINstaticCOR(m_beams_rot, dofs,par,
    Fe_rot);


%% Start of load step 2
% Step 2.1: positive rotation about x
%Setting the buckling load as a preforce
```

```
F_M_pre_end_node_step2 = F_M_end_rot;

% placing it in a vector with all loads on all nodes
% PreFe2 = force_end_node_generate(F_pre_end2,m_beams2);
PreFe2 = force_end_node_generate(F_M_pre_end_node_step2,m_beams2_rot); %
    here m_beams or

% placing it in a vector
F_M_end2 = zeros(6,1); % F_M_end = [Fx, Fy, Fz, Mx, My, Mz]'; all 0 since
    we only apply a rotation here


% constraints imposed in this step besides the already present pre force
ep1_step2    = [0 0 0];
theta1_step2 = [0 0 0];

ep2_step2    = [nan nan nan];
theta2_step2 = [pi/3 nan nan];


[m_beams4_unnec, dofs2, par, Fe2] = m_beam_generate_CSD_IyyIzzJA (CSD,
    H_factor, B_factor, h_factor, b_factor, Iyy_factor, Izz_factor,
    J_factor, A_factor, nodal_coordinates, F_M_end2, ep1_step2,
    theta1_step2, ep2_step2, theta2_step2,timesteps, iterations,
    convergence_err,N_nodes);


% solve step 3, aka load step 2: here the rotation is applied on a beam
% kept at the unstable equilibrium by having the pre force equal to the
% buckling load
% different solver than the previous solving steps 2 due to PRESENCE of
    pre force
[history2_rot, m_beams3_rot] = solveNONLINstaticCOR_w_PreF(m_beams2_rot,
    dofs2,par,Fe2,PreFe2);


%% Finding the deformations of the end node for each time step using the

% so deformations of step 2 for the final node are
deformation_per_timestep_step2 = zeros(timesteps, 3);

% here you cannot use the deformations function because the displacement
    is
% between two beams that are both already deformed instead of one being
% simply a given set of beam coordinates for an unloaded beam
for i =1:timesteps
deformation_per_timestep_step2(i,:) = [history2_rot(i).m.D(N_nodes,1:3) -
    history_rot(timesteps).m.D(N_nodes,1:3)];
end


rotation_per_timestep_step2 = rotations(timesteps,N_nodes,history2_rot);


%% force - displacement, moment angle for when you are applying a
    displacement or rotation
```

```
% % plots reaction force - displacement, moment - rotations


reaction_forces_moments_per_timestep_step2 = zeros(timesteps,6);
for n = 1:timesteps
reaction_forces_moments_per_timestep_step2(n,:) = reaction_RF_RM_generate(
    history2_rot,n, ep2_step2, theta2_step2)';
end

All_RF_RM_per_timestep_step2_pos_rot(2:timesteps+1,N3:N3+5) =
    reaction_forces_moments_per_timestep_step2;

% max(size(All_RF_RM_per_timestep_step2_pos_rot))

Reaction_moment_x_final = All_RF_RM_per_timestep_step2_pos_rot(timesteps
    +1,4);
RMx_buck = Reaction_moment_x_final;







    Fapplied = 1.1*Fapplied;

    loopcount_while_loop = loopcount_while_loop+1
end
RMx_buck;
deformation_per_timestep_step2;
final_displacements_xyz = deformation_per_timestep_step2(max(size(
    deformation_per_timestep_step2)),:)
loopcount_while_loop;

remain_RMx = RMx_buck/RMx_unbuck;
stiffness_decrease_percent = (1 - (RMx_buck/(pi/3))/(RMx_unbuck/(pi/3)))
    *100;
runtime = toc;
Fz_estimated_buckling_y_based
Fapplied_final = Fapplied/1.1
lat_defl_y = final_displacements_xyz(1,2)

% as a test I want to display dims to track down the point at which the
    file cannot
% converge


%% create the 3D figure
%
% % solve step 1: application of the buckling load
% % Here the deformed beam is plotted
% figure
% hold on
% % Solve step 1, aka load step 1
% PlotBeamsCrossSections(m_beams,par, 'deformed')
% PlotBeamsCrossSections(m_beams2,par, 'undeformed')
```

```
% PlotBeamsCrossSections(m_beams2,par, 'deformed')
%
% % solve step 2, rotated equivalent of solve step 1 aka load step 1
% PlotBeamsCrossSections(m_beams2_rot,par, 'undeformed')
% PlotBeamsCrossSections(m_beams2_rot,par, 'deformed')
%
% % solve step 3, applying a rotation about the local longitudinal axis of
% % the final alement which is coinciding with the global x-axis
% PlotBeamsCrossSections(m_beams2_rot,par, 'undeformed')
% PlotBeamsCrossSections(m_beams3_rot,par, 'deformed')
%
% xlabel('x')
% ylabel('y')
% zlabel('z')
% title('undeformed and deformed configurations ')
% legend('Step 1A: undeformed inital beam','Step 1A: deformed initial beam
    ','Step 1B: undeformed and rotated','Step 1B: deformed and rotated','
    Step 2: undeformed prefroce present','Step 2: deformed preforce and
    longitudinal rotation')
% hold off
end % this is the end of the if commands



end


%% matlab
Put your code here.
```

Bibliography

[1] A Andrade, D Camotim, and P Providência e Costa. “On the evaluation of elastic critical moments in doubly and singly symmetric I-section cantilevers”. In: *Journal of Constructional Steel Research* 63.7 (2007), pp. 894–908.

[2] Anisio Andrade, Dinar Camotim, and P Borges Dinis. “Lateral-torsional buckling of singly symmetric web-tapered thin-walled I-beams: 1D model vs. shell FEA”. In: *Computers & Structures* 85.17-18 (2007), pp. 1343–1359.

[3] Rujuta A Bhat and Laxmikant M Gupta. “Moment-gradient factor for perforated cellular steel beams under lateral torsional buckling”. In: *Arabian Journal for Science and Engineering* 45.10 (2020), pp. 8727–8743.

[4] Virote Boonyapinyo, Hitoshi Yamada, and Toshio Miyata. “Wind-induced nonlinear lateral-torsional buckling of cable-stayed bridges”. In: *Journal of Structural Engineering* 120.2 (1994), pp. 486–506.

[5] Mary Brettle. *Lateral torsional buckling and slenderness*. Oct. 2006.

[6] Noël Challamel and Chien Ming Wang. “Exact lateral–torsional buckling solutions for cantilevered beams subjected to intermediate and end transverse point loads”. In: *Thin-Walled Structures* 48.1 (2010), pp. 71–76.

[7] A Lokman Demirhan et al. “Experimental and numerical evaluation of inelastic lateral-torsional buckling of I-section cantilevers”. In: *Journal of Constructional Steel Research* 168 (2020), p. 105991.

[8] Justus Laurens Herder. *Energy-free Systems. Theory, conception and design of statically*. Vol. 2. 2001.

[9] Oguz Kayhan, A Kemal Nennioglu, and Evren Samur. “A skin stretch tactor for sensory substitution of wrist proprioception”. In: *2018 IEEE Haptics Symposium (HAPTICS)*. IEEE. 2018, pp. 26–31.

[10] Sepehr Movaghati. “Strengthening beam sections of industrial buildings against lateral torsional buckling”. In: *Proceedings of the Annual Stability Conference Structural Stability Research Council*. Vol. 1. 2019, pp. 1–12.

[11] R Piotrowski and A Szychowski. “Lateral-torsional buckling of beams elastically restrained against warping at supports”. In: *Archives of Civil Engineering* 61.4 (2015), pp. 155–174.

[12] Ioannis G Raftoyiannis and Theodore Adamakos. “Critical lateral-torsional buckling moments of steel web-tapered I-beams”. In: *The Open Construction and Building Technology Journal* 4.1 (2010).

[13] Access Steel. “NCCI: Elastic critical moment for lateral torsional buckling”. In: *Access Steel* (2005).

[14] Simon Herman Venter et al. “The effect of the adjacent span on the lateral-torsional buckling capacity of overhang beams”. PhD thesis. University of Pretoria, 2017.

[15] Marilyn B Wagner, Paul J Vignos Jr, and Chris Carlozzi. “Duchenne muscular dystrophy: a study of wrist and hand function”. In: *Muscle & Nerve: Official Journal of the American Association of Electrodiagnostic Medicine* 12.3 (1989), pp. 236–244.

[16] Wei-bin Yuan, Boksun Kim, and Chang-yi Chen. “Lateral–torsional buckling of steel web tapered tee-section cantilevers”. In: *Journal of Constructional Steel Research* 87 (2013), pp. 31–37.